# DEVELOPMENT OF A LOW COST LINEAR FRESNEL SOLAR CONCENTRATOR

Gregg Stuart Walker

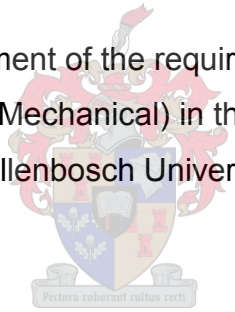

Thesis presented in partial fulfilment of the requirements for the degree of Master of Science in Engineering (Mechanical) in the Faculty of Engineering at Stellenbosch University

Supervisor: Prof TW von Backström

Co-supervisor: Mr P Gauché

December 2013

# DECLARATION

By submitting this thesis electronically, I declare that the entirety of the work contained therein is my own, original work, that I am the sole author thereof (save to the extent explicitly otherwise stated), that reproduction and publication thereof by Stellenbosch University will not infringe any third party rights and that I have not previously in its entirety or in part submitted it for obtaining any qualification.

# ABSTRACT

This study describes the design and construction of a low-cost linear Fresnel solar concentrator. Ray-trace simulation models that analyse optical performance were developed and then used to perform sensitivity analyses of various characteristics of linear Fresnel concentrators. The design of a small-scale concentrator was optimised using the simulation models, after which the concentrator was constructed in the solar laboratory. The concentrator consists of a single-motor tracking system, flat primary mirrors and a low-cost secondary concentrator that approximates a compound parabolic concentrator. Testing revealed satisfactory performance that was comparable to the simulation models' prediction. The construction of a low-cost solar concentrator that can replace existing thermal sources for the generation of power and process heat is thus achievable.

# OPSOMMING

Die ontwerp en konstruksie van 'n laekoste- lineêre Fresnel-sonkonsentreerder word in hierdie studie beskryf. Stralingsimulasiemodelle wat optiese werksverrigting analiseer is ontwikkel en gebruik om sensitiwiteitsanalises van die verskillende eienskappe van lineêre Fresnel-konsentreerders te doen. Die modelle is verder gebruik om die ontwerp van 'n kleinskaalse konsentreerder te optimeer, waarna die konsentreerder in die sonlaboratorium gebou is. Die konsentreerder bestaan uit 'n enkelmotorvolgingstelsel, plat primêre spieëls en 'n laekoste- sekondêre konsentreerder soortgelyk aan 'n saamgestelde, paraboliese konsentreerder. Toetsing dui bevredigende werksverrigting aan, vergelykbaar met wat die simulasiemodelle voorspel het. Dit is dus moontlik om 'n laekoste-sonkonsentreerder wat bestaande termiese bronne vir kragopwekking en proseshittegenerasie kan vervang, daar te stel.

# DEDICATION

This thesis is dedicated to my family for their unwavering support and belief.

Also, may this work be one of many small steps needed for South Africa to move towards a more conscious and sustainable way of living.

# ACKNOWLEDGEMENTS

The financial assistance of the National Research Foundation (NRF) and the Centre for Renewable and Sustainable Energy Studies (CRSES) (SANERI Hub) towards this research is hereby acknowledged. Opinions expressed and conclusions arrived at, are those of the author and are not necessarily to be attributed to the NRF or CRSES.

To Professor Theo von Backström and Mr Paul Gauché, thank you for all the guidance and expertise. The constant support and patience was greatly appreciated.

The author would like to thank the Solar Thermal Energy Research Group (STERG) for financing equipment and experiment construction through funds from the DST/NRF solar thermal spoke and SU Hope Project. Also, gratitude is expressed to fellow members of STERG for the valuable input and discussions.

# TABLE OF CONTENTS

# LIST OF TABLES

# LIST OF FIGURES

# NOMENCLATURE

Latin symbols

| | | |
|---|---|---|
| A | rad | Azimuth angle |
| $A_1$ | m | Aperture of full mirror |
| $A_2$ | m | Aperture of unshaded mirror |
| $A_p$ | $m^2$ | Area of pipe |
| Cp | kJ/kg.°C | Specific heat of water at constant pressure |
| d | m | Radius of applied force |
| D | m | Diameter of absorber tube |
| $DNI_{ew}$ | $W/m^2$ | DNI projected onto East-West plane |
| F | N | Applied force |
| $F_{p\rightarrow rec}$ | | View factor (dimensionless) |
| g | $m/s^2$ | Gravitational acceleration |
| H | m | Height of receiver |
| h | $W/m^2.K$ | Heat transfer coefficient |
| $L_1$ | m | Shading vector x intercept |
| $L_2$ | m | Unshaded vector x intercept |
| $\dot{m}$ | kg/s | Mass flow rate |
| $Q_n$ | m | Mirror centre point x coordinate |
| $Q_{n+1}$ | m | Centre point of adjacent mirror |
| $Q_R$ | W | Radiation heat loss |
| $Q_C$ | W | Convection heat loss |
| $\dot{q}$ | W | Heat transfer rate/Power |
| Re | | Reynolds number (dimensionless) |
| $r_0$ | m | Radius to offset pivot centre |
| T | Nm | Applied torque |
| $T_p$ | K | Absorber pipe temperature |
| $T_{rec}$ | K | Receiver/ambient temperature |
| V | $W/m^2$ | Vector to sun |
| $V_e$ | $W/m^2$ | Projection on east direction |
| $V_n$ | $W/m^2$ | Projection onto north direction |
| $V_z$ | $W/m^2$ | Projection onto zenith |
| w | m | Mirror width |
| $w_{receiver}$ | m | Receiver width |

| | | |
|---|---|---|
| $x_n$ | m | Relative offset pivot in x |
| $y_n$ | m | Relative offset pivot in y |

Greek symbols

| | | |
|---|---|---|
| $\alpha$ | rad | Offset pivot deflection angle |
| $\Delta T$ | K | Change in temperature |
| $\Delta x$ | m | Absolute offset pivot in x direction |
| $\Delta y$ | m | Absolute offset pivot in y direction |
| $\delta_{x1,spillage}$ | m | Spillage to east in horizontal plane |
| $\delta_{x2,spillage}$ | m | Spillage to west in horizontal plane |
| $\varepsilon$ | | Emissivity of pipe (dimensionless) |
| $\theta_n$ | rad | Tilt angle of mirror |
| $\theta_{n+1}$ | rad | Adjacent mirror tilt angle |
| $\theta_z$ | rad | Zenith angle |
| $\mu$ | Pa.s | Dynamic viscosity |
| $\xi_0$ | rad | Sun subtend angle |
| $\rho$ | rad | Projected sun angle on East-West plane |
| $\sigma$ | $W.m^{-2}.K^{-4}$ | Stefan–Boltzmann constant |
| $\varphi$ | rad | Mirror position angle to receiver |

# LIST OF ABBREVIATIONS

| | | |
|---|---|---|
| CFD | - | Computational Fluid Dynamics |
| CLFR | - | Compact Linear Fresnel Reflector |
| CPC | - | Compound Parabolic Concentrator |
| CSP | - | Concentrated Solar Power |
| DC | - | Direct Current |
| DNI | - | Direct Normal Irradiance |
| DTI | - | Department of Trade and Industry |
| EOT | - | Equation Of Time |
| GFRP | - | Glass Fibre Reinforced Plastic |
| GPS | - | Global Positioning System |
| GUI | - | Graphical User Interface |
| IPCC | - | Intergovernmental Panel on Climate Change |
| LFR | - | Linear Fresnel Reflector |
| LEC | - | Levelized Electricity Cost |
| MTOE | - | Million Tons of Oil Equivalent |
| NMEA | - | National Marine Electronics Association |
| NRF | - | National Research Foundation |
| NREL | - | National Renewable Energy Laboratory |
| PET | - | Poly Ethylene Terephthalate |
| PSA | - | Plataforma Solar de Almeria |
| PV | - | Photo Voltaics |
| RPM | - | Revolutions Per Minute |
| SEGS | - | Solar Energy Generating Systems |
| SPG | - | Solar Power Group |
| SHP | - | Solar Heat and Power |
| STERG | - | Solar Thermal Energy Research Group |
| TERC | - | Tailored Edge Ray Concentrator |

# CHAPTER 1. INTRODUCTION

## 1.1. MODERN ENERGY PRODUCTION

As the global population continues to grow and the industrialization of emerging economies increases, so does global energy demand. In 1973 total primary energy supply amounted to 6107 Mtoe (Million tonnes of oil equivalent) which has now doubled to 12717 Mtoe by 2010 (International Energy Agency 2012). This has been driven by the rapid expansion in emerging economies as well as an increase in passenger vehicles and freight transport. Figure 1 below shows the change in market share of the main energy types.

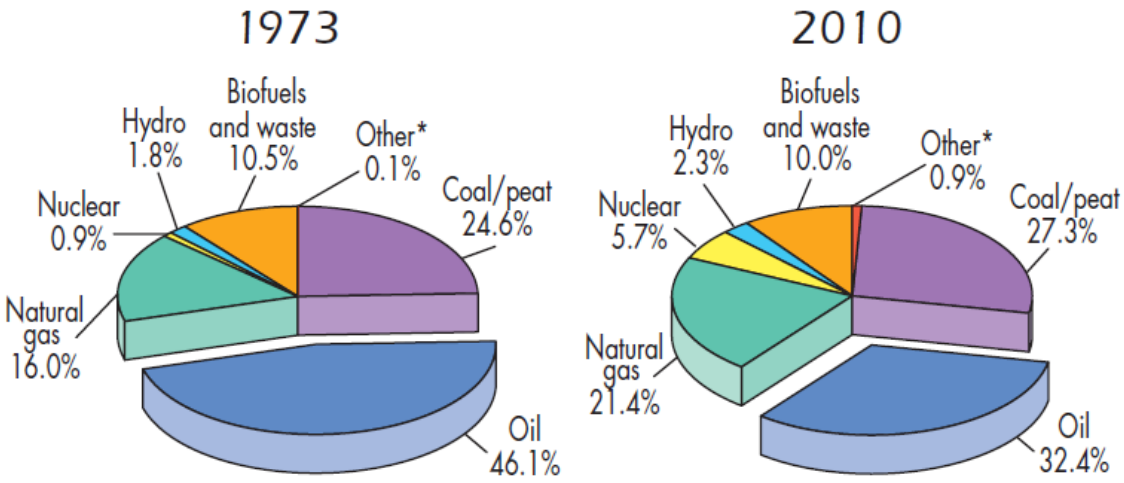


**Figure 1 Global fuel share of primary energy supply** Source: (International Energy Agency 2012)

While the market share of oil has decreased and coal has increased by only 3 %, in absolute terms there has been a dramatic increase in fossil fuel use. In comparison, renewables (included in “Other”) have made little impact on global energy supply. A surge in natural gas production and nuclear have been the greatest change to the global energy mix in the last three decades.

This dependency on fossil fuels for primary energy production has led to increasingly noticeable levels of atmospheric $CO_2$ and other greenhouse gasses. The Intergovernmental Panel on Climate Change (IPCC) has found in their latest assessment report that: “most of the observed increase in the globally averaged temperature since the mid-20th century is very likely due to the observed increase in anthropogenic greenhouse gas concentrations” (IPCC 2007). Climate change not only affects the weather but studies have identified changes in terrestrial ecosystems and marine environments (IPCC 2007). With global food

production and water resources already under strain, governments have identified the importance of climate change mitigation measures. One such measure is the move from predominantly fossil fuel use to renewable energy sources (IPCC 2011).

Wind power has had the greatest impact on renewable energy production over the last decade due in part to it being a mature technology thus making it more competitive. As the availability of economically feasible sites decline, more expensive options such as offshore wind are being investigated. At the same time, incentives and technology developments have made solar power an attractive option. Solar power technologies operate ideally in arid regions where urban development is scarce and land is readily available. The much greater availability of suitable land and potential future cost reductions have made solar photovoltaics (PV) and concentrated solar power (CSP) the forerunners in potential renewable energy production. By 2035 it is estimated that solar and wind power in combination will account for one third of global electricity production (International Energy Agency 2012).

For countries in the world's sun-belt, such as South Africa, CSP plants have the potential to contribute a large portion towards future energy production. This includes the production of both electric and thermal energy. Industry could benefit from the local production of thermal energy directly from concentrated sunlight. The production of electricity in a coal power plant, transmission of this energy and then conversion back to heat is an inefficient process. Local production of heat would reduce these losses which in turn would further reduce reliance on fossil fuels. Therefore the development of CSP plants is of particular interest for developing economies that wish to grow industrial sectors sustainably and provide renewable energy to citizens.

## 1.2. CSP TECHNOLOGY TYPES

CSP is a technology that has been around for a number of decades already. The Solar Energy Generating System (SEGS) plants in the USA have been operating for over 25 years producing power from solar radiation and had produced over 9 $TWh_{el}$ by 2002 (NREL 2002). The plants were constructed initially to demonstrate the technology and gain operational experience in these new types of plants. A major driver was also the oil crisis of the time and new ways of generating energy were being investigated. However, after the construction of the SEGS plants there was a long period in which little new development occurred in the CSP industry due to the oil price stabilising again. In the last decade though there has been

renewed interest in CSP due mainly to increasing awareness of climate change as well as increasing fuels costs of fossil fuel power plants. The rising fuel costs and constant improvements in CSP technology have brought it close to grid parity.

CSP plants concentrate the incoming beams of direct sunlight using various optical devices to heat a fluid and then extract work from this fluid using a heat engine. The method of concentrating sunlight as well as the type of heat engine used defines the type of solar thermal technology. The two most common methods of concentrating solar radiation are line focusing and point focusing. The most notable differences between the two major solar thermal types is that concentration ratios are higher for point focus technology but these require two axis tracking as opposed to single axis tracking for line focus type. Figure 2 below shows examples of the four sub types of CSP plants.

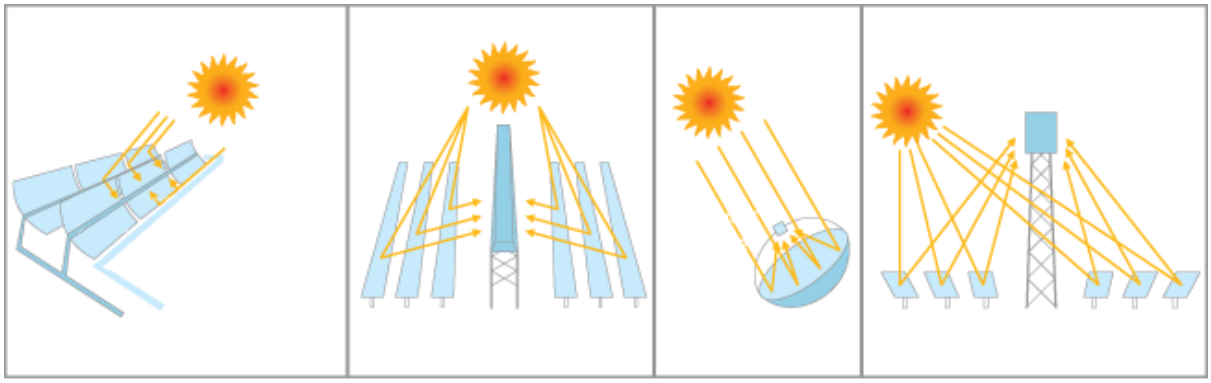


**Figure 2 CSP technology types** Source: www.iea.org, accessed: 17/11/2012

Parabolic trough plants are the most mature of the CSP technologies and the majority of worldwide installed capacity is of this type. They offer an acceptable performance level but some limitations do still exist. The curved mirrors are relatively expensive and aspects such as the need for flexible couplings and strong foundations to combat wind loads result in a high cost per kWh. The scope for future cost reduction is also limited. The other line focusing type, the linear Fresnel reflector (LFR), is comparatively new and offers much potential for cost reduction. It is not as efficient as the parabolic trough but is projected to have a lower investment cost per kWh (Häberle, *et al*. 2002). The technology also uses simpler parts that could be manufactured locally.

Central receiver plants offer the highest potential efficiency of all CSP plants. The higher concentration ratio and working fluid temperature lends itself to combined cycle operation.

The more sophisticated nature of the technology means that at first, components would be manufactured abroad and therefore contribute less to a local CSP industry. The second point focus type, dish Stirling, is a very scalable technology in terms of selecting the number of units to match the required load. Dish Stirling has much potential for small scale off grid applications in Africa. It does not benefit much from economies of scale and therefore may not be appropriate for large base load installations.

## 1.3. SOLAR THERMAL ENERGY IN THE SOUTH AFRICAN CONTEXT

The rising cost of fuel, the depletion of the country's coal reserves and the current shortfall in electricity base-load capacity has caused the South African government to investigate the inclusion of CSP plants into the country's electricity generation mix. The Integrated Resource Plan 2010 has included the construction of CSP power plants in order to meet demand as well as the beginning of climate mitigation measures. Currently 600 MW of new CSP capacity has been allocated for the period up to 2030 with an option of an extra 400 MW (Department of Energy 2010). The inclusion of CSP plants as a renewable energy option is because of the excellent solar resource available over much of the country. In particular, the Northern Cape has some of the best solar resource available worldwide in terms of DNI as shown in Figure 3 below.

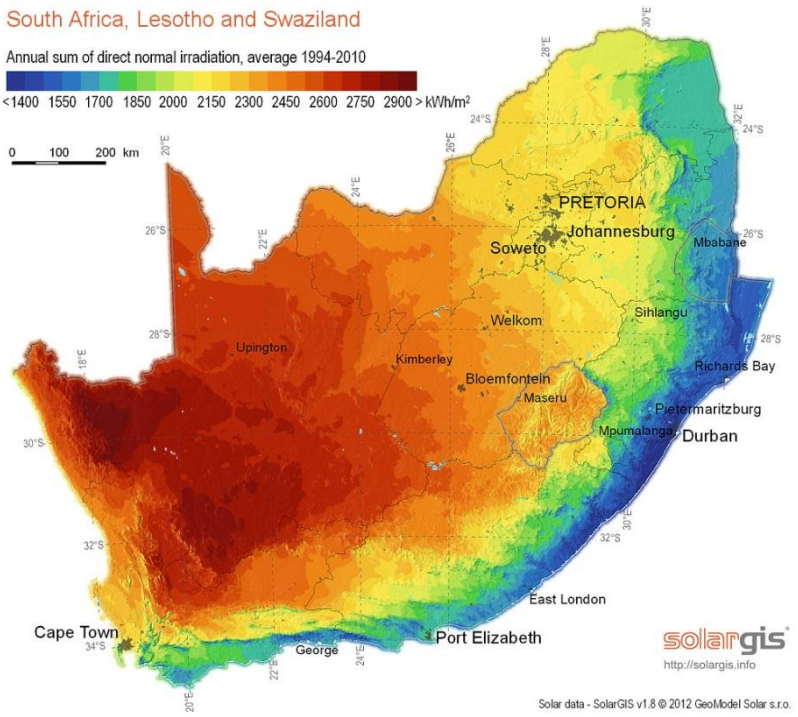


**Figure 3 DNI map of South Africa** Source: www.geosun.co.za, accessed 17/11/2012

This level of unlimited and clean energy resource puts South Africa in an enviable position to generate a large percentage of its power demand from renewable sources. Unfortunately there is no historical presence of CSP operations in South Africa. The main options in implementing CSP locally is to either develop the expertise locally and then build plants or to import the technology first and then attempt to replicate it locally. Whilst the first option would provide the greatest benefit to the economy, it would take many years to establish local expertise. There is also the situation in South Africa in which high levels of poverty and inequality exist that demands the greatest share of government funding and attention. The establishment of a CSP industry would require much funding and firm commitment from the regulatory bodies in the change from fossil fuels to renewables.

In the short term, the first CSP plants to be built will be by international technology suppliers. The first 100 MW plant scheduled for construction in Upington has an estimated cost of R4.466 billion of which R4.020 billion will be imported labour and equipment (African Development Bank 2011). This demonstrates the importance of establishing local industries for parts and services in CSP if the full potential boost to the local economy is to be achieved. With this in mind, new research activities have been funded by the National Research Foundation (NRF) and the Department of Trade and Industry (DTI) that will hopefully kick start the local CSP sector.

One such research area that has been identified is the potential that LFR power plants may have in Southern Africa. It is inherently a much simpler technology that may find application in either stand-alone power generation or process heat for industry. The level of local manufacture of parts is also a driver for the technology. Very little of the plant would need to be sourced outside of the country if the correct support industries are established.

## 1.4. HISTORY OF LINEAR FRESNEL POWER PLANTS

LFR technology is one of the youngest concentrating solar power technologies that has been proven both in demonstration plants and scaled up to full commercial plants. Work to prove the feasibility of the technology intensified in the 1990's with the main research groups working independently on the design of LFR demonstration plants. Later, various partnerships emerged that often resulted in the formation of start-up LFR companies.

The first modern LFR demonstration plant was the Solarmundo prototype built in Liège, Belgium in 2001. It was a small kW size installation but successfully demonstrated the technology. Figure 4 below shows the completed Solarmundo prototype. Some Solarmundo employees then formed Solar Power Group GmbH (SPG) to scale-up and commercialise the technology. Solar Power Group formed a consortium with other German research institutes and constructed a 1 MW plant at the Plataforma Solar de Almeria (PSA) in Spain in 2007. This plant was the first to successfully demonstrate direct steam generation by a LFR plant.

**Figure 4 Solarmundo prototype** Source: (Häberle, et al. 2002)

Research at the same time in Australia by Dr. David Mills and Professor Graham Morrison resulted in the Compact Linear Fresnel concept (CLFR) that is introduced in a widely cited paper (Mills and Morrison 2000). Mills and Morrison formed the company Solar Heat and Power Ltd (SHP) which built a 1 MW pilot plant at Liddell Power Station, Australia. After demonstrating successful integration with the Liddell coal power plant, Solar Heat and Power was bought by a USA investor and rebranded into Ausra. Ausra then proceeded to build a 5 MW demonstration plant in Kimberlina, USA. This was completed in 2008 and the first phase is shown in Figure 5. In order to scale up operations Ausra was then sold to the much larger Areva who rebranded it to Areva Solar.

**Figure 5 Kimberlina CSP plant** Source: Ausra, accessed: 14/11/2011

http://www.ausra.com/news/photographs.html

Another CSP start-up company specialising in LFR, Novatec Solar, was formed in 2006 and completed a 1 MW plant in Spain called Puerto Errado 1. A 30 MW plant has since been completed at the same site. The table below lists the existing and planned commercial scale LFR plants worldwide (as of July 2012).

**Table 1 Linear Fresnel CSP plants worldwide**

| Plant name | Country | Size (MW) | Status | Company |
|---|---|---|---|---|
| Fresdemo | Spain | 1 | Operational 2007 | SPG, DLR, MAN |
| Liddell | Australia | 1 | Operational 2007 | Solar Heat and Power Ltd |
| Kimberlina | USA | 5 | Operational 2008 | Areva Solar |
| Liddell Phase 2 | Australia | 3 | Operational 2009 | Areva Solar |
| Puerto Errado 1 | Spain | 1 | Operational 2009 | Novatec Solar |
| Puerto Errado 2 | Spain | 30 | Operational 2012 | Novatec Solar |
| Himin Solar | China | 3 | In construction | Himin Solar Energy Group |
| Kogan Creek Solar Boost Project | Australia | 44 | In construction | Areva Solar |
| Reliance Areva | India | 125 | In construction | Reliance Power |

| Plant name | Country | Size (MW) | Status | Company |
|---|---|---|---|---|
| CSP 1 | | | | |
| Reliance Areva CSP 2 | India | 125 | In construction | Reliance Power |
| Collinsville Solar | Australia | 150 | Planned | Transfield Services Pty Ltd |
| Mejillones | Chile | 5 | Planned | |
| Sundt Solar Boost Project | USA | 5 | Planned | Areva Solar |
| Novatec FG Emvelo Upington 1 | South Africa | TBA | Planned | Novatec Solar |
| Solar Dawn Kogan Creek | Australia | 250 | Planned | Areva Solar |
| Aurum Renewables | India | 125 | Planned | Aurum Renewables Pvt Limited |
| Bokpoort | South Africa | 7 | Planned | Solar Heat and Power Ltd |
| | | | | |
| **Totals** | | **(MW)** | | |
| Operational | | 41 | | |
| In construction | | 297 | | |
| Planned | | 542 | | |

(Source: CSP Today http://www.csptoday.com/global-tracker/content.php, accessed 03/07/2012)

## 1.5. RECENT PILOT PLANTS

The increasing awareness of LFR technology and its potential market segment in the growing CSP industry has led to a number of existing companies to branch out into CSP. The LFR technology is relatively simple in comparison with the more mature CSP technologies like parabolic troughs and has allowed companies with manufacturing backgrounds, but not necessarily CSP research backgrounds, to build their own prototypes. A number of the more recent pilot plants built are listed in the table below.

**Table 2 Recent LFR pilot plants**

| Plant | Description |
|---|---|
|  | BBE, South Africa.<br>A mine heating and ventilation company that built a prototype.<br>Source: BBE, accessed: 12/09/2011<br>http://www.bbe.co.za/index.php?option=com_phocagallery&view=categories&Itemid=5 |
|  | FERA, Sicily.<br>An Italian research consortium formed with the purpose of developing LFR technology and creating a CSP supply chain industry in Italy.<br>Source: FERA, accessed: 04/07/2012<br>http://www.ferasolar.it/en/la-tecnologia-csp-fresnel |
|  | CNIM, France.<br>An established heavy industry manufacturer with future interests in renewable energy.<br>Source: CNIM , accessed: 04/07/2012<br>http://www.cnim.com/en/cnim-and-solar-energy.aspx |
|  | Industrial Solar, Germany.<br>A Fraunhofer ISE spinoff with specific focus on LFR for process heat and cooling. A number of plants have been installed around Europe and the Middle East.<br>Source: Industrial Solar, accessed: 04/07/2012<br>http://www.industrial-solar.de/cms/en/ |

| | |
|---|---|
|  | Solar Euromed, France.<br>A French research entity that evolved out of parabolic trough research. A larger pilot plant is planned for the island of Corsica.<br>Source: Solar Euromed, accessed: 04/07/2012<br>http://www.solareuromed.com/en |

The only South African based manufacturer of LFR plants, BBE, has won a contract to build a demonstrator at the Eskom renewable energy research offices in Johannesburg. Construction is underway and Eskom employees will evaluate the system's performance during 2013.

## 1.6. RESEARCH OBJECTIVE

The core aim of the work undertaken was to design and construct a low cost LFR concentrator that could successfully demonstrate operation of the technology. Due to safety concerns and the lack of a heat extraction system, the experiment was not designed to produce steam for a heat engine. An emphasis was placed on designing the system with locally sourced components and to use low-tech components where it would not jeopardise the system's operation.

The aim of the experiment was firstly to demonstrate that such a system could be built locally and to investigate the areas in which further work would be needed to develop a commercial product. Functionality was built into the experiment to allow future alterations and upgrades as may be required by the research group.

## 1.7. SCOPE AND METHODOLOGY

Similar to the research efforts mentioned in section 1.5 above, the aim of this thesis was to develop the tools required to understand the various design aspects of LFR systems with the eventual aim of building a small working prototype. The Solar Thermal Energy Research Group (STERG) at Stellenbosch University has a rooftop laboratory, termed the solar roof, on which the prototype was built. The width in the North-South orientation as well as budget

constraints placed limits on the potential size of the experiment. Approximately 8m total in length by 5m in width was the area available.

The thesis focuses on the design and construction of both the collector and receiver. This includes the tracking system and the water/heat exchanger surfaces. The chief design aim was to build a low cost LFR system from components sourced locally. The experiment was to operate automatically with little outside control as may be the case in an industrial environment. It was not designed to provide steam to a heat engine, however, its operation demonstrates the LFR technology principle through the heating of water to just below boiling point.

An overview of existing LFR plants and published research efforts formed the basis of the preliminary review work. This influenced the decision to develop simulation models that can predict system performance. These models were firstly used to perform sensitivity analyses on the various design parameters of the primary collector. The layout of the experiment could then be optimised for the allowable footprint on the solar roof. A second model was used to perform ray trace simulations of potential secondary concentrator designs for the receiver. This resulted in a low cost design with relatively high performance.

Following simulation results, the experiment was designed and constructed primarily by the author, members of STERG and the Mechanical Department. Testing was conducted and the experimental results were compared to what the earlier models predicted.

## 1.8. REQUIREMENTS AND SPECIFICATIONS

The main aim of the thesis is to design and build a low cost LFR demonstrator. In order to achieve this objective a number of core requirements were initially identified. These form the basis of benchmarks against which the success of the project can be measured. During the literature review and design process a number of additional desired characteristics were identified. These requirements, and the quantity or capability against which they are measured, are listed in Table 3 below.

**Table 3 Requirements and specifications**

| Item number | Description | Quantifiable measure |
|---|---|---|
| **1.0** | **Core** | |
| 1.1 | Demonstrate linear Fresnel principle | Power curve similar to model prediction and literature (within 10 %) |
| 1.2 | Construction cost within acceptable budget limits | System is similar in price compared to existing thermal systems |
| 1.3 | Experiment to be built at the solar roof laboratory | Experiment fits in allowable 4 m × 8 m footprint |
| 1.4 | Design should strive to achieve low cost and local manufacturing potential | 75 % of total cost relates to locally sourced components |
| 1.5 | Allow various configurations to be tested such as mirror sizes, spacing and receiver design | Flexibility of final design to allow conversions |
| 1.6 | System to automatically track the sun | Only input needed is to switch on experiment |
| 1.7 | Must include measurement instruments to validate operating conditions | Instrument system to output data of experiment's performance over a day |
| 1.8 | Structurally sound to withstand inclement weather and wind loads | No damage present after rough weather |
| 1.9 | Sufficient design life to allow future testing, up to 10 years | No degradation of mirrors or metal surfaces within design life |
| | | |
| **2.0** | **Desired** | |
| 2.1 | Ability to turn mirrors upside down to enable washing or protect from hail | Full rotation of mirrors achievable (360°) |
| 2.2 | Modular design to allow additional arrays to be connected at later stages | No major alterations required to add additional array module |
| 2.3 | Design life similar to commercial plants (20-30 years) | |
| 2.4 | Mirror mounts to be easily removable to aid replacing broken mirrors or fitting new | Mirror must be removable without significantly disrupting operation |

| | | |
|---|---|---|
| | surfaces | |
| 2.5 | Single drive to actuate all mirrors | |
| 2.6 | Where possible, cheap flat mirrors must be used | |

The number of LFR pilot plants and commercial installations that are already operational allows for an early investigation into the likely problems to be encountered when designing an experimental system. While much of this information is the proprietary knowledge of the few LFR start-up companies, there is still significant literature available to inform the direction in which a low cost LFR prototype could take. The following section provides a review of this literature study.

# CHAPTER 2. LITERATURE REVIEW

## 2.1. INTRODUCTION

The majority of published work on linear Fresnel solar concentrators is concerned with the quantification of the efficiency with which different designs convert incoming Direct Normal Irradiance (DNI) into thermal power. The common approach is to use ray tracing methods to model the performance of the optics in the array. Such tools can calculate the statistical chance that an incoming ray will be reflected correctly and strike the absorber tube. Simulations can be run that predict the efficiency of a collector at different times of the day and then compare this with DNI data for specific locations. This allows the potential annual energy production to be calculated and then compared to other forms of energy production to see whether a linear Fresnel plant would be economically feasible.

Some of the earliest work on LFR concentrators was performed by a consortium of research groups that formed the Solarmundo initiative. The pilot plant that was built had the aim of validating the ray trace models as well as investigating mechanical and operational aspects. In (Häberle, *et al.* 2002) the Solarmundo collector was theoretically scaled up to a commercial plant size and compared to an existing parabolic trough plant. The comparison is shown in the figure below. While the Fresnel collector didn't perform as well as the parabolic trough in terms of optical efficiency (34.5 % compared to 50.1 %), because of its much lower investment and operational cost it actually had a lower lifetime cost per kWh.

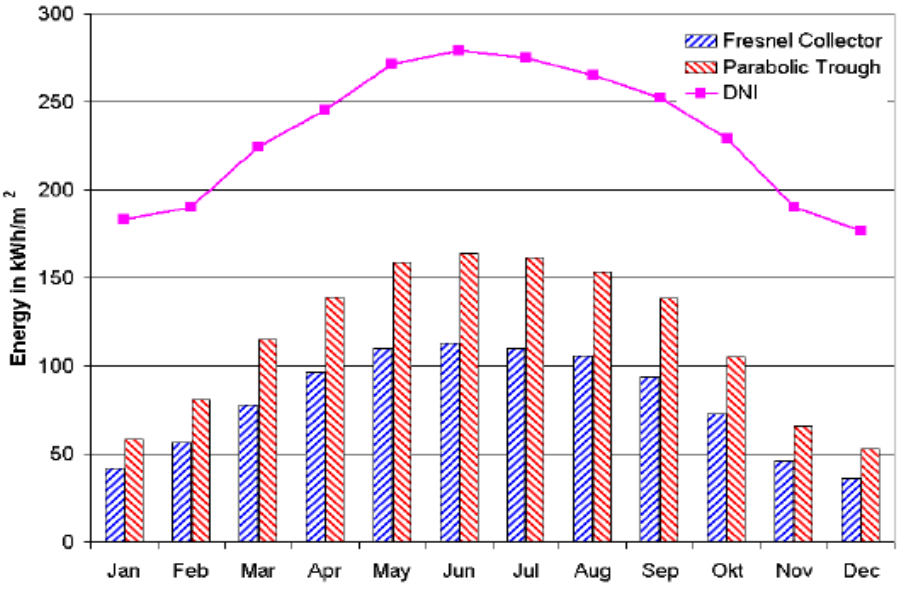


**Figure 6 Solarmundo Fresnel comparison with parabolic trough** Source: Häberle *et al*, 2002

Ray tracing methods also allow the investigation of what effect the changing of various features will have on the performance. In this way the design of a collector can be optimised and trends in the performance can be predicted for a number of variables. For instance, the effect of reducing the accuracy of tracking systems in order to save costs can be evaluated. As linear Fresnel collectors have traditionally had lower efficiencies than parabolic troughs, much research has been focussed on increasing the performance while maintaining the lower cost advantage that LFR has. Collector optimisation is discussed more in section 2.3 below.

Another area of research has been the evaluation of the potential of direct steam generation in LFR plants such as the Supernova concept proposed by Novatec (Morin, Mertins, *et al*. 2011) and research being conducted by CNIM (Alliotte 2011) and Areva Solar (Conlon, Johnson and Hanson 2011). A related study on the effect of thermal stress on receiver tubes in the different stages of direct steam generation in LFR plants has been conducted (Eck, *et al*. 2007). In order to obtain direct steam generation a number of key operating conditions and plant features must be designed. The production of superheated steam requires high temperatures and pressures. The higher pressures are easier to obtain in LFR plants than parabolic trough plants because the steam piping is all fixed with no flexible joints. There is the problem, however, that line focusing CSP plants require many kilometres of steam piping which introduces pressure drop. (Eck, *et al.* 2007) used the predicted pressure drop to determine the optimum length of preheater, evaporator and superheater sections. The required total length can be split into parallel lines for each section to obtain the same total heat transfer but reduce the pressure drop.

The obtaining of higher steam temperatures is a more complicated problem. To reach higher steam temperatures, the concentration of the solar radiation must be higher and creates the need for very accurate tracking, curved primary reflectors and secondary concentrators. The flux distribution for a typical LFR absorber tube is shown below in Figure 7. This flux distribution is an ideal one for preheater and evaporator sections as the majority of flux is concentrated at the bottom of the tube where the liquid water is and therefore the highest heat transfer occurs. The flux concentrations to either side of the centre of the tube are due to the secondary concentrator.

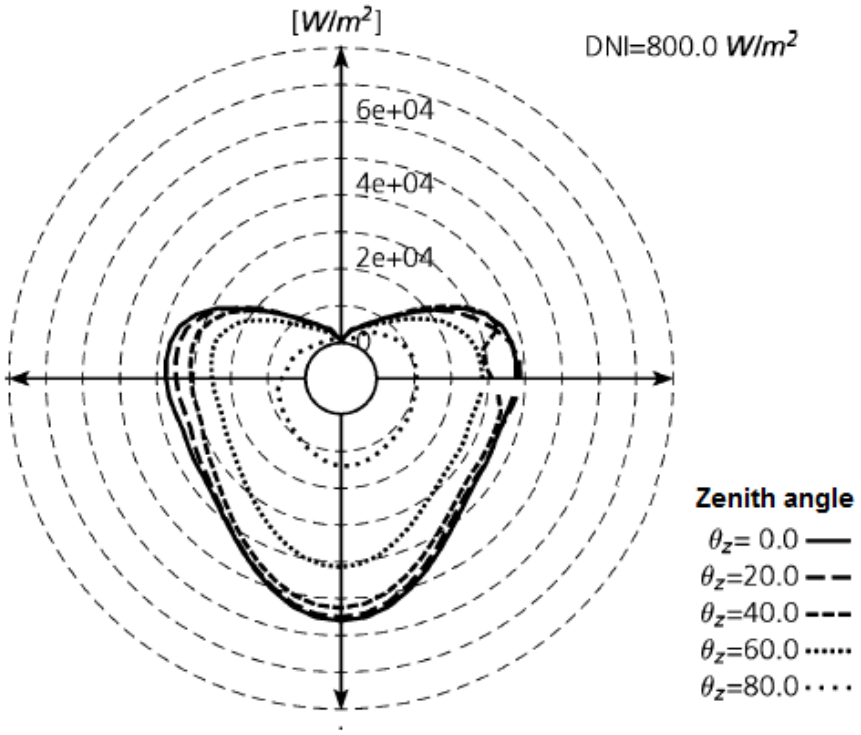


**Figure 7 Heat flux distribution at absorber tube for different zenith angles** Source: Eck *et al*., 2007

The flux distribution can become a problem in the superheater section as the lower heat transfer of superheated steam causes the absorber tube to heat up at the bottom to a higher temperature than the top and induce thermal stress. The absorber tube temperature must also not increase higher than 500 °C or degradation of the selective coating will occur. It was found by (Eck, *et al*. 2007) that in the worst case scenario, defocusing of mirrors may be needed in the superheater section to prevent this degradation. In order to investigate such problems and improve designs, very accurate ray tracers and system modelling must be performed.

## 2.2. RAY TRACING AND CFD WORK

Two common methods of ray tracing are the Monte Carlo and geometric edge ray tracing techniques. Monte Carlo is a statistical approach that uses random rays generated in a number of statistical ways such as Gaussian distributions. The rays are randomly generated in terms of angle of incidence and origin on the sun disk. The path of each ray is then traced from origin through any reflections until it either hits the absorber tube or is lost to the environment. This is usually the most accurate but many rays are needed for a meaningful result and the computational time can be long. The number of striking rays and their flux

values are then integrated to calculate the relative concentration ratio or flux distribution for that collector. Most commercial ray tracing programs make use of Monte Carlo.

The edge ray method is a much simpler approach but can provide results quickly that are relatively accurate. This method can be used in optimisation algorithms in which computational time must be a minimum for each optimisation loop. (Mathur, Kandpal and Negi 1991) introduce a number of edge ray tracing methods tailored for linear Fresnel collectors. The basic concept is that a ray for each mirror is calculated at each particular time of day to specularly reflect a ray from the centre of the sun disk to the centre of the absorber tube. This results in a particular tilt angle for each mirror at that time of day. Edge rays are then traced from the sun disk to reflect off the outermost edges of each mirror at the same tilt angle towards the absorber tube. The point at which these edge rays strike some predefined surface such as a horizontal receiver surface is then recorded. The concentration ratio is then calculated from the geometry of each reflected beam that hits the receiver.

The edge ray method assumes homogeneously distributed flux levels across the width of the incoming radiation. There is also the assumption that if the edge rays are calculated to hit a receiver, then all the rays in between the edge rays will also hit the receiver. This method is not as accurate as Monte Carlo because the specularity of mirror surfaces is not taken into account unless the beam is split into a number of different rays that strike different surfaces on the mirror. Both methods can take into account errors such as tracking errors, spillage, blocking, shading and edge losses.

Two well documented ray tracers used for linear Fresnel are the OptiCAD tool developed by Fraunhofer ISE and EDStar developed by RAPSODEE Laboratory (Barale, *et al.* 2010) (Veynandt, *et al*. 2006) (De La Torre, *et al*. 2010). Both tools use Monte Carlo ray tracing. OptiCAD was used by the Solarmundo team to evaluate the optical efficiency of their design. In Häberle *et al.* (2002) the system analysed had 48 mirrors each 0.5 m wide and a receiver comprising a selectively coated 18 cm diameter steel tube with a glass pane to seal the receiver. OptiCAD predicted a 61 % efficiency of incoming DNI transformed to heat at the absorber tube. This efficiency did not include radiation and convention heat losses. The figures below show examples of the ray traces performed.

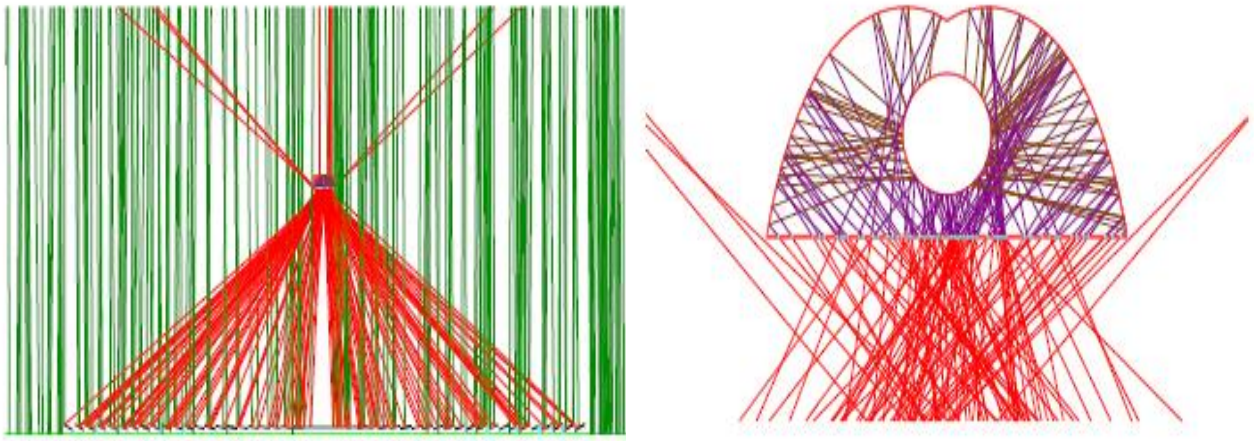

**Figure 8 Solarmundo ray trace (Left) Collector (Right) Receiver** Source: (Häberle *et al*, 2002)

Ray trace tools are often coupled with transient solvers to perform CFD simulations and calculate heat transfer and loss on the receiver parts. The Solarmundo study used TRANSYS to simulate losses in the receiver and the results are shown in the Figure 9 below. This study indicates that the majority of heat loss is through the glass pane below the absorber tube. This is corroborated by (Larsen, Altamirano and Hernández 2012) who state that around 91 % of heat loss is through the bottom of the receiver at a temperature of 200 °C.

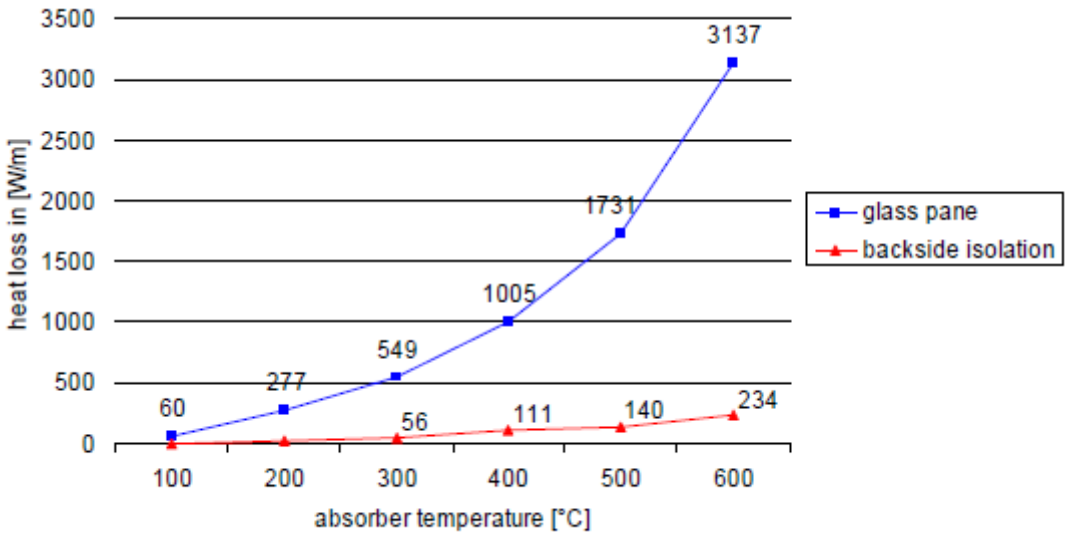


**Figure 9 Heat loss from Solarmundo receiver** (Source: Häberle *et al*, 2002)

Ray tracers are also used to analyse the effects that specific attributes have on system performance. (Veynandt and Bézian 2011) used the EDStar tracer to investigate the effect

that optical accuracy has on the performance. Tracking, specular and curvature errors were combined into a global error that was applied across the mirror surface in a statistical manner. Figure 10 below shows the effect primary mirror error has on the flux distribution on the receiver.

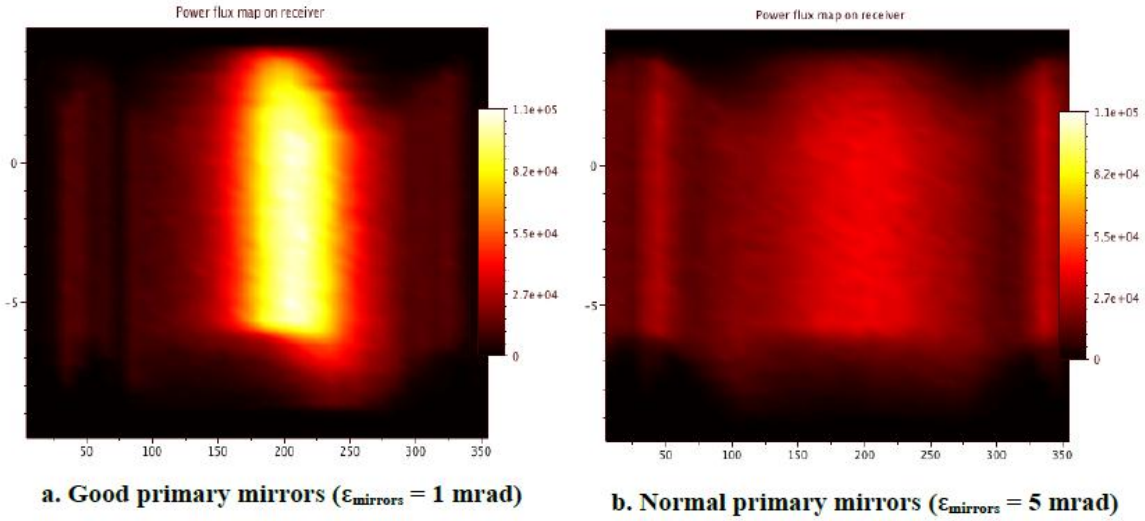


**Figure 10 Effect of primary mirror precision** (Source: Veynandt & Bézian, 2011)

Veynandt *et al*. concluded that primary mirror precision was the most important and that the global precision should be kept below 2 mrad (approximately 0.115 degrees). For the system they analysed, a precision above 5 mrad (0.286°) resulted in 25 % spillage loss. A study by Heimsath *et al*. was conducted on the characterization of specular surfaces using the Fringe Reflection Technique (Heimsath, et al. 2008). This method creates local surface gradient maps and can be used to analyse the actual specular performance of a mirror. The aim of the study was to develop a technique that can be used to evaluate the effect of various stages of the construction process in LFR plants such as mirror gluing and mechanical bending.

## 2.3. COLLECTOR OPTIMISATION

The design of a LFR plant will differ depending on what the intended use is. For example, direct steam generation or low temperature process heat. During the design process it is useful to conduct sensitivity analyses to investigate the effect of changing component dimensions. In this way trends can be identified that help in the optimisation of receiver performance. Prior to developing a prototype, Veynandt *et al*. used EDStar to explore the changes in performance when varying receiver height and width separately (Veynandt, et al.

2006). Similar work in Sicily resulted in optimisation of the design of another prototype (Barale, *et al*. 2010). (Morin, Platzer, *et al.* 2006) also performed sensitivity analyses in their design when scaling up the Solrmundo prototype to the plant later built at PSA, Spain. Figure 11 below shows some of the results from the project (Mertins, *et al*. 2004).

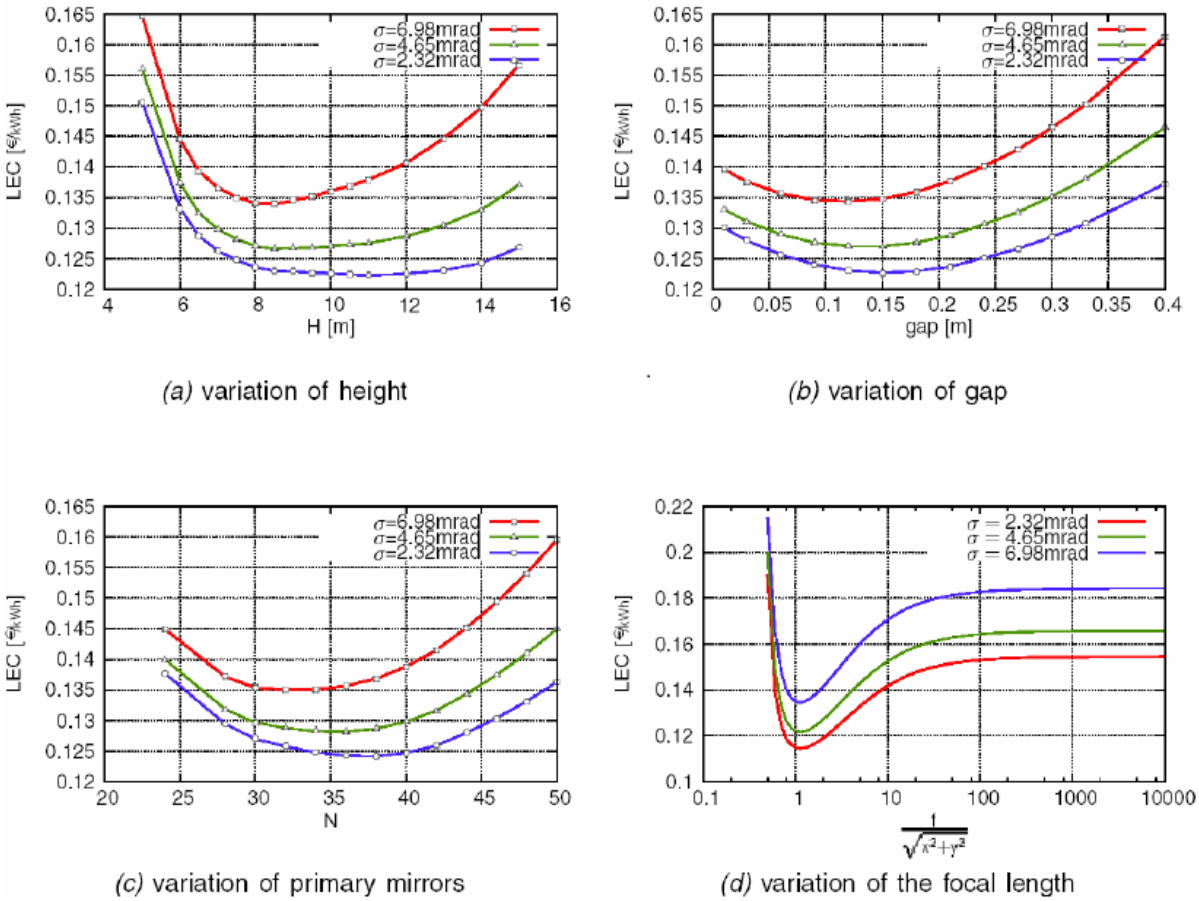


**Figure 11 Sensitivity analyses** (Source: Mertins *et al*, 2004)

In the above sensitivity analyses, LEC was chosen as the desired optimisation function. Some very evident trends develop and give an indication of where the first guesses for optimisation should begin.

## 2.4. TRACKING SCHEMES AND MIRROR ORIENTATION

The two major causes of efficiency losses in LFR systems are the blocking and shading effects. In an attempt to reduce their impact a number of alternative tracking schemes have been proposed. Mills and Morrison proposed the CLFR that was later incorporated into Ausra plants (Mills and Morrison 2000). The blocking effect is the highest at the edge of an array due to the more oblique angle to the receiver. To overcome this it was proposed that

certain mirrors at the edge be oriented to reflect to an adjacent receiver. The change in tilt angle prevents other mirrors from being blocked. The concept is shown in Figure 12.

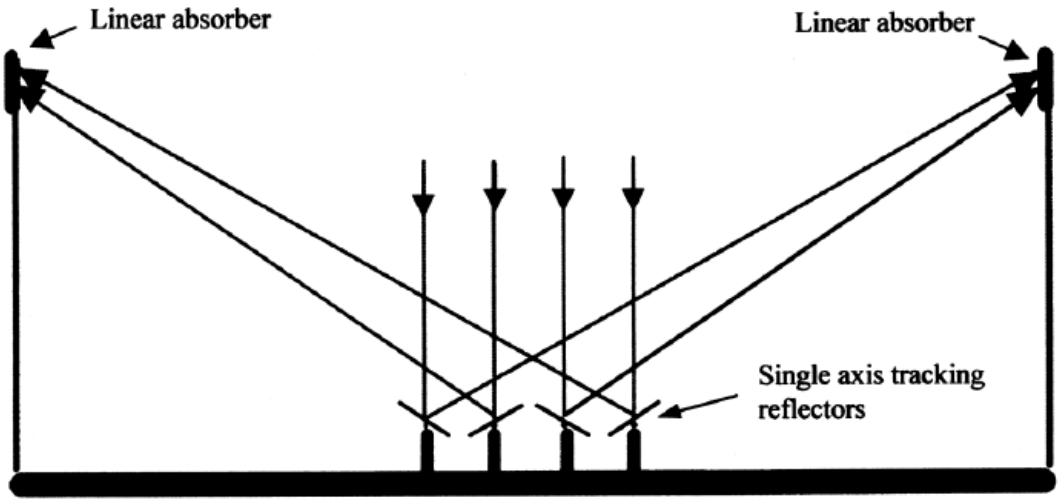


**Figure 12 CLFR concept** Source: (Mills and Morrison 2000)

This technique allowed the receiver height to be reduced and the array to be more closely packed, both of which will reduce the cost of the plant. They found that for optimum receiver performance there was the need for a secondary concentrator near the receiver that allowed the rays from the outermost mirrors to be reflected to the absorber tube. There was an optimum size of the receiver at which point increasing its size to allow further collection was outweighed by the increase in shadowing. It was also found that a standard mirror curvature over the whole collector array had no noticeable difference in performance than for a system where the curvature is varied for each mirror. This improves the manufacturability and construction of the LFR plant.

A more recent concept is the “Etendue matched” CLFR design which is said to take advantage of ideal non-imaging optics to reduce blocking and shading errors (Chaves and Collare-Pereira 2010). Etendue is the extent to which incoming radiation diverges, thus losing flux concentration. The conservation of Etendue means that the incoming beams do not diverge further than the subtend angle of the sun and perfect reflection is achieved. The primary mirrors are positioned along an Etendue conserving curve in cross section. The variation in mirror location along the curve reduces optical losses and also allows reflection of the incoming rays to two different receivers. The concept is said to improve optical efficiency to just below 70 % (Canavarro, Collares-Pereira and Guerreiro 2011). Figure 13 below illustrates the mirror layout.

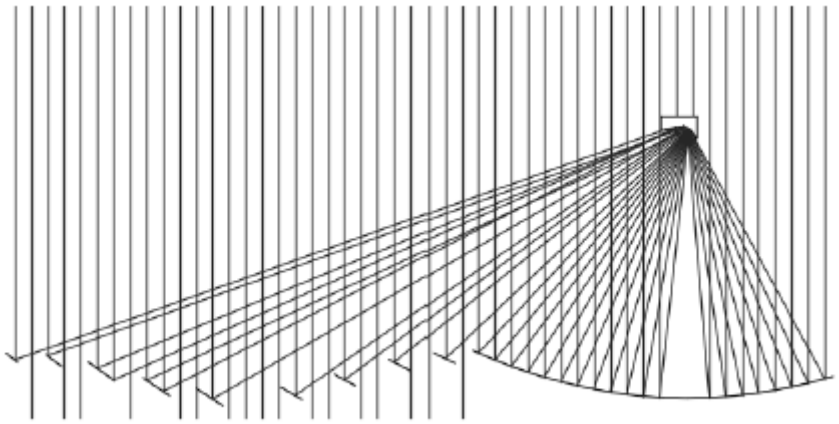

**Figure 13 Etendue matched CLFR** Source: (Horta, et al. 2011)

The receiver design has also been modified for this concept. It uses a non-evacuated asymmetric secondary concentrator called a Tailored Edge Ray Concentrator (TERC). This receiver can also be situated closer to the ground.

Another interesting tracking concept that was proposed is the Solar Island concept (Olcese and Amorosi 2011). This system uses fixed linear Fresnel mirror arrays that are instead rotated in the azimuth plane on a large scale turn-table. The arrays track so that the azimuth is along their length. The concept is stated to achieve a 22 % increase in optical performance while using 30 % less land. This brings the Solar Island LFR within 10 % of the performance range of a parabolic trough. Figure 14 shows a conceptual image of it.

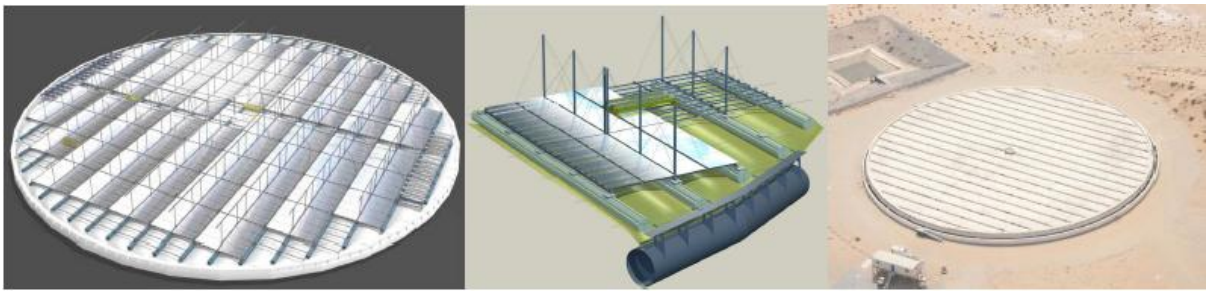

**Figure 14 Solar Island concept** (Source: (Olcese and Amorosi 2011))

Whilst the concept does show dramatic improvements in efficiency and land use, the complicated turn-table may increase costs to beyond a feasible level.

# CHAPTER 3. SIMULATION OF COLLECTOR

## 3.1. INTRODUCTION TO COLLECTOR SIMULATION

As one of the aims of the project is to design a LFR prototype that is cost effective yet as efficient as possible, it was decided to develop a simulation tool that can model any particular design of a LFR collector and calculate its expected performance. A simplified ray trace model was used such as those commonly found in the literature. Mathur *et al.* present a method to model the concentration ratio achieved by any particular LFR design (Mathur, Kandpal and Negi 1991).

The method of modelling a horizontal absorber from Mathur *et al*. was chosen as the most appropriate model for this study. This is because the reflected beams are modelled until they strike the horizontal surface below what would be the entrance to the secondary concentrator. This allows the performance and concentration ratio of the collector to be evaluated separately from the performance of the secondary concentrator. The performance of the secondary concentrator is investigated further in Chapter 4. The azimuth and zenith angles of the sun vector at any given time are transformed onto an East-West plane so that the North-South oriented collector can be approximated by a two dimensional slice. The DNI is also transformed onto this plane so that the incoming ray can be represented by the angle to the vertical axis, denoted by the sun-angle ρ in Figure 15 below.

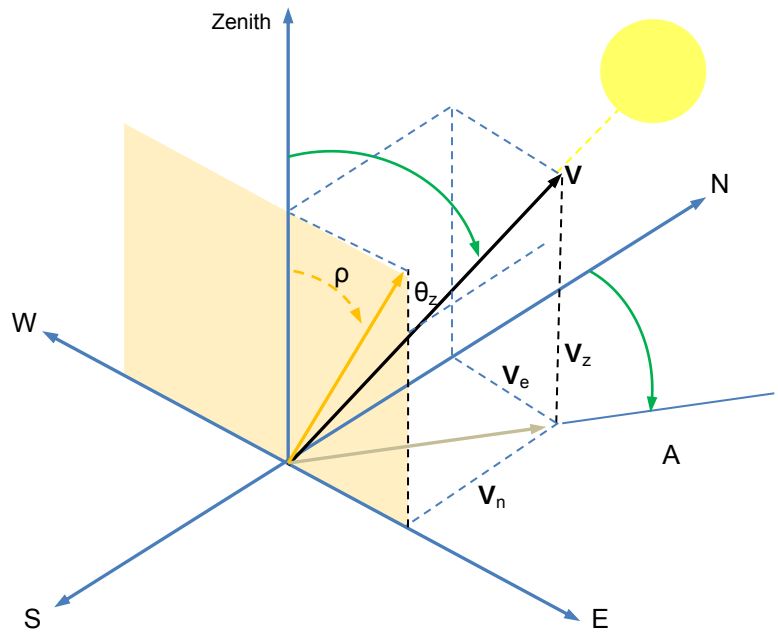


**Figure 15 Coordinate system for solar angles**

The vector V that points to the centre of the sun disk can be transformed into its component vectors as shown in Equations 1 to 3 below.

$$V_z = V\cos(\theta_z) \quad (1)$$

$$V_e = V\sin(\theta_z)\sin(A) \quad (2)$$

$$V_n = V\sin(\theta_z)\cos(A) \quad (3)$$

The transformed sun-angle ρ is then:

$$\rho = \arctan\left(\frac{V_e}{V_z}\right) = \arctan\left(\frac{\sin(\theta_z)\,\sin(A)}{\cos(\theta_z)}\right) \quad (4)$$

If vector V's quantity represents the DNI then the portion of DNI in the East-West plane is:

$$DNI_{ew} = \frac{V_z}{\cos(\rho)} = \frac{V\cos(\theta_z)}{\cos(\rho)} = \frac{DNI\,\cos(\theta_z)}{\cos(\rho)} \quad (5)$$

While the above equation does take into account the cosine loss of the collector, the vector $V_n$ must be used to calculate the end losses of the collector. The basic geometry of the collector simulation program is shown in Figure 16 below.

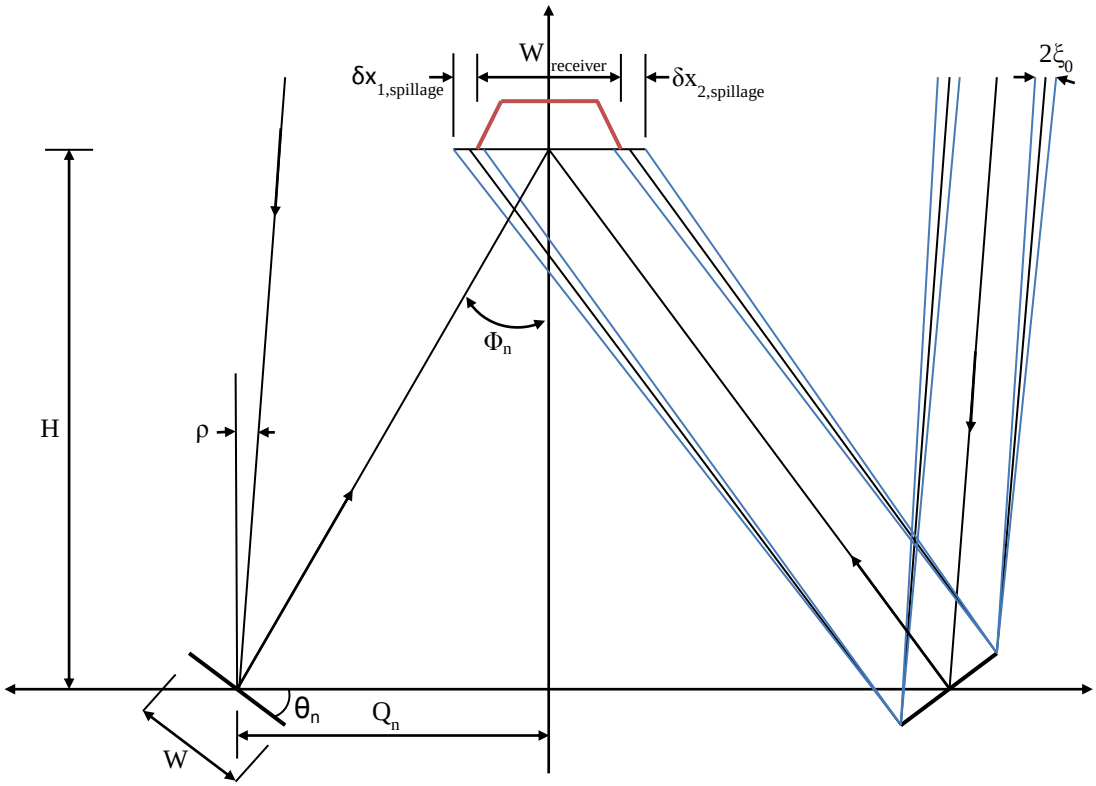


**Figure 16 Ray trace layout and variables**

For any random mirror N, the ray from the centre of the sun disc is designed to hit the centre of the mirror and reflect to the centre of the receiver tube. The incoming edge rays of the mirror, which are diverging due to the sun's subtend angle $\xi_0$, reflect to the horizontal surface below the receiver. The relative concentration of the $N_{th}$ mirror can be calculated by the coordinates of the reflected beam compared to the incoming beam aperture. There are, however, losses that must first be taken into account as discussed in section 3.2 below.

The tilt angle of a mirror $\theta_n$, is a function of the current sun-angle and the geometry for that mirror:

$$\theta_n = \frac{\varphi_n - \rho}{2} \tag{6}$$

Where

$$\varphi_n = arctan\left(\frac{Q_n}{H}\right) \tag{7}$$

$Q_n$ is the position of the $N_{th}$ mirror and $H$ is the height of the receiver above the axis of rotation of each mirror. The tilt angle is the angle to which that particular mirror must be positioned at that particular time of day to reflect to the receiver and is needed by the control electronics to track the sun.

In order to simulate the performance of LFR collectors a model was developed in MATLAB as it is a flexible tool and allows easy graphical representation of the system. A number of input variables were chosen to enable flexibility in the design of multiple systems. The variables include:

- Number of mirrors
- Width of each mirror
- Height of the receiver
- Width of the receiver
- Spacing between each mirror
- Increment of mirror spacing
- Offset pivot spacing

The offset pivot spacing is a variable that allows investigation of a concept that was developed and is discussed further in section 3.5. A graphical user interface (GUI) was also developed for the simulation model as an interactive tool that allows variables to be changed and the result to be displayed immediately in a graphical form. The GUI is shown below.

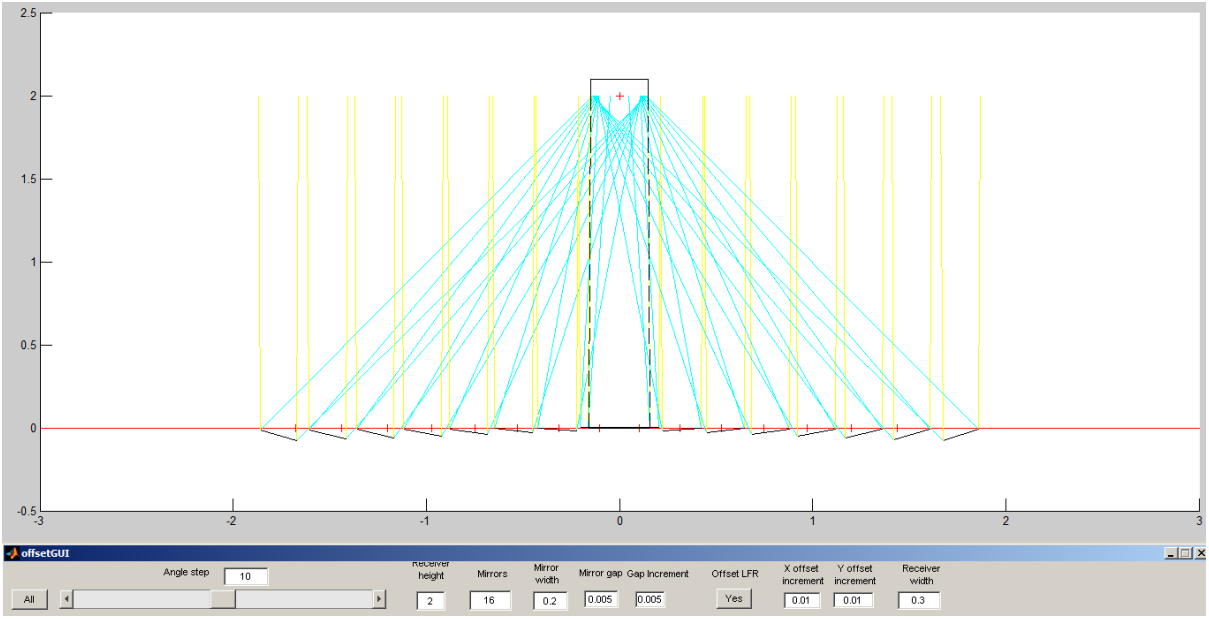


**Figure 17 GUI for LFR modelling**

## 3.2. LOSSES IN THE SYSTEM

When the tilt angles of the mirrors in a particular design are known and the geometry of the incoming radiation is defined a number of losses in the system can be calculated. There are losses associated with the geometry of a LFR collector that prevent portions of reflected beams from reaching the receiver. These and other mechanical causes of losses are listed in the table below.

**Table 4 List of collector losses**

| Type of loss | Description |
|---|---|
| Shading | Adjacent mirrors shade each other from incoming sunlight |
| Blocking | Adjacent mirrors block outgoing reflected rays from mirrors to the receiver |
| Spillage | Due to diverging reflected beams or narrow receivers, a portion of the reflected beam misses the receiver |
| Specular | Inconsistencies on mirror surfaces |
| Transmissivity | Impurities in glazing and glass mirrors |
| Tracking | Mechanical and manufacturing tolerances |
| Receiver shading | When the shadow of the receiver obscures a mirror |
| End loss | Declination of the sun causes losses at the ends of collector arrays |

The shading loss is a loss that is more significant for LFR collectors when compared to other CSP technologies. The loss for a given mirror is calculated from the geometry and tilt of adjacent mirrors in comparison to it. Figure 18 below shows an example in which the sun is rising in the east and a particular mirror N is shaded by the mirror that is further to the east in the array, the N+1 mirror. This case is for the situation in which all the mirrors' centre of rotation are on the same horizontal plane.

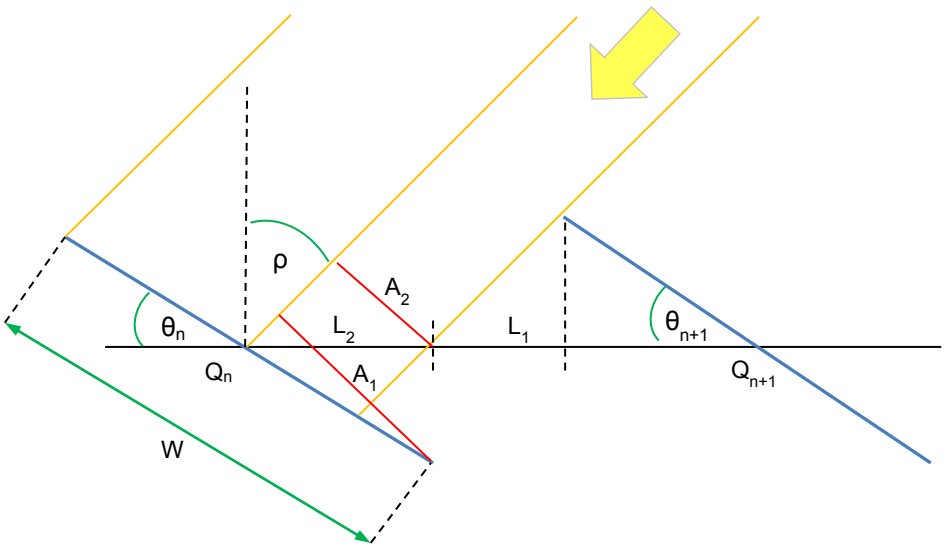


**Figure 18 Example of shading loss geometry**

Shading occurs when the aperture of the incoming beam $A_2$ is less than the aperture of the mirror $A_1$ (both shown by red lines in Figure 18). A ray striking the centre of the mirror is taken as reference point for both $A_1$ and $A_2$. This means that if shading goes beyond this point, then the relative difference between $A_1$ and $A_2$ becomes negative. In both cases the difference is added to the other half of the mirror aperture. When the difference is negative, this merely means it is subtracted from the other half of the aperture. The aperture of half the mirror is:

$$A_1 = \sin(90 - \rho + \theta_n) \times \frac{W}{2} \quad (8)$$

And the unshaded aperture is:

$$A_2 = L_2 \times \sin(90 - \rho) \quad (9)$$

Where the positions of the mirror centre points $Q_n$ and $Q_{n+1}$ are used to calculate $L_2$:

$$L_2 = Q_{n+1} - \left(\frac{W}{2} \times \cos(\theta_{n+1})\right) - L_1 - Q_n \quad (10)$$

And $L_1$ is:

$$L_1 = \tan(\rho) \times \sin(\theta_{n+1}) \times \frac{W}{2} \quad (11)$$

Substituting (11) into (10) and then (10) into (9) yields:

$$A_2 = \left(Q_{n+1} - \left(\frac{W}{2} \times \cos(\theta_{n+1})\right) - \left(\tan(\rho) \times \sin(\theta_{n+1}) \times \frac{W}{2}\right) - Q_n\right) \times \sin(90 - \rho) \quad (12)$$

If $A_2$ is greater than or equal to $A_1$ then no shading occurs. If it is less than or negative, then shading losses will be present. The blocking loss can be calculated using similar geometric comparisons between adjacent mirrors.

### 3.3. MATLAB SIMULATION TOOL

The simulation tool begins with the input of the particular design case variables as well as the DNI data selected for the evaluation. In all simulation results presented in this text the DNI data selected is for Stellenbosch, however, any DNI data set can be used for performance evaluation at a particular site. The model then calculates the potential losses for each particular mirror at a given sun-angle. The logic flow diagram of the program is shown in Figure 19. The code listing for the simulation tool can be found in Appendix A.

The model simulates the collector's performance over the course of a day, according to which DNI data was selected. To run the simulation using standard LFR designs takes approximately 1 minute 30 seconds for a full day simulation at 1 minute intervals of DNI data. The simulation of the offset concept discussed later in section 3.5 takes significantly longer at approximately 4 minutes. This is because of the more complex calculation of the tilt angle.

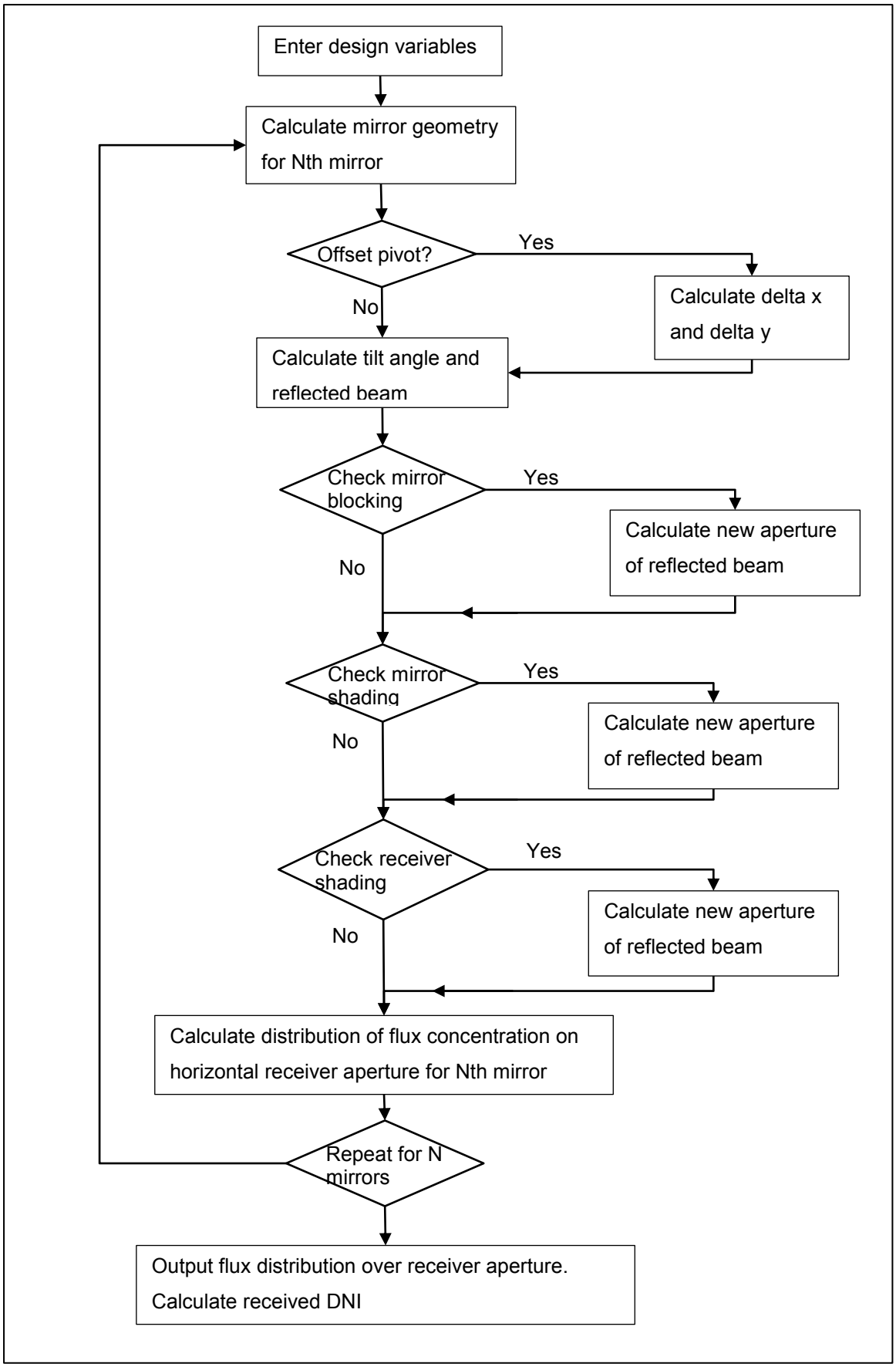


**Figure 19 MATLAB simulation model logic flow**

## 3.4. SENSITIVITY ANALYSIS

There are a number of variables to be considered in the design of a LFR collector and to better understand the effect of changing each variable a number of sensitivity analyses were conducted. One variable is changed over a feasible range while the rest of the variables are held constant and the relative change in predicted thermal energy production over the course of a summer day is compared. Limitations on the design include a maximum 4 m wide footprint and a 3 m high receiver as this is the allowable space on the solar roof. The ultimate aim of the sensitivity analyses is to understand how changing certain variables effect the thermal energy production with the desire of maximising it.

### 3.4.1. Number of mirrors

The effect of changing the number of mirrors on the performance was investigated and the design cases are shown in Table 5 below.

**Table 5 Sensitivity analysis setup**

| Case | Mirror width (m) | Mirror gap (m) | Receiver height (m) | Receiver width (m) |
|---|---|---|---|---|
| 1 | 0.2 | 0.01 | 2 | 0.25 |
| 2 | 0.25 | 0.01 | 2 | 0.3 |
| 3 | 0.3 | 0.01 | 2 | 0.35 |
| 4 | 0.35 | 0.01 | 2 | 0.4 |
| 5 | 0.4 | 0.01 | 2 | 0.45 |
| 6 | 0.5 | 0.01 | 2 | 0.55 |

Mirror widths of standard size were chosen as this would improve manufacturability. The mirror gap was set to 1 cm as this will result in a closely packed array. The receiver height of 2 m is in the middle of the range of the specifications and allows flexibility for increasing or decreasing as required. The receiver width is the width of the mirror plus an additional 5 cm to allow for diverging reflected beams.

The number of mirrors for each design case above was then incremented from two to thirty-two. Initially this was done with no limitation on the footprint on the array. The trend in energy production increase is shown in Figure 20.

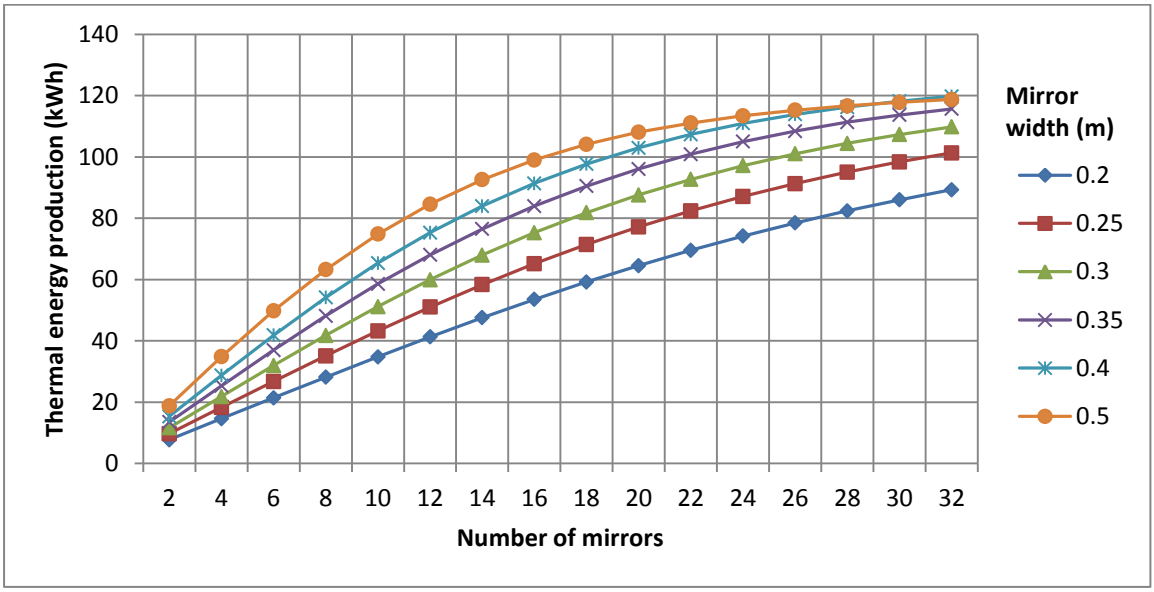


**Figure 20 Thermal energy trend for number of mirrors**

The thermal energy production increases rapidly for the first number of mirrors that were added but this rate drops off as the array gets wider. This reduced rate in the increase of thermal energy production is due to the added mirrors being further away from the receiver and the reflected beam diverging to a greater extent. For a very wide array, adding additional mirrors may not have a noticeable effect on the thermal energy production but the footprint will still be increasing. The widest mirror that was evaluated was 0.5 m in width and this mirror showed the greatest rate of increase in energy as additional mirrors are added. This is because it adds a relatively wider aperture for each extra pair of mirrors.

The data from the above results that were within the 4 m footprint specification was then selected and the allowable design envelope for the solar roof is shown in Figure 21. The 0.5 m wide mirror obviously requires fewer mirrors to fill the 4 m footprint than the 0.2 m wide mirror.

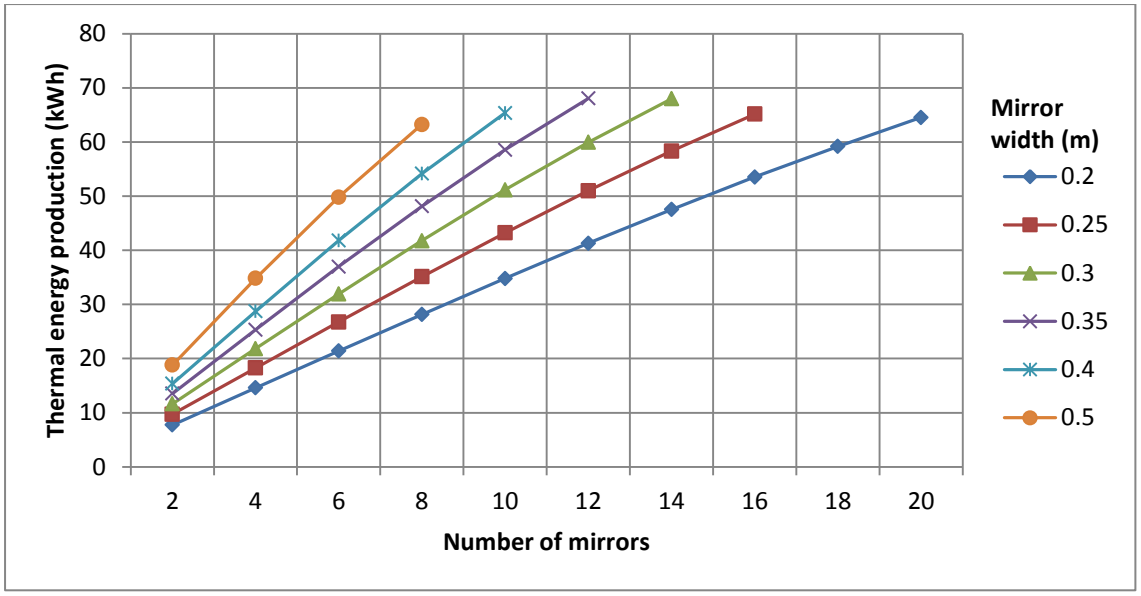


**Figure 21 Thermal energy trend for allowable footprint**

All the different mirror sizes produce roughly the same thermal energy when the array size is at the limit of the allowable footprint. The rates of energy increase, however, are noticeably different which may be useful when deciding on a particular design and the exact number of mirrors to install. For instance, if the 0.5 m mirror is chosen then the cost of the extra motors needed to drive two additional mirrors may be offset by the relatively large increase in thermal energy for those two mirrors. This may not be the case if the 0.2 m mirror is chosen as it adds less extra thermal energy for each new mirror row. However, in terms of reduction of performance for each mirror row that either breaks or if the motor fails, the 0.2 m mirror is the better option as the loss in performance will be the lowest.

### 3.4.2. Receiver height

The next sensitivity analysis that was performed was to investigate the effect the receiver height above the mirrors has on the thermal energy production. The design of each case was as shown in Table 5 except that now the receiver height was varied and the number of mirrors was set as the maximum number for each mirror size for the allowable footprint as shown in Figure 21. The result is shown below.

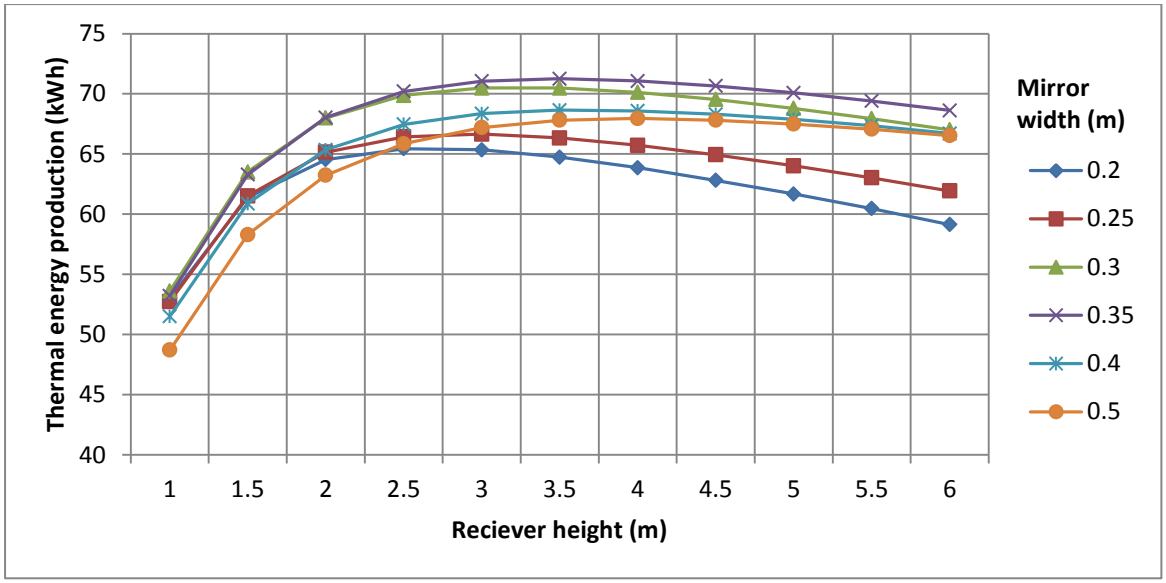


**Figure 22 Thermal energy trend for receiver height**

The receiver height has significant effect on the produced thermal energy at the lower spectrum for receiver heights. This is due to the increased effect of blocking loss on the system. As the receiver height increases, the thermal energy production approaches a maximum value and then gradually reduces again. This behaviour is because once the receiver height varies above its optimum, the reflected beam continues to diverge until the width of the receiver aperture does not receive all the flux and spillage occurs. The optimum receiver height for each mirror width ranges from about 2.5 m to 3.5 m for the case where the footprint is limited to 4 m wide. If the allowable footprint was increased then the optimum receiver heights would also increase.

### 3.4.3. Receiver width

The effect of varying the receiver width was also investigated for the design cases in Table 5. Receiver height was set at 3 m as this is the middle of the optimum range deduced in section 3.4.2 above. Figure 23 below shows the sensitivity of receiver width variation.

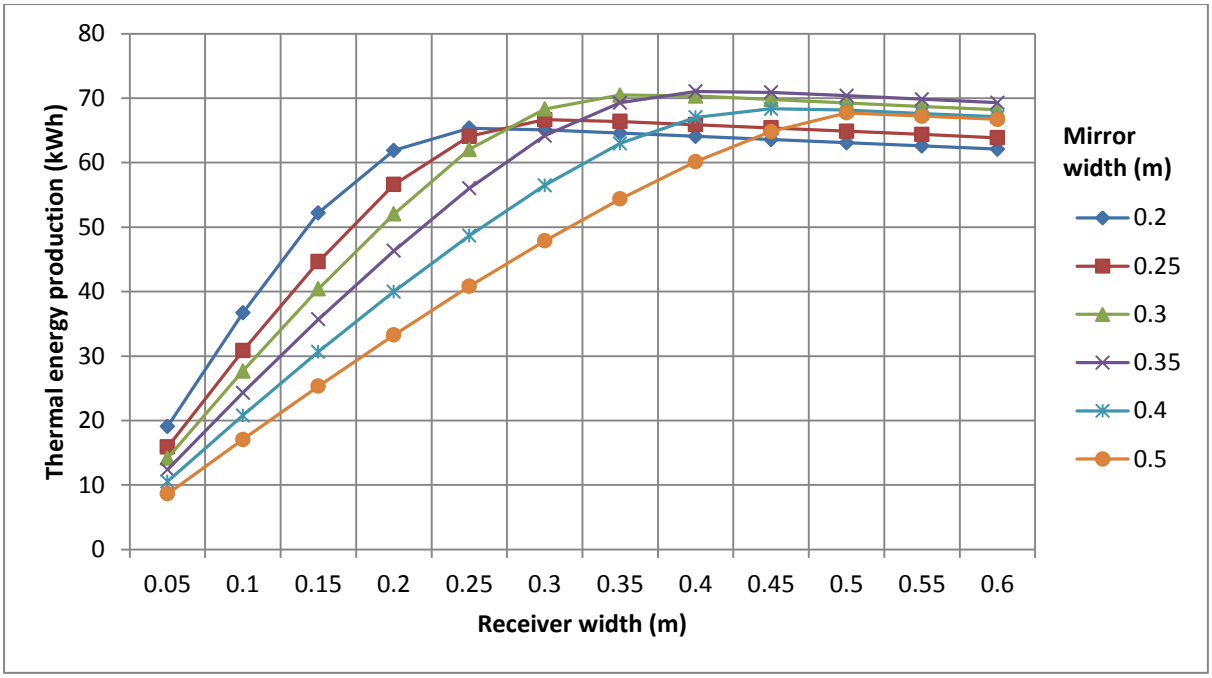


**Figure 23 Thermal energy trend for receiver width**

The trends shown above indicate that for each particular mirror size the optimum receiver width is approximately the width of the mirror plus 5 cm. This is only valid for flat mirrors used within the limitations set by the 4 m footprint. For receiver widths below the width of the particular mirror, there is a dramatic reduction in performance as significant spillage occurs. Once the receiver width increases beyond its optimum length then the effect of receiver shading of the mirrors below the receiver becomes more noticeable and a gradual reduction in produced thermal energy is evident.

### 3.4.4. Combined receiver height and width sensitivity

Varying the receiver height and receiver width individually shows that there is a range for each of the variables in which the optimum configuration can be found. The two variables, however, are linked as there is an optimum receiver height for each specific receiver width. To find the best possible combination the variables must be varied simultaneously. The receiver width was varied between 0.1 to 0.6 m and the receiver height was varied between 1 to 7 m. This was performed for each mirror width and the resulting sensitivity curves are shown in Figure 24 to Figure 27 below.

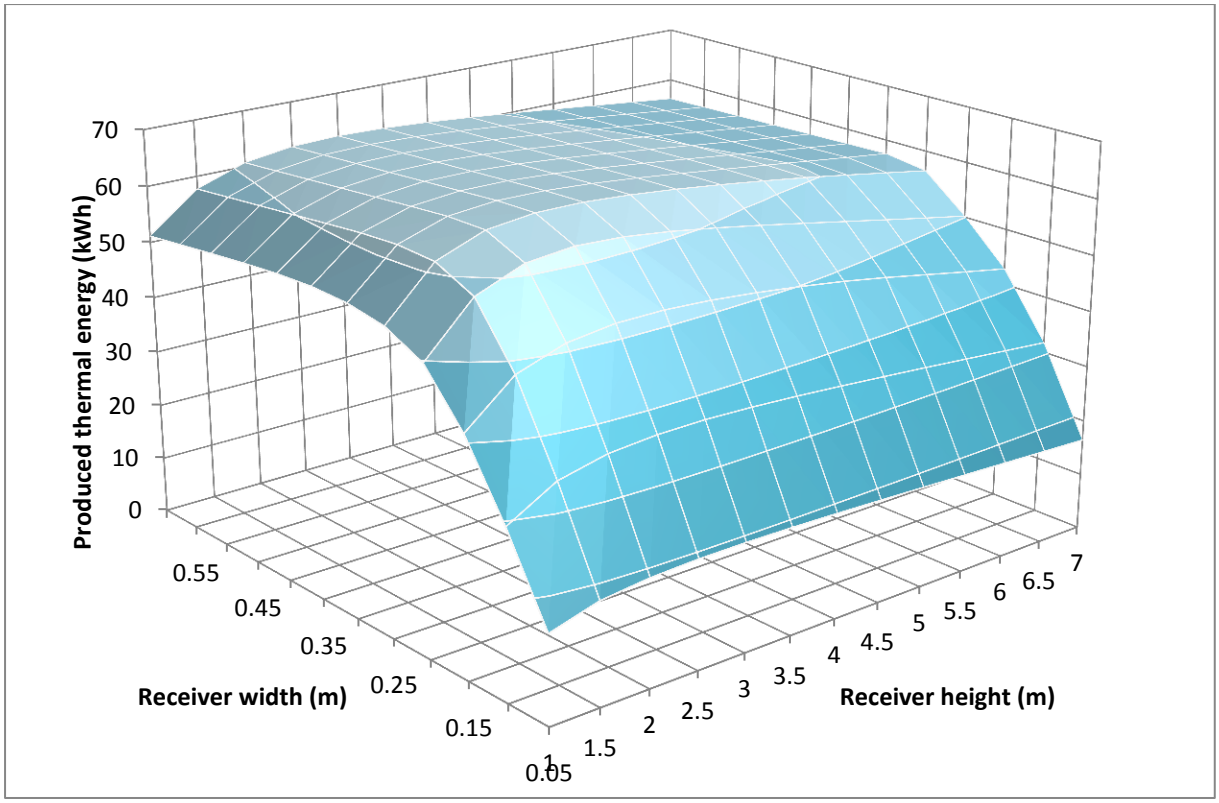


**Figure 24 Thermal energy production for 0.2 m mirror over design space**

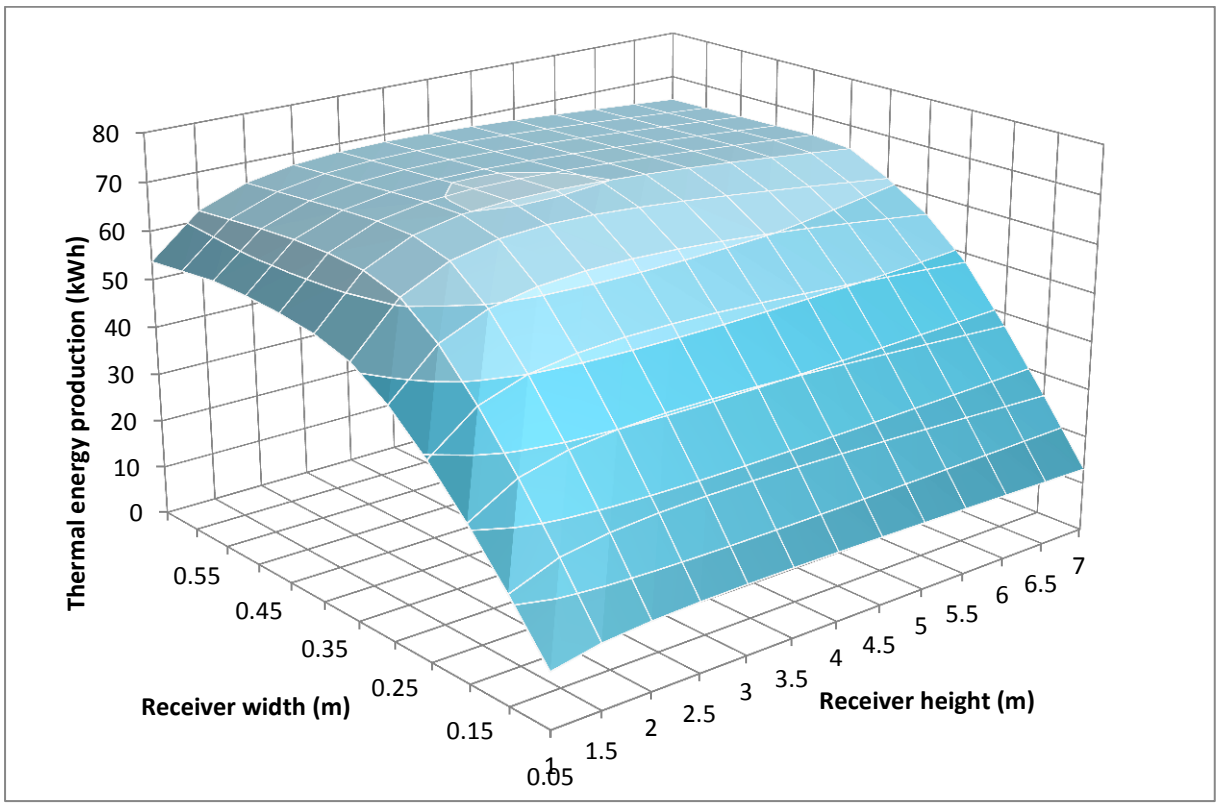


**Figure 25 Thermal energy production for 0.3 m mirror over design space**

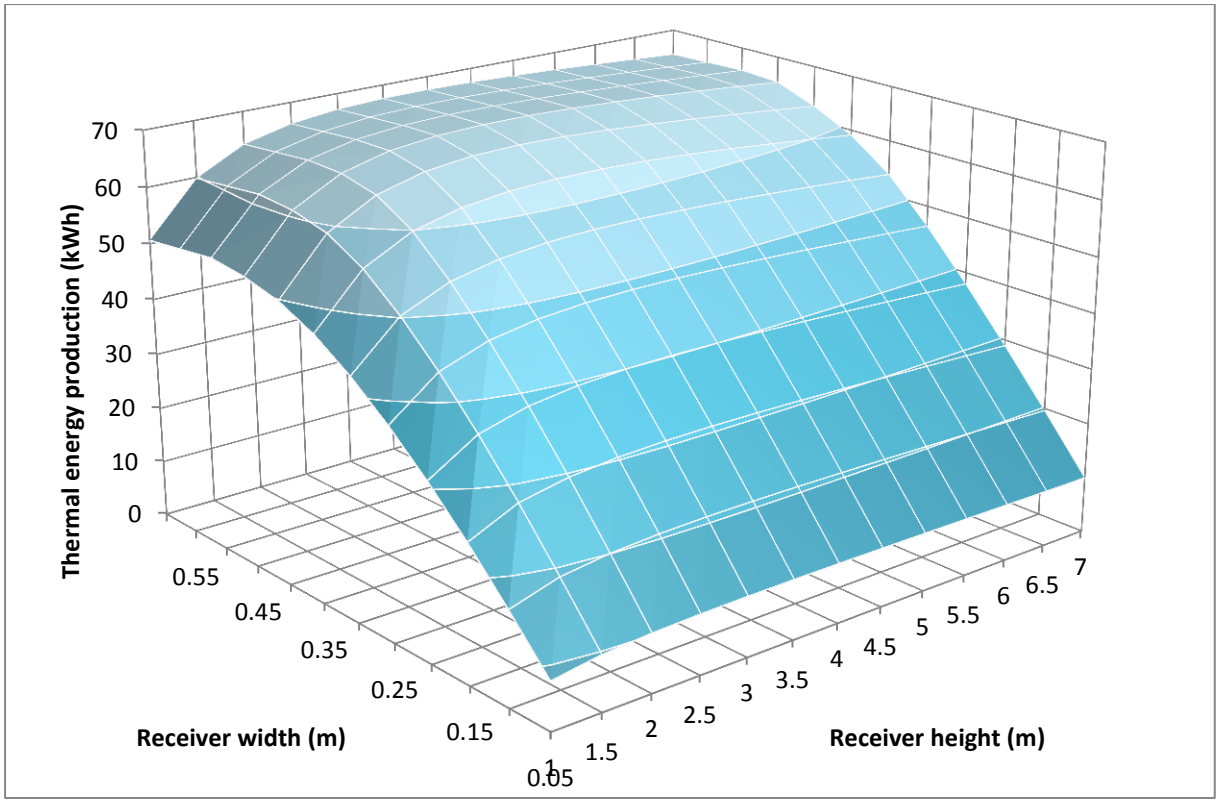


**Figure 26 Thermal energy production for 0.4 m mirror over design space**

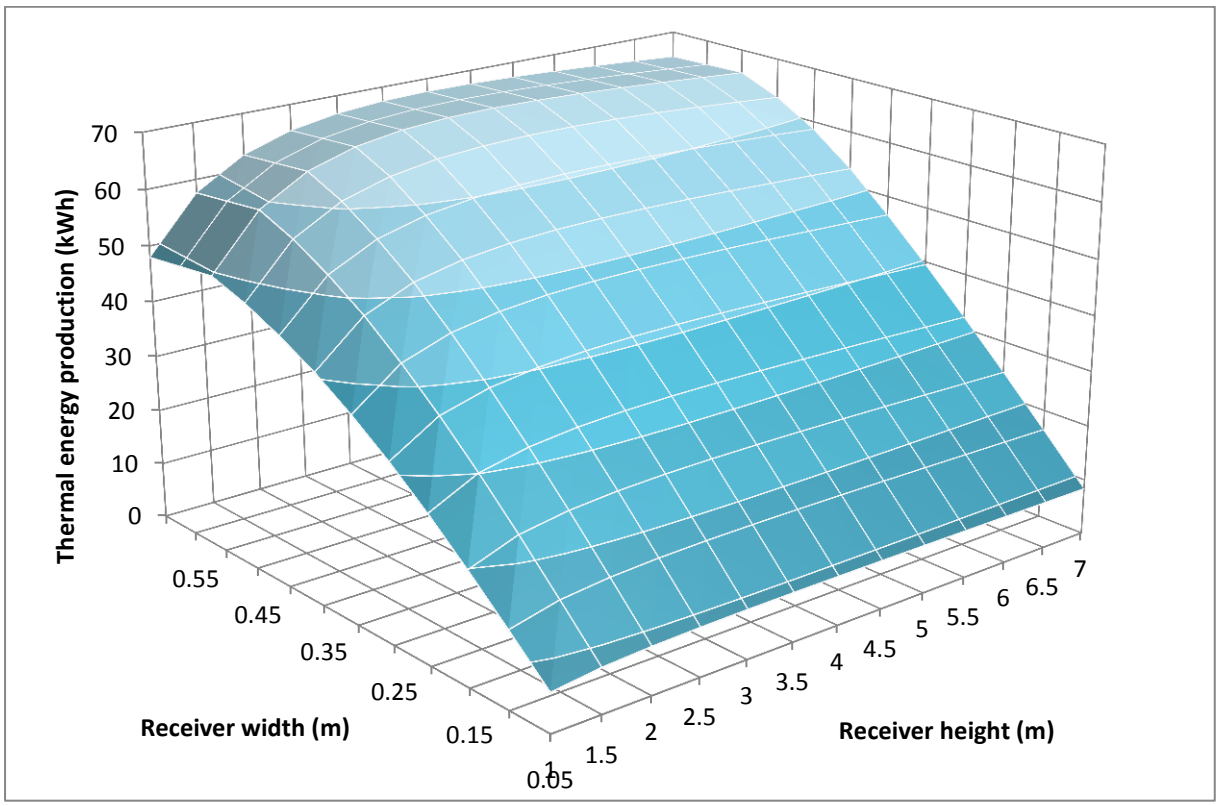


**Figure 27 Thermal energy production for 0.5 m mirror over design space**

The four figures above indicate areas of maximum performance for each mirror size. It is evident that for receiver heights above 1 m there is only a gradual effect on system performance as the height increases. For the 4 m footprint and utilising a 1 cm gap between mirrors the sensitivity analyses indicate the preferred dimensions shown in Table 6.

**Table 6 Ideal dimensions**

| | Mirror width (m) | | | |
|---|---|---|---|---|
| | 0.2 | 0.3 | 0.4 | 0.5 |
| Receiver height (m) | 2.5 | 3 | 3 | 4 |
| Receiver width (m) | 0.25 | 0.35 | 0.45 | 0.55 |

### 3.4.5. Mirror gap

The gap between adjacent mirrors will dictate how closely packed an array of mirrors is and therefore the amount of blocking that occurs. Increasing the mirror gap will reduce blocking but mirrors will spread out further and this will increase both the divergence of reflected beams and the footprint that the array occupies on the ground. Figure 28 below shows the expected increase in thermal energy as mirror gap increases.

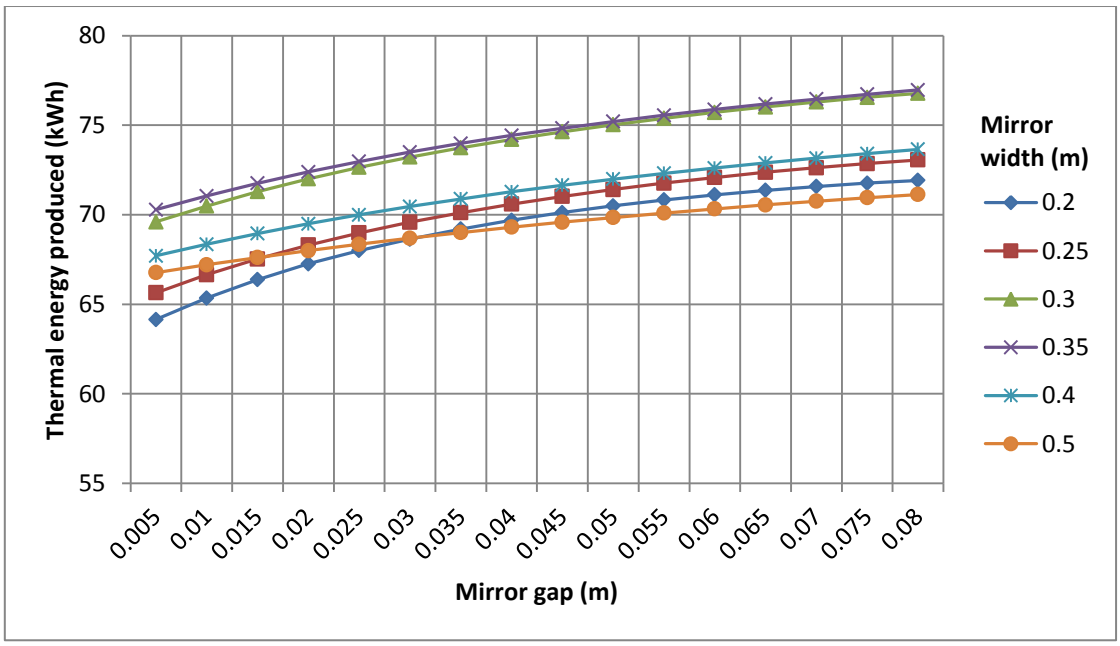


**Figure 28 Thermal energy trend for varying mirror gap**

While the increase in thermal energy by increasing mirror gap is noticeable, it does come at the expense of increasing the footprint. When the footprint is an important factor to consider such as on the solar roof, then a compromise must be made between the increase in thermal energy and the increase in footprint. Figure 29 shows the relative increase in thermal energy and footprint when the mirror gap was increased from 1 cm to 10 cm for each of the mirror widths previously investigated.

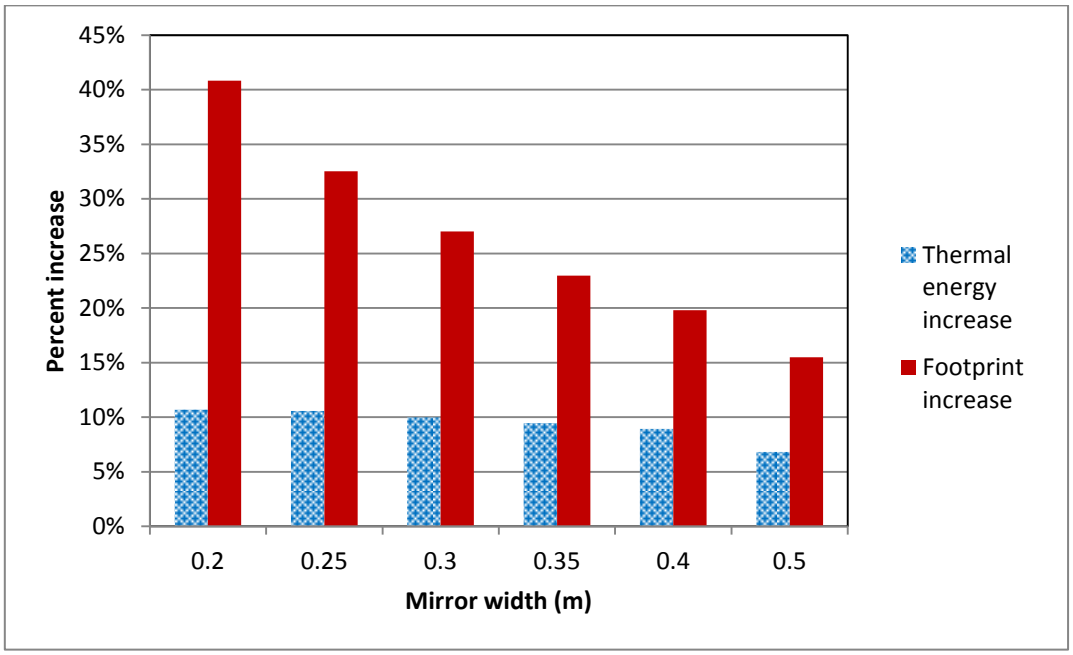


**Figure 29 Increase of thermal energy vs footprint increase**

It is clear that for the 0.2 m wide mirror the increase in footprint is four times the expected increase in thermal energy, therefore for smaller size mirrors the gap should not be too large. This ratio is much smaller for the larger mirrors and it may prove beneficial to do an optimisation of the cost of the increased footprint versus the increase in thermal energy.

## 3.5. OFFSET PIVOT CONCEPT

In an attempt to reduce the effects of shading, an alternative method of mounting the collector mirrors was investigated. This method aims to increase the aperture of the collector at high zenith angles by pivoting mirrors around an axis of rotation instead of merely rotating on an axis through the centre of the mirror. The principle is shown in Figure 30 below. Mirrors are offset to different directions on either side of the centre of the collector.

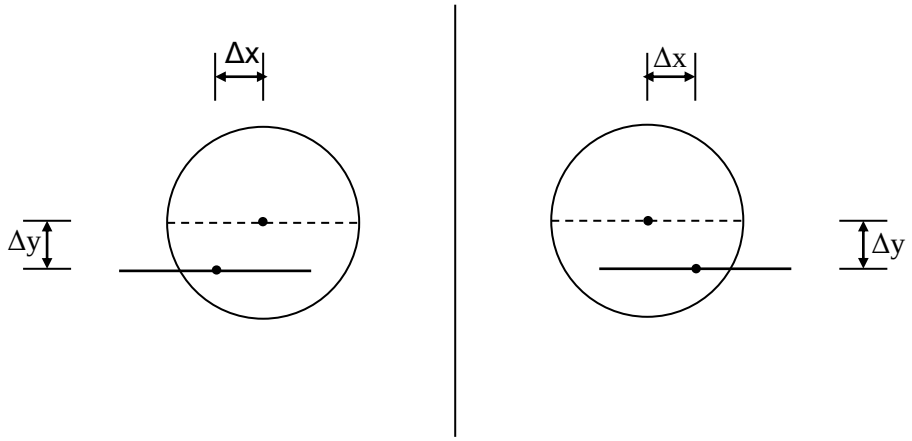


**Figure 30 Offset pivot basic concept**

At early morning, the east side of the collector drops below the horizontal plane while the west side rises up slightly. The reverse is true for late afternoon as shown in the figure below. This has the effect that the shading of adjacent mirrors is reduced when the sun is close to the horizon.

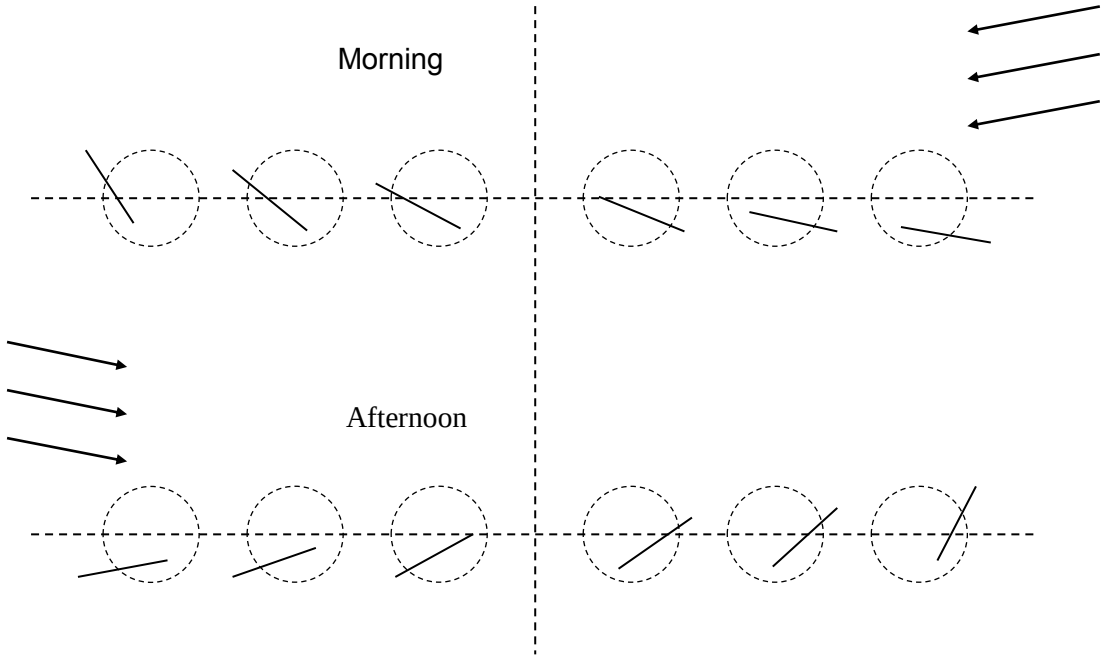


**Figure 31 Collector mirror positions at high zenith angles**

### 3.5.1. Modelling the concept

Calculating the tilt angle $\theta_n$ of Equation 6 for standard LFR is a basic exercise as only the sun-angle changes for a particular layout. For the offset pivot, the relative x and y offsets from the centre of the mirror to the fixed centre of rotation are constantly changing. They are indicated below by $X_n$ and $Y_n$. Only when a mirror is horizontal or vertical are the offset coordinates equal to the fixed Δx and Δy design values as shown in Figure 30. In all other instances, the x and y coordinates shown in Figure 32 below must be calculated.

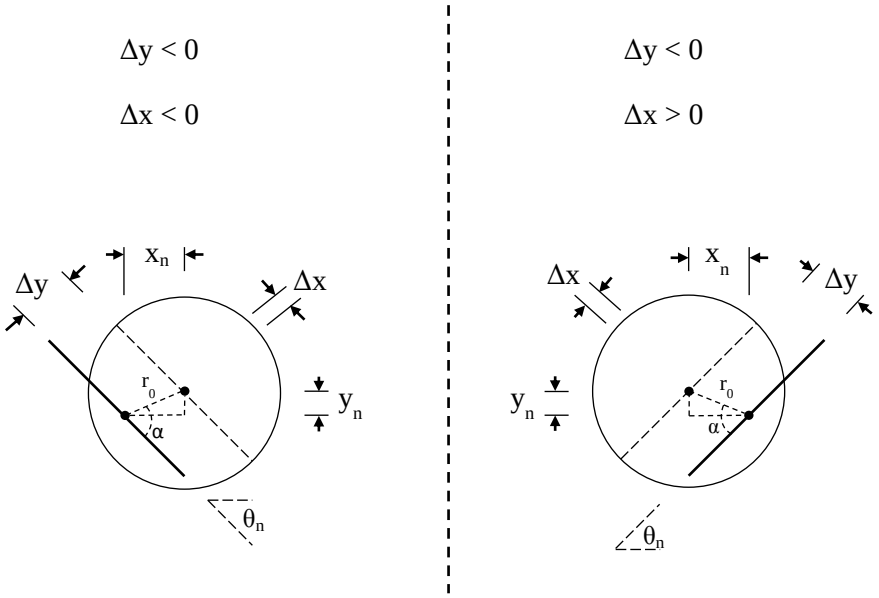


**Figure 32 Offset geometry**

The offset radius is simply:

$$r_0 = \sqrt{(\Delta x)^2 + (\Delta y)^2} \quad (13)$$

And the angle between $r_0$ and the mirror surface:

$$\alpha = tan^{-1}\left(\frac{\Delta y}{\Delta x}\right) \quad (14)$$

The offset coordinates x and y are then:

$$x_n = r_0 \times cos(\alpha - \theta_n) \quad (15)$$

$$y_n = r_0 \times sin(\alpha - \theta_n) \quad (16)$$

The altered geometry of the offset pivot results in:

$$tan(\varphi_n) = \frac{Q_n + x_n}{H + y_n} \quad (17)$$

Assuming specular reflection and rearranging equation, then substituting in $x_n$ and $y_n$:

$$tan(2\theta_n + \rho) = \frac{Q_n + r_0 \times cos(\alpha - \theta_n)}{H + r_0 \times \sin(\alpha - \theta_n)} \quad (18)$$

In the Equation 18 above $\theta_n$ is the only unknown, however, it must be solved either through an iterative process or using a solver function such as those available in MATLAB.

### 3.5.2. Evaluation of the concept

The offset pivoting concept does show noticeable increases in aperture over standard Fresnel. The maximum increase in aperture was found to be when the offsets in both the x and y direction were incremented when moving from the innermost mirrors to the outer mirrors. This results in the mirrors directly below the receiver being similar to standard Fresnel while the outer mirrors have the highest offset. Figure 33 shows the aperture gain for a 0.2 m wide mirror design of 16 mirrors. This specific case relates to the allowable footprint on the solar roof. The offsets Δx and Δy were incremented by 2 cm for each mirror in the direction of the edge of the array.

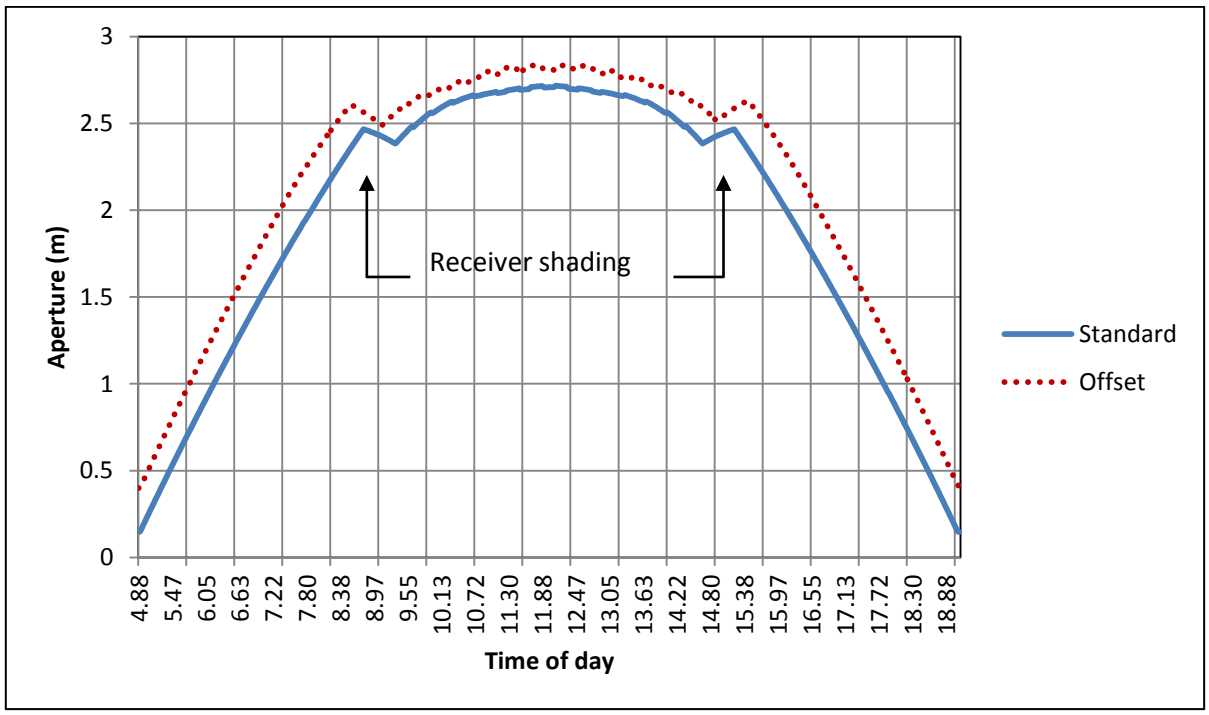


**Figure 33 Aperture gain for offset pivot**

The increase in aperture over standard Fresnel is noticeable over the entire day. At high zenith angles, this increase is usually in the order of 100 %. This doubling of aperture, however, is the doubling of an already small aperture and does not contribute dramatically to the thermal power production over the course of the day. This fact can be seen in Figure 34 where the power curves of the two cases are very close at early morning and late afternoon. The gap does widen though when the DNI starts to increase. The sharp dips in aperture evident at mid-morning and mid-afternoon are caused by receiver shading taking effect.

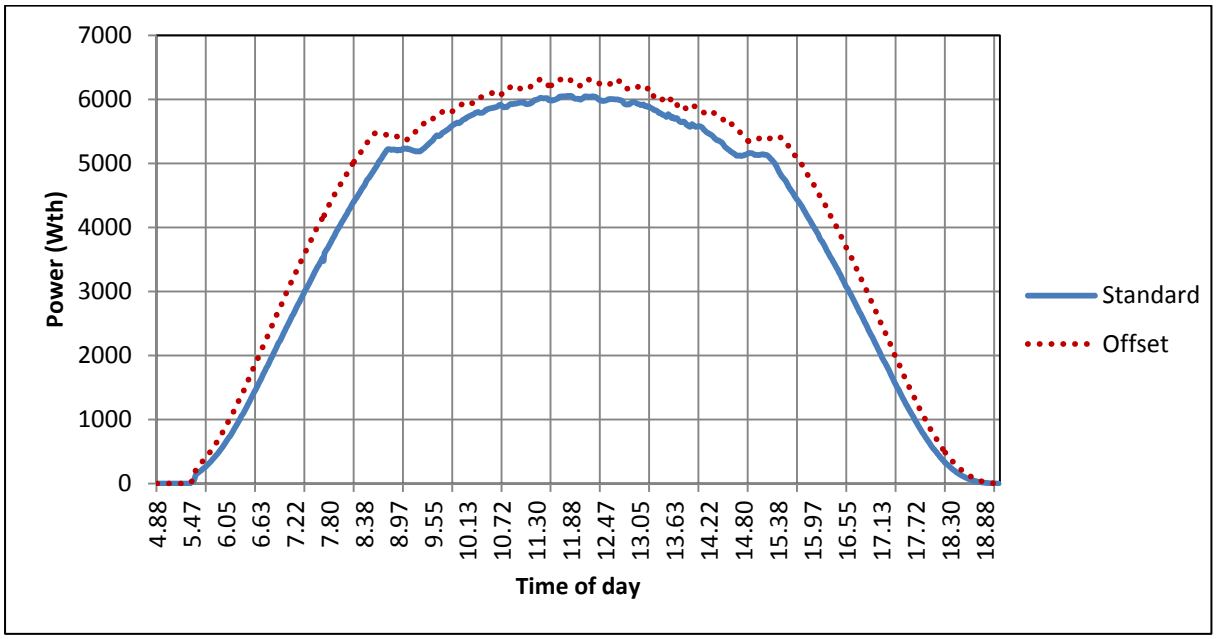


**Figure 34 Thermal power over average Stellenbosch summer day**

Whilst the offset pivot idea does show promise in increasing the efficiency of LFR systems, the design is more complicated and places greater requirements on mounting systems and drive motors. The above instance shows an 8.9 % increase in power in summer and a 9.5 % increase in power in winter. This corresponds with a 10.5 % increase in the footprint of the system. Therefore the trade-off between increased efficiency and increased land use will need to be evaluated for any particular design. The complexity of the offset pivot as well as the increased load on bearings and drive systems due to moments will drive up costs.

The proposed new pivoting concept would also increase the shading of adjacent arrays at sunrise and sunset. This may counteract the gain in aperture at these times. The offset pivot concept was not pursued further because it was found that almost the same increase in thermal power production could be achieved by choosing the correct spacing between mirror

rows. If the gap between adjacent mirrors' axis of rotation is incremented toward the edge of the array, then the blocking loss can be minimized.

## 3.6. SELECTION OF COLLECTOR DESIGN CHARACTERISTICS

The sensitivity analyses conducted indicate that the produced thermal energy for a number of different mirror sizes is basically the same for the specified allowable footprint if the array is closely packed with a 1 cm mirror gap. The preferred receiver heights and widths as indicated in Table 6 correspond to the ideal dimensions for a test rig on the solar roof. It was decided that the test rig should be flexible in order to test the offset pivot concept as well as different spacing's between mirrors. For example in order to test the concept, the number of mirrors for a 0.2 m wide mirror design must be reduced from 20 to 16 as this will allow the increase in spacing to be tested.

The 0.2 m wide mirror design was chosen for a number of reasons. Firstly, the smaller mirrors result in less blocking loss in the system. This is important when attempting to achieve the highest concentration ratio possible. The smaller mirrors also reduce the wind loading on the array and the receiver width is comparatively smaller too. A low receiver height is also ideal as it will cause less shading on other experiments on the roof and the 0.2 m wide mirror has the lowest requirement for a receiver height of all the mirrors tested. A single drive system was also proposed that would drive many mirrors off a single motor. The greater number of mirrors that is achievable for the allowable footprint by the 0.2 m wide mirror over bigger mirrors allows such a drive system to be tested. Table 7 below shows the chosen design for the solar roof test rig.

**Table 7 Chosen collector design**

| Dimension | Value |
|---|---|
| Width of mirrors | 0.2 m |
| Number of mirrors | 16 |
| Receiver height | 2 m |
| Receiver width | 0.3 m |
| Mirror gap | Flexible |
| Width of array | 4 m |
| Length of array | 3 m |

# CHAPTER 4. SECONDARY CONCENTRATOR OPTIMISATION

A number of different secondary concentrators and receivers have been investigated in literature (Abbas, R; Munoz, J; Martinez-Val, J M 2012). While some have focused on using Compound Parabolic Concentrator (CPC) type secondary concentrators, a number have investigated the much simpler trapezoidal type that uses flat reflective surfaces (Facão and Oliveira 2011) (Singh, Sarviya and Bhagoria 2010). The use of flat mirrors in the primary concentrator as well as the inherent divergence of reflected beams in LFR creates the need for some form of secondary concentrator. The entire aperture width of the receiver can be comprised of multiple tubes that will capture all incoming flux without the need for a secondary concentrator but this results in much lower concentration ratios. This may be ideal for situations in which large quantities of warm water are needed but in most applications a higher temperature is desired. Using fewer tubes also saves costs as boiler tube is expensive and so a number of different secondary concentrator designs have been developed.

## 4.1. SECONDARY CONCENTRATOR DESIGNS

The receiver design will depend largely on the collector design as well as the intended application of the LFR array. Parabolic surfaces for concentrators are ideal when the incoming flux is normal to the aperture plane of the receiver, i.e. when the Φ angle in Figure 16 is zero. In LFR concentrators this is almost the case for the mirrors directly below the receiver but the incoming rays from mirrors at the outer edges of the array are at an angle to the normal of the aperture plane. The maximum angle that rays make to the normal for a particular collector design, known as the acceptance angle, depends on the height of the receiver and the width of the collector.

CPC's have been developed that are more flexible than a single parabolic surface and allow wider acceptance angles. CPC surfaces allow a single tube to be used which lowers costs and raises steam temperatures. LFR arrays with a CPC design for the receiver do, however, require accurate tracking. Alternatively, the trapezoidal secondary concentrator with multiple tubes can be used. This is a simpler design that is much easier to manufacture but it will not produce very high temperatures unless the steam circuit is a multiple pass type.

The aim of the secondary concentrator optimisation exercise was to develop a tool that could evaluate different secondary concentrator surfaces by comparing the expected absorption of flux. Table 8 below shows the secondary concentrator surfaces that were evaluated.

**Table 8 Secondary concentrator surfaces**

| Graphic | Description |
|---|---|
| 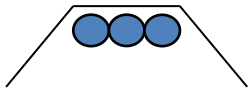 | Trapezoidal |
| 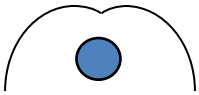 | CPC |
| 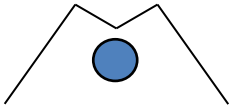 | M type |
| 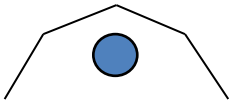 | Peak type |

## 4.2. RAY TRACE MODEL

The model was developed in MATLAB and allowed any particular secondary concentrator surface and tube arrangement to be analysed for a given collector design. The tool imports beam data from the collector simulation tool discussed in 3.3 above. The beam data contains information for each mirror regarding coordinates of the edges of the beams as they strike the receiver aperture plain as well as the incidence angle.

The beam is then split into rays 1mm apart and each ray is traced as it travels through the receiver. For each reflection in the secondary concentrator an efficiency loss is deducted according to what type of reflector material was used. When a ray strikes an absorber tube

the model records this as absorbed flux according to its incoming flux value minus any reflection losses. The percentage of absorbed flux to total incoming flux is then the function value used to rate the performance of the secondary concentrator. The rays are assumed to specularly reflect when striking a reflective surface as shown in Figure 35.

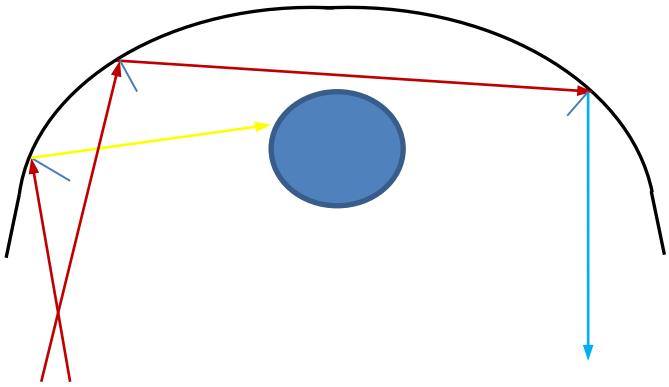

**Figure 35 Ray propagation through receiver**

In the ray trace graphics produced, the incoming and reflected beams are shown as red lines which change to yellow when the ray strikes a tube or to blue when the ray misses and travels out the receiver. Different secondary concentrator surfaces can be chosen such as those shown in Table 8. The simulation model inputs the surface functions between different domains. When a ray is traced and it does not strike the absorber tube directly, the model checks to see which reflected surface it hits. The surface normal at that point is then calculated and the ray is specularly reflected again as shown in Figure 35.

The figures below show examples of ray traces. Figure 36 is a ray trace for a single mirror at a particular time of day (noon in this example). The shown traced mirror is from the edge of the array and it is evident that a portion of the beam reflects back out the receiver and is lost. Figure 37 is an example for the same surface in which all sixteen mirrors are traced. The density of the ray trace makes it hard to visually discern the actual performance of the secondary concentrator.

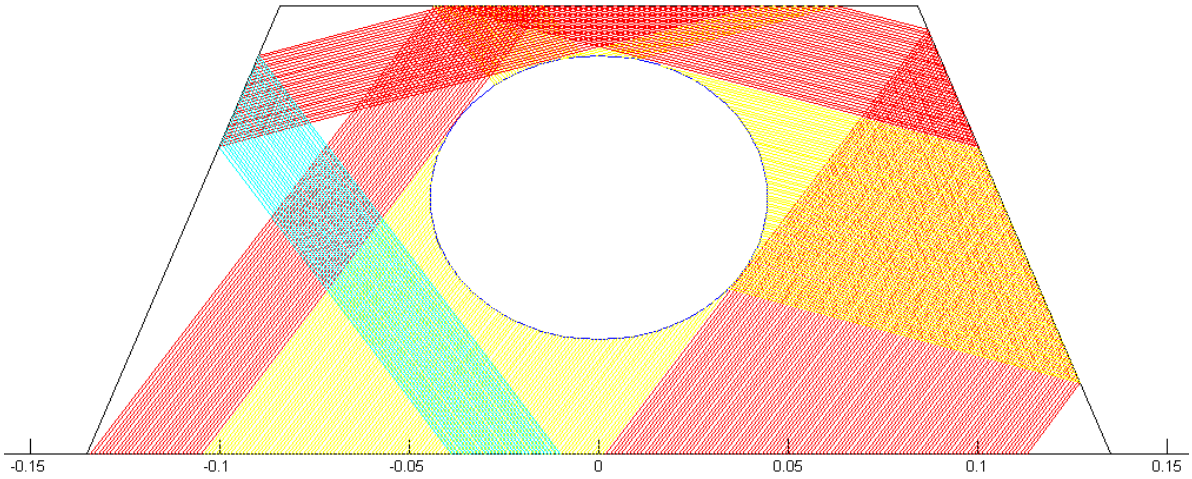


**Figure 36 Ray trace example - single mirror**

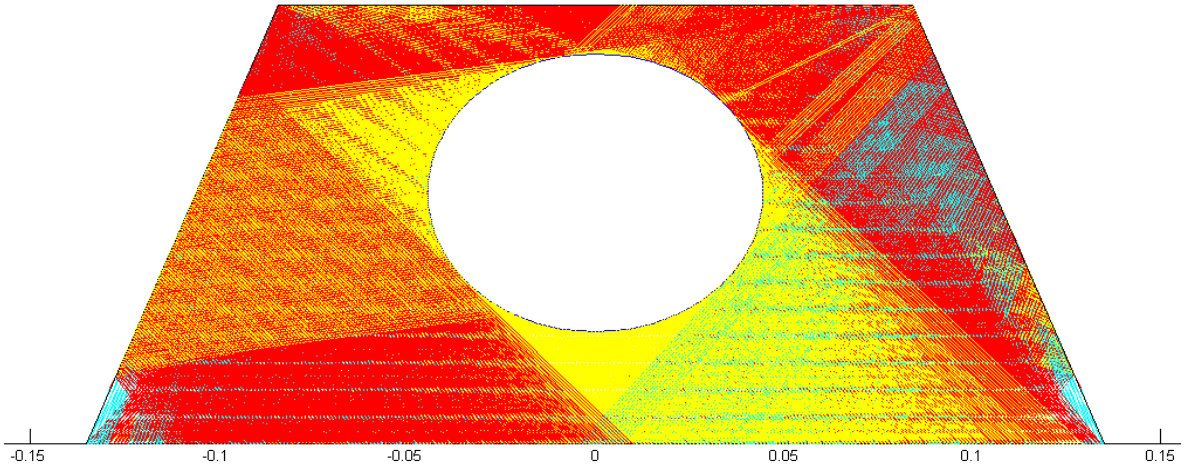


**Figure 37 Ray trace example - multiple mirrors**

Figure 38 below shows the logic flow for the ray trace model. The MATLAB code for the secondary concentrator model is listed in Appendix B.

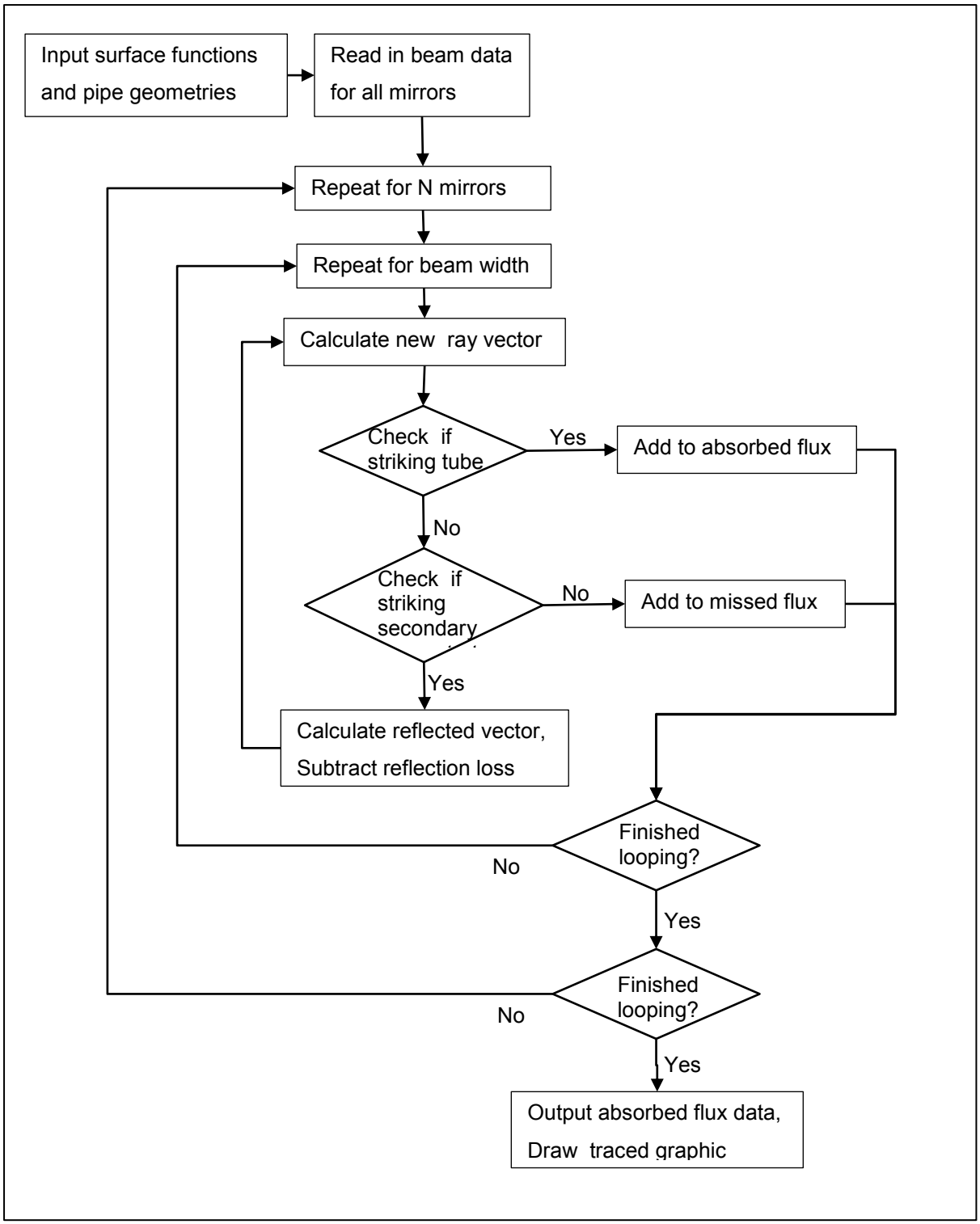


**Figure 38 Secondary concentrator model logic flow**

## 4.3. SECONDARY CONCENTRATOR SURFACE PERFORMANCES

The model was used to firstly evaluate designs of secondary concentrators currently operating around the world. The CPC is often stated to achieve the best concentration ratios or temperatures and this was examined. A research aim was to investigate other designs that could achieve concentrations close to the CPC values but with a much simpler reflection profile. Flat surface profiles for example would allow cheap flat mirrors to be used in a potential plant and thus reduce the cost of the secondary concentrator. Another aim was to use a single tube where possible as this would reduce complications with different flux levels on tubes and resulting problems such as mixing at headers and different thermal expansion on the tubes.

The different surface types were analysed by varying both the geometric parameters and the absorber pipe dimensions and position. The absorber pipe diameters that were investigated corresponded to standard steel tube piping sizes that are commonly available. The number of pipes was also varied to investigate the affect this would have on the absorbed flux distribution across the receiver aperture. The total absorbed flux is compared to the total circumference of all pipes. In this way, an average concentration ratio can be computed and used to rate the performance. The best results for each combination are listed in Table 9 below.

The receiver ray trace model sums up the flux of each ray as it hits the absorber tube. The flux values are reduced due to reflection losses for each ray. This is compared to the total flux of the incoming rays resulting in a percentage flux efficiency for the surface. The geometric performance of the system is also calculated by summing up the number of rays that hit the absorber compared to the total number. This percentage of reflective efficiency is always higher than the flux efficiency.

**Table 9 Secondary concentrator surface performances**

| Surface type | Pipe configuration and diameter | Flux efficiency (%) | Geometric efficiency (%) | Average concentration ratio |
|---|---|---|---|---|
| Compound parabolic | 1 pipe, 88.9 mm | 87.99 | 97.56 | 8.76 |

| | | | | |
|---|---|---|---|---|
| Compound parabolic | 2 pipes, 60.3 mm | 90.22 | 98.58 | 5.82 |
| Trapezoidal | 1 pipe, 88.9 mm | 81.76 | 88.66 | 7.15 |
| Trapezoidal | 2 pipes, 60.3 mm | 81.74 | 89.14 | 5.27 |
| Trapezoidal | 3 pipes, 50.8 mm | 90.49 | 95.89 | 4.08 |
| M type | 1 pipe, 88.9 mm | 82.35 | 90.08 | 7.20 |
| M type | 2 pipes, 60.3 mm | 84.77 | 92.35 | 5.47 |
| Peak | 1 pipe, 88.9 mm | 73.87 | 82.09 | 6.46 |
| Peak | 2 pipes, 60.3 mm | 78.73 | 82.31 | 5.08 |
| **Extended peak** | **1 pipe, 88.9 mm** | **84.39** | **92.40** | **7.38** |
| Extended peak | 2 pipes, 60.3 mm | 87.42 | 94.39 | 5.64 |

As expected from the literature, the CPC performed the best out of the secondary concentrator surfaces. The CPC with two pipes obtained almost perfect reflection of rays to the absorber. 98 % was achieved for the geometric efficiency. This translated to just over 90 % for the flux efficiency due to losses when rays reflected off the secondary concentrator surfaces. The average concentration ratio achieved was almost 9 which means higher temperatures will be obtainable than for the other surfaces.

While the CPC does exhibit the best performance, it is also the hardest secondary concentrator surface to manufacture due to the accuracy needed to achieve the correct parabolic surface. In order to reduce costs, surfaces with flat profiles were investigated and compared to the CPC benchmark. The trapezoidal profile, which exists in currently operating Fresnel plants, performed very well in terms of collected flux when multiple tubes are used. This however means that the flux is spread across a wider area and concentration is not as high. There is also the added complication of using multiple tubes and the problems with different flux levels across them over the course of the day.

The M type surface performed better than the peak type but there were advantageous aspects of both that became evident in the sensitivity analysis. The peak surface was beneficial for the rays coming from mirrors directly below the receiver and the M type was appropriate for the rays coming from mirrors at the edge of the array. These characteristics were combined in a concept called the extended peak. In this surface, an additional angular plane was added to each side so that there were three angles to optimize for reflection. This allowed the shape of the secondary concentrator to approximate a compound parabolic

shape with flat mirror segments. The two examples listed at the end of Table 9 show that for both the single and double tube arrangement the performance is significantly improved.

## 4.4. OPTIMUM SURFACE SELECTION

The extended peak type mentioned above was chosen as the most appropriate secondary concentrator surface. Firstly, because it attains approximately 84 % flux efficiency with a single tube and a relatively high average concentration ratio around 7.4. This means higher temperatures will be achievable than if the trapezoidal or M type surfaces were used. The single tube greatly simplifies flow conditions. Secondly, the surface uses flat mirror segments to approximate a CPC shape and is therefore much cheaper to manufacture. The particular extended peak type surface that achieved the above mentioned performance is shown in Figure 39 below.

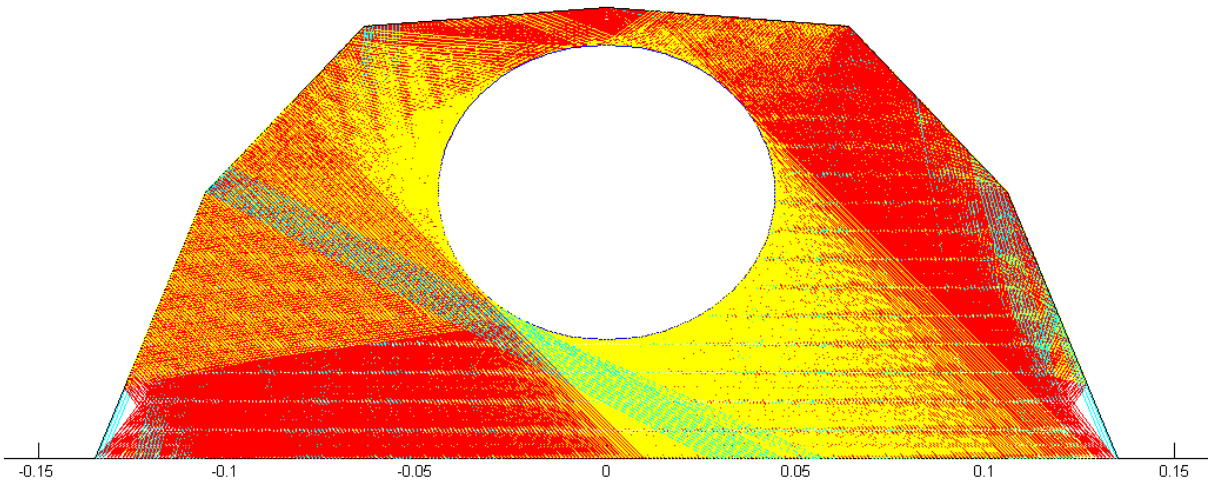


**Figure 39 Final secondary concentrator ray trace**

This surface has an inclination of 70 degrees to the horizontal for the first plane, then 50 degrees and finally 5 degrees. The 70 degree inclination corresponds to the acceptance angle of the receiver plus an additional 15 degrees. This means that rays from any of the mirrors will be reflected deeper into the receiver.

# CHAPTER 5. EXPERIMENT DESIGN AND CONSTRUCTION

## 5.1. SUPPORT STRUCTURE

The support structure for a LFR array generally comprises the concrete support bases and the steel frame on which the mirror bearing mounts are secured. The mirrors are usually installed in segments of a few metres long between bearings as it becomes difficult to support the mirrors over longer lengths due to the requirements for far more rigid and therefore heavier structures that prevent sagging. It was decided to use steel tubing as the main support base of the mirrors as it is readily available in lengths up to 6 metres and in many different profiles. Following some testing, the 6 metre lengths were found to sag too much when supported only at either end. This was halved to 3 metres and found to be sufficiently rigid.

The array was therefore designed to be constructed in modules 3 metres in length and 4 metres width. The support structure was constructed from trusses made from welded steel square tubing that was then galvanized. The trusses bolt together to allow easy transportation and erection on the solar roof. Additional trusses can easily be added at a later stage to increase the size of the array. The trusses were first designed in Inventor 2012 and then manufactured by the workshop of Stellenbosch University. The phases are shown in the figures below. The support structure sits on adjustable feet and not fixed steel supports set in concrete foundations as in commercial plants. The height of each foot is adjusted to make the support structure level on the uneven surface of the solar roof.

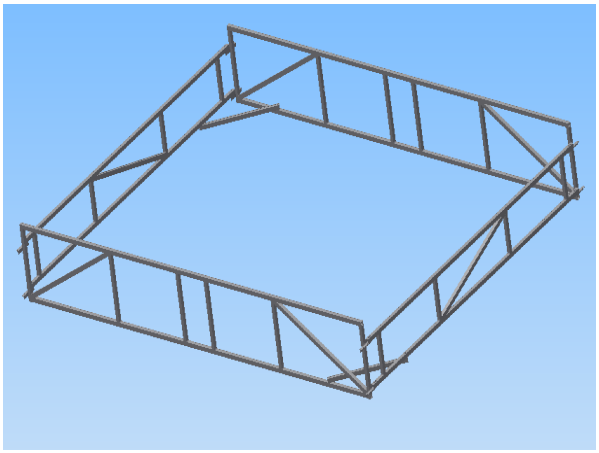

**Figure 40 Inventor model of structure**

**Figure 41 Assembled structure on solar roof**

## 5.2. MOUNTING SYSTEM

The mirrors in existing plants are usually supported by a frame made of either aluminium or steel structural members. Ausra makes use of corrugated steel backing on the mirrors which is then secured to a truss system below the mirrors. This is a very rigid design but makes use of much material. In contrast, systems such as the Novatec plants make use of pressed steel segments that are assembled into the support structure. Both systems would be expensive for a small scale experiment and are also designed for permanent installation of over 20 years.

Because of the experimental nature of the system on the solar roof, flexibility must be built in to test various aspects of LFR technology. The sensitivity analyses of section 3.4 showed that the performance is affected by various factors such as mirror width and mirror spacing. Therefore an experimental setup should be able to investigate these characteristics if desired. A mounting system was designed that would allow spacing between mirrors to be adjusted as well as the size or number of mirrors. Figure 42 below shows the design in Inventor.

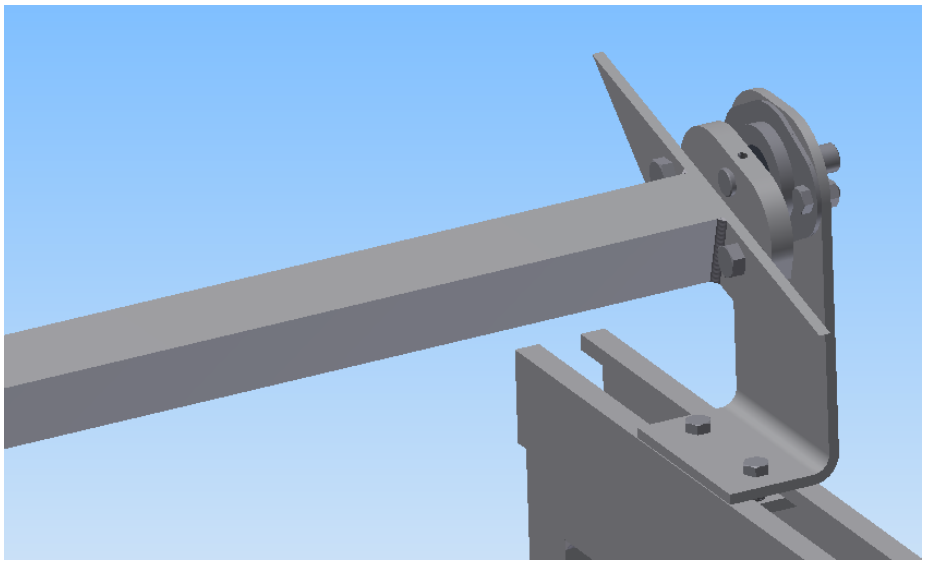

**Figure 42 Mirror mounting system**

The bearing unit is mounted on a rail with bolts and this allows the unit to be moved to a particular location and secured. The mirror support beam is also removable without the need to de-couple the drive system or adjacent mirrors. This design would, however, not be appropriate for a commercial plant as it requires much calibration on site.

### 5.2.1. Mirror support structure

The means of securing or mounting the mirror on the support structure is an important consideration. The support structure must not significantly add to the weight but it must also protect the mirror from the elements. The method of bonding the mirror to the support structure is also important as the mirror surface must not be compromised. A number of materials were investigated for their potential of being lightweight and able to withstand exposure to the elements. It became apparent that the thermal expansion was also an important aspect. Table 10 lists a number of materials and their thermal expansion over a 3 m length at a temperature rise of 50 degrees above ambient.

**Table 10 Comparison of material properties**

| Material | Density ($kg/m^3$) | Coefficient of thermal expansion | Expansion over 3 m at $\Delta T$ of 50 °C |
|---|---|---|---|
| Glass | 2400-2800 | $8.5 \times 10^{-6}$ | 1.28 mm |
| Steel | 7470-8030 | $13 \times 10^{-6}$ | 1.95 mm |
| Aluminium | 2500-2700 | $22 \times 10^{-6}$ | 3.3 mm |
| Acrylic | 1180-1200 | $70 \times 10^{-6}$ | 10.5 mm |
| PET | 1300-1400 | $50 \times 10^{-6}$ | 7.5 mm |
| GFRP | 1700-1900 | $7.4 \times 10^{-6}$ | 1.1 mm |

While acrylic and PET materials are the lightest, their thermal expansion is too great when paired with the thermal expansion expected from glass mirrors. This would result in stress in the bonding material between the surfaces. Steel does have an appropriate coefficient of thermal expansion although it might be too heavy as a backing material. Aluminium and Glass Fibre Reinforced Plastic (GFRP) have the ideal combination of low density and low coefficient of thermal expansion. GFRP was chosen as the backing material due to it being much cheaper than aluminium.

The glass mirrors were initially bonded to the fibre glass with Alcolin “Fix All” glue. This glue is stated to have no effect on the reflective silver backing of mirrors. However, after six months of exposure to the elements it was found that the glue became brittle and started to detach from the mirror. A replacement glue, Pattex PL700 Total Fix, was then found that had a higher silicon content and was therefore more flexible and resistant to water.

The mirror and backing was attached to the support beams by means of countersunk machine screws in the backing and bent steel brackets that fitted around the square tubing. This allows the mirrors to be removed as needed.

## 5.3. TRACKING SYSTEM DESIGN

### 5.3.1. Tracking concepts

The tracking system for a LFR plant needs to be accurate while maintaining the lower cost aspect that makes LFR attractive over other CSP technologies. The tracking accuracy is not as stringent as for power towers or parabolic troughs but some form of accurate tracking is required to optimise power production. The drive systems for LFR plants will typically comprise some gear reduction system and these systems must require as little recalibrating as possible during the life of the plant.

The first Ausra plants move on a system of large diameter rings that are supported below on rollers. The drive system is a motor connected to the periphery of these rings by either a friction drive or chain and sprocket. The relatively large diameter of the ring provides the reduction ratio. The rings do, however, shade mirrors slightly and may not be aesthetically desirable.

Another method for the tracking drive that has been employed is a direct connection to the rotation shaft of the mirrors. There are a number of planetary gearboxes that allow the motor, gearbox and driven shaft to all be on the same axis of rotation. While the direct drive configuration is less noticeable during operation than the ring system, it prevents an adjacent mirror row from being connected at the drive point.

Both of the drive systems discussed above necessitate the use of a motor for each mirror row. While this allows control of each mirror row individually and hence smarter tracking algorithms, this may be undesirable for small scale applications in which the multiple mirror rows would mean a large number of motors. To reduce the number of motors and tracking electronics needed, a common drive train for all mirrors is possible which may significantly reduce costs. Such drive trains may not be feasible for large plants, however they do have application for use in pilot plants and industrial heating applications. The Solarmundo prototype used a worm gear set. A common shaft drives multiple mirrors through worm wheels on each mirror shaft.

A second form of the common drive system is a Novatec design that uses a linear actuator to drive an arm on which cranks are connected. These cranks then turn a number of mirrors off a single linear arm. Table 11 shows examples of each drive system.

**Table 11 Drive systems**

| Description | Example |
|---|---|
| Ring/friction drive<br><br>Source: Ausra, accessed:14/11/2011 http://www.ausra.com/news/photographs.html |  |
| Direct drive<br><br>Source: BBE, accessed:12/09/2011 http://www.bbe.co.za/index.php?option=com_phocagallery&view=categories&Itemid=5 |  |
| Geared drive<br><br>Source: Solarmundo, (Häberle, et al. 2002) |  |
| Linear/lever arm drive<br><br>Source: Novatec, presentation 2012. |  |

The above systems each have their advantages and disadvantages when looked at in the context of a pilot plant. The direct drive and ring drive allow smart tracking algorithms but require a number of motors and drive controls. Similarly, the geared drive requires a number of worm gearboxes which can be expensive to machine or purchase. The linear drive is relatively cheap but is not that flexible when changing aspects such as mirror gap. It was decided to use a combination of the concepts. A sprocket and chain system was designed that uses a sprocket on the shaft of each mirror row with a common drive chain running over all sprockets. A single sprocket is then driven by the motor and gearbox to actuate all 16 mirrors. In order to change mirror gaps or number of mirrors, the grub screw of the particular sprocket is loosened and the mirror mounts can be moved before tightening the grub screw again. The installed drive system is shown in Figure 43 below.

**Figure 43 Common drive system**

The reason a single drive system can be used is because the relative change in sun position for a given time period is the same for each mirror. The starting angle for each mirror is different though and this can be set prior to the tracker operating. In order to ensure accurate tracking with this system, the tension in the chain must be enough to ensure a change in motor position is translated to the same change in position for all the mirrors. Any backlash or slack will reduce tracking accuracy.

### 5.3.2. Tracking system

A calculation of the actual torque required to actuate the 16 mirrors together was performed and resulted in a required torque of 40 Nm at the driven sprocket. This calculation is shown in Appendix C. This relatively high torque must be balanced by a motor's ability to move with a high precision for the mirror tracking. There is a variety of different motor types, each with their own advantages and disadvantages. DC motors are cheap and good at providing acceptable levels of torque but it is more complicated to accurately control the shaft's rotational position as they normally rotate at high RPM's. Servo motors can be accurately positioned but they cannot continuously rotate through full revolutions and require detailed control electronics. Stepper motors are good at accurately stepping through specific angles but typically do not provide enough torque.

It was decided that a stepper motor would satisfy the tracking requirements of the collector the best. A large stepper motor would be required which is more expensive than a DC equivalent but the built in stepping function is ideal. The control board for the large stepper would need to provide the higher currents drawn which also increased cost.

It was found that the average change in angular position of each mirror every second comes to approximately 0.2 degrees for summer and 0.3 degrees for winter due to different day lengths. Standard stepper motors available can provide either 200 steps a revolution or 400 steps a revolution using micro-stepping. Micro stepping may provide higher resolution although this requires the motor to constantly be drawing current which is not desirable when using high torque and therefore high current motors. 200 steps a revolution, or 1.8 degrees a step, is too low a resolution and therefore it was decided to use a worm gear set to further reduce the ratio. The chosen 50:1 worm gear set provides 0.036 degrees a step which allows the collector to accurately track the sun every second if desired. The 50:1 worm gear set allows a higher driven torque to be achievable from a given motor. The worm gear also prevents the driven load from turning back the motor when power is removed. It is therefore a built in brake for the drive train.

The driver board for a stepper motor requires a low step pulse to step the motor a single step. This pulse can be provided by any standard micro-controller. Most modern controllers can perform basic functions such as trigonometric calculations which are required for calculating the sun angles for tracking. A simple yet relatively powerful micro-controller is the Arduino open source controller. It is a widely used controller that is cheap and uses basic C programming.

One of the requirements for the LFR system is to have the functionality that the experiment can be switched off for any period of time. The system must be able to be switched on and immediately be able to start tracking. This necessitates that the microcontroller has an external time source that is not reliant on battery power to maintain the time. Accurate time can be provided by basic GPS chips with a one second resolution. These chips constantly transmit strings of characters serially that correspond to standard National Marine Electronics Association (NMEA) strings. There are a number of choices of standard strings with different information and the most appropriate for a solar tracker is the “ZDA” string. The format is as follows:

*$GPZDA,hhmmss.ss,day,month,year,ltzh,ltzn*cs<CR><LF>*

The Arduino board can read this character string in through its serial port and extract the time and date information. The controller then calculates the azimuth and zenith angle at that particular moment. This is then compared to the current position of the motor. If there is a difference greater than the step size, the motor is stepped until it reaches the required tilt angle. This comparison happens every second but the motor may only need to step once a minute. The GPS can also be used to determine the exact location of the array but this only needs to be done once and the coordinates are then programmed into the tracking algorithm.

### 5.3.3. Tracking algorithm

The tracking algorithm is programmed in C using the Arduino’s standard development environment. The tracker is designed to be in a stow position at night and during rainy periods by facing the mirrors downwards. This position corresponds to “home” for the tracker. The driven shaft of the tracking system has a mechanical limit switch that is enabled when the tracker is at “home”. At start-up the tracker steps the mirrors until the limit switch is engaged. In this way the tracker resets itself every time it is switched on. Then the process begins of comparison with the calculated sun angles from the GPS. The tracker will only move the mirrors to face upwards once the zenith angle is below 90 degrees, in other words the sun has risen. It also turns the mirrors to stow position once the zenith angle goes above 90 degrees again at sunset. Figure 44 shows the logic flow of the tracking algorithm.

A number of algorithms have been proposed to calculate the sun angles and normally use some form of mathematical approximation to calculate the Equation of Time (EOT). (Lamm 1981) (Stine and Harrigan 1986) (Michalsky 1988). The algorithms vary in complexity and accuracy depending on the application. Lamm's EOT equation is very simple to implement but loses accuracy due to calculating the EOT only down to the day of the year. Michalsky's EOT equation calculates the EOT down to the specific hour of the day. Michalsky's overall formula for azimuth and zenith angles is stated to be one of the most accurate. It does, however, have the limitation that it is meant only for use in the northern hemisphere. In order to improve its performance and also add applicability to the southern hemisphere, a team at the PSA present a modified version of the Michalsky formula (Blanco-Muriel, *et al*. 2001).

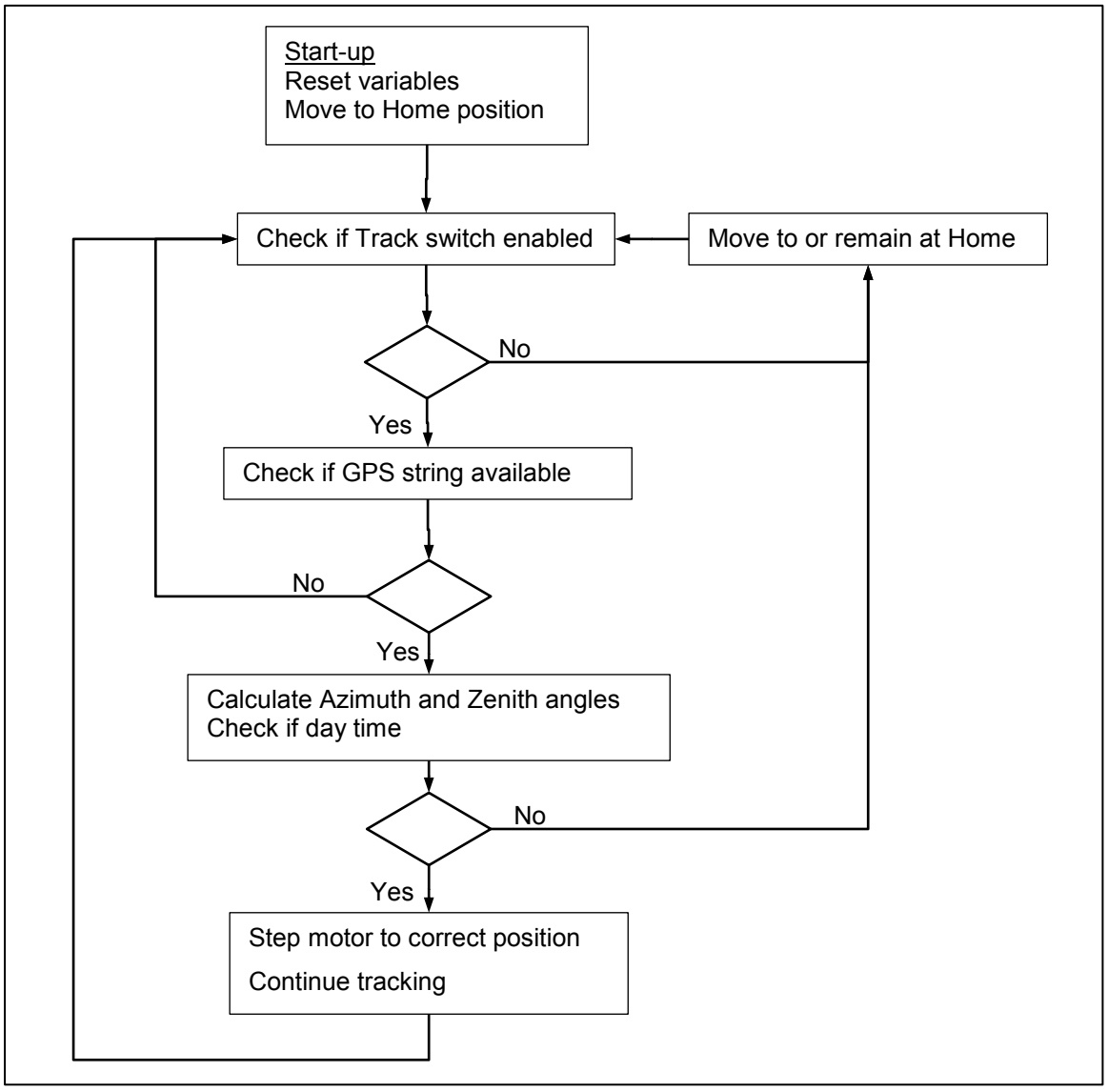


**Figure 44 Tracking algorithm**

The track switch mentioned in the diagram above is a toggle switch that is installed on the side of the tracker. Its purpose is to reset the tracker and turn the mirrors to the stow position. This for instances in which rapid defocusing of the concentrator is required or when heavy rain or hail is falling. The code for the tracker is listed in Appendix D.

## 5.4. RECEIVER DESIGN

The receiver width of 0.3 m was found in section 3.6 to be ideal for the size of collector designed. The secondary concentrator surface described in section 4.4 was designed to fit in this receiver width. In order to support the secondary concentrator and absorber pipe a frame was fabricated from galvanized steel tubes similar to the support structure. A stainless steel shell was fixed to this to act as the sides and top of the receiver. 6 mm glass slide rails were then fastened to the bottom of the receiver sides to locate the glazing below the receiver and also to support the secondary concentrator. The aim of the glazing is to seal the bottom of the receiver and reduce convective losses.

The receiver was built to include a 2 m overhang on the southern side of the collector. This is so that the receiver can collect the reflected radiation in winter which tends to have a large cosine loss associated with it. The absorber pipe used was a 88.9 mm diameter mild steel tube that was coated with a high heat resistant black paint. The pipe is supported at either end of the receiver by thick steel plates that also act as plugs for the end of the receiver. The weight and height of the receiver above the ground caused the need for steel cables that prevent the receiver swaying in high winds. Figure 45 below shows the receiver.

**Figure 45 Installed receiver**

The secondary concentrator was constructed out of a welded metal support structure and sections of flat mirrors. In order to obtain the correct reflective angles as optimised in section 4.4, struts were laser cut out of mild steel to the correct profiles. The laser cutting was an accurate method of machining profiles in a repetitive manner. These profiles were welded to steel frames acting as the structural members. The mirrors were then fixed to the strut profiles with glue. Because of lessons learnt when mounting the primary collector mirrors, it was decided to include a secondary backup fixture in the event of the glue melting. This was performed using thin wire wrapped around the mirror and metal struts. The secondary concentrator design done in Inventor is shown in Figure 46.

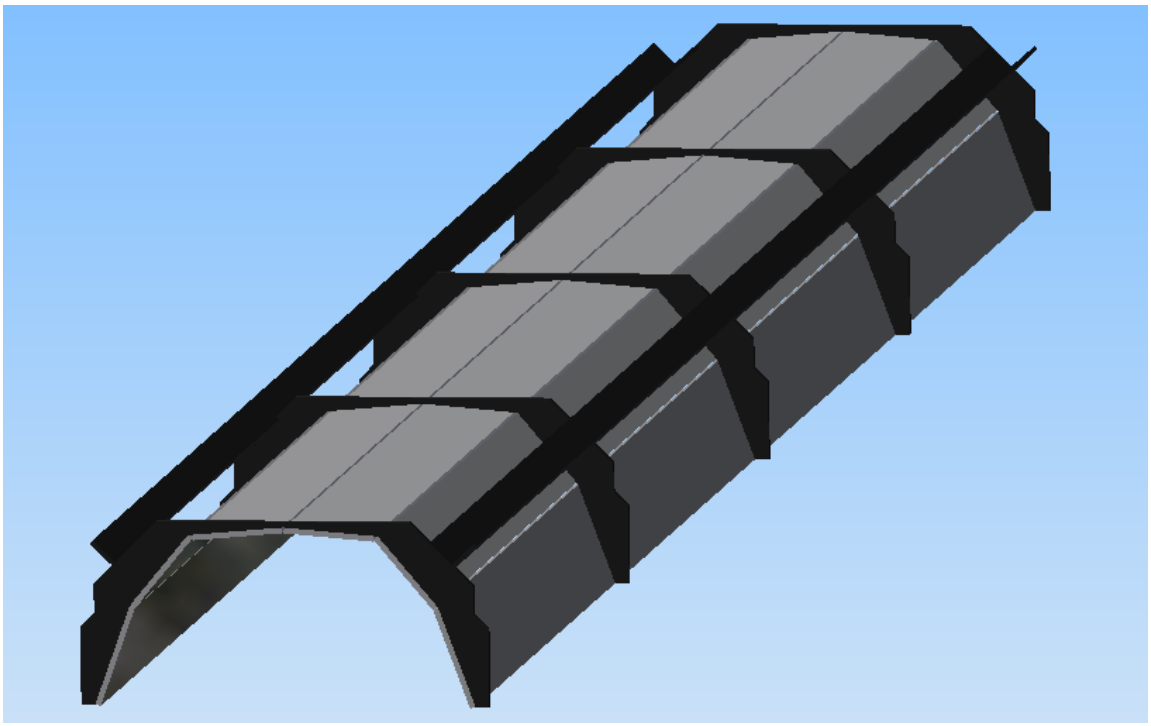

**Figure 46 Secondary concentrator assembly**

This assembly was designed to slide into the receiver from either side over the absorber tube. This allows the secondary concentrator surface to be changed in future and easily reassembled. In Figure 46 above, the black material is the welded steel strut system which is coated in a black high heat resistant paint. The grey surfaces are the backs of the mirrors which face inwards towards the absorber tube.

## 5.5. FINAL INSTALLED EXPERIMENT

The completed experimental rig is shown in Figure 47 below. The piping connected to the absorber tube is first routed to above the receiver and then through a 180 degree bend on both the entrance and exit. The reason for this is that when the pump is pumping water through the circuit it is always to a level above the absorber tube. This means that the absorber tube is always completely full with no pockets of air so that the heat transfer is at a maximum.

**Figure 47 Completed LFR experiment**

After the assembly was completed, a number of adjustments were required to improve the accuracy of the concentrator. The North-South lines painted on the solar roof were not accurate enough for a line concentrator and resulted in skewed reflections. Manufacturing tolerances also caused misalignment of the mirrors on their tracking axes as well as their horizontal levels. The flexible design of the experiment allowed relatively simple adjustment of the orientation and rotation of mirrors. Following these calibrations, the concentrator was ready for testing.

# CHAPTER 6. TESTING AND RESULTS

## 6.1. TEST PROCEDURE

The main objective of the test process was to investigate the rate of heat input into the circulated water. This level of thermal power would then be compared to the predicted thermal power from the model. In order to simplify the test process it was decided to keep the circulated water in the liquid phase so that two phase flow and measurement did not become a problem. To accomplish this, a high flow rate was set so that the temperature rise was not excessive. The required flow rate was calculated from the basic equation:

$$\dot{q} = \dot{m} \times C_p \times \Delta T \qquad (19)$$

To keep the temperature rise below 60 degrees above ambient, a flow rate of 1.17 l/min is required (mass flow of 0.02 kg/s). At the same time, in order to save water, it was decided to recirculate the water by having a 500 l tank as a reservoir. This means that the water in the tank will be recirculated at-least once a day. A variable speed pump was chosen that had a flow rate much higher than the minimum stated above. This built in a safety factor so that there was not a large temperature gradient between inlet and outlet. The flow rate settings of the variable speed pump corresponded to a mass flow rate of 0.1455 kg/s and 0.35 kg/s. The volume of water in the tank was such that even on the hottest day the average recirculated water temperature never exceeded 60 °C.

While the inlet temperature did rise over the course of the day, it was the difference between inlet and outlet that was important. To measure this difference, two thermocouples were installed at both inlet and outlet. A data acquisition system then logged the temperatures over the day. It was found that due to the large diameter of the absorber tube and the volume of water in the tube, at low flow rates the flow in the absorber tube exhibited laminar flow behaviour. This was evident in the different temperature readings at the outlet. One of the thermocouples was installed to take readings from the centre of the flow stream and the second thermocouple was approximately 2 cm higher.

The Reynolds number for each of the flow rates was calculated using the equation below:

$$Re = \frac{4\dot{m}}{\mu\pi D} \qquad (20)$$

The dynamic viscosity for water at 40 °C was used and the Reynolds number for the flow rates was calculated to be 3191 and 7677 respectively. This indicates that at the lower flow rate the flow regime was transitional flow which is inadequate for proper mixing. If turbulent flow was present, there would be enough mixing that the two outlet temperature readings would be similar. This was not the case and meant that the water closest to the bottom of the tube was heating up but not transferring this energy further into the tube quick enough. This is undesirable because a high level of mixing would mean higher heat transfer characteristics.

The higher mass flow rate of 0.3 kg/s was chosen because it clearly resulted in turbulent flow (Reynolds number greater than 4000) but it was also not too high and therefore the temperature difference between outlet and inlet would be noticeable. The mass flow rate was measured using a timed mass method. A bucket was held under the outlet for a given period and then the bucket was weighed.

## 6.2. THERMAL POWER PRODUCTION

The experiment was run over a number of test days to firstly calibrate the mirrors and tracking system and then to perform full day tests from sunrise to sunset. The resulting thermal power trend for a specific day (19/11/2012) is shown in Figure 48 below. This is plotted on the primary vertical axis while the DNI for that particular day is plotted on the secondary axis.

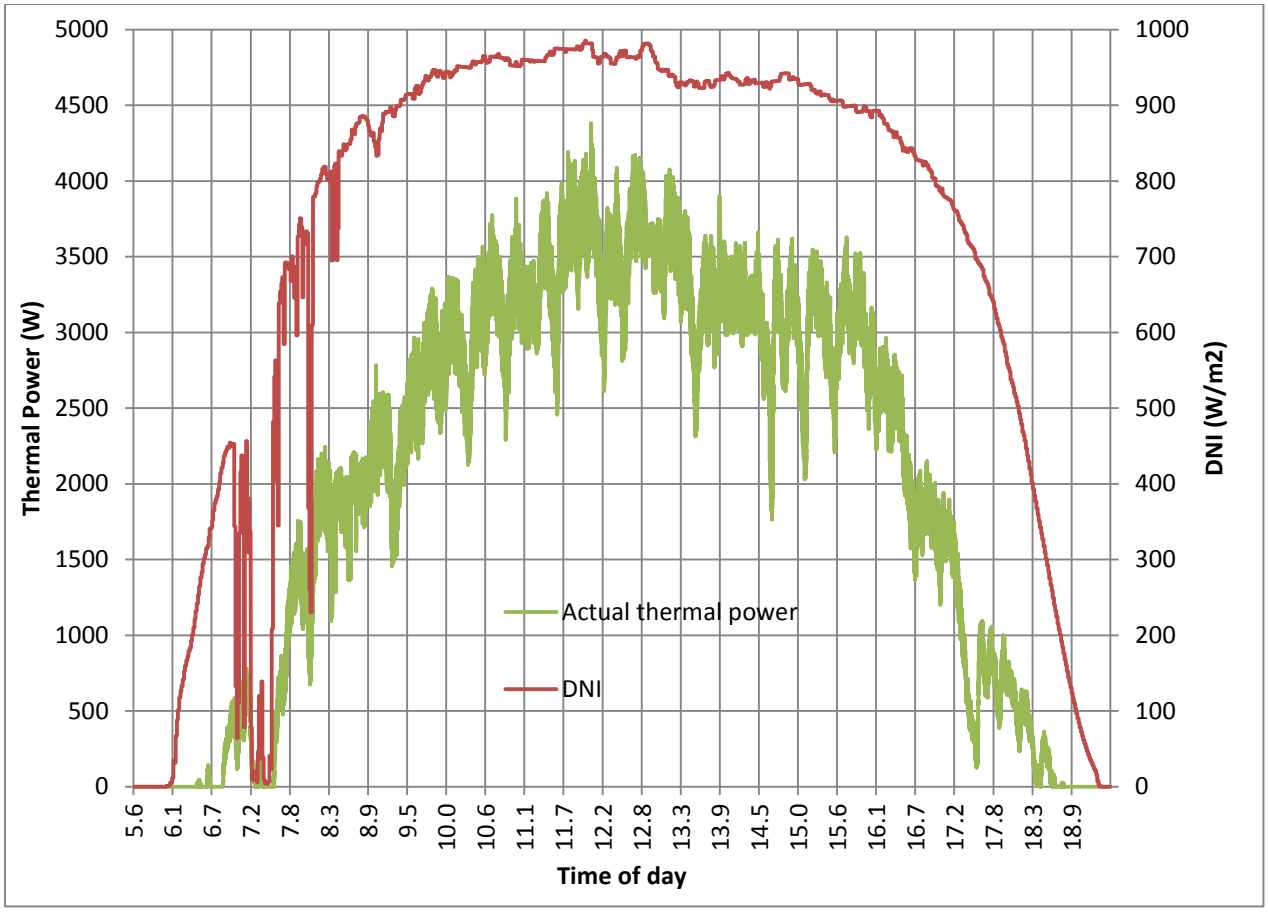


**Figure 48 Actual thermal power production vs DNI**

A noticeable irregularity in the graph is that around 7 am the DNI drops sharply. This was due to clouds passing over the experiment. It is evident that cloud cover poses a significant problem for smooth power production. The graph does indicate a degree of thermal inertia in the system but this is inadequate to mitigate extended cloud cover.

The measured thermal power has a high level of variability and this may be due to a number of reasons. The temperature readings may have a degree of uncertainty which would be amplified in the calculation of power from Equation 19. The most likely cause though is that the single drive tracker is not ideal for each mirror at a given time. The chain and sprocket design does introduce issues when the chain is not perfectly tensioned. The mirrors closest to the drive sprocket will track the best while there may be slack in the chain that incrementally worsens until the last mirror. Chain backlash also poses a problem and is visible in the movement of a mirror when an external force is applied to it, either manually or through wind loading.

The tracker algorithm may also cause this defocusing if the calculation of solar time is not accurate enough. The equation used for the tracker is stated to be sufficiently accurate but electronics issues such as the floating point arithmetic of the relatively cheap Arduino board may be an issue.

During testing it was noticed that at times the tracker was lagging the sun's movement. Sometimes a full reset of the tracker was needed to refocus the mirrors. A possible reason for this lagging is that the stepper motor was missing a step at times due to the motor and driver board being operated at the high end of their limits. This could be because the driver board is supplying current for a step but it is not sufficient for the torque required for an actual step. The board would then falsely think it has stepped the motor. In order to accurately test if slipping is happening, a shaft encoder would be needed.

## 6.3. COMPARISON WITH MATLAB MODEL

In order to ascertain whether the experiment represents adequate performance of a LFR system, the experimental results were compared to what the MATLAB model of section 3.3 predicts for the power production. The DNI data for each particular day was used to run the model such as the DNI shown in Figure 48 above. The comparisons are shown in Figure 49 to Figure 51 below.

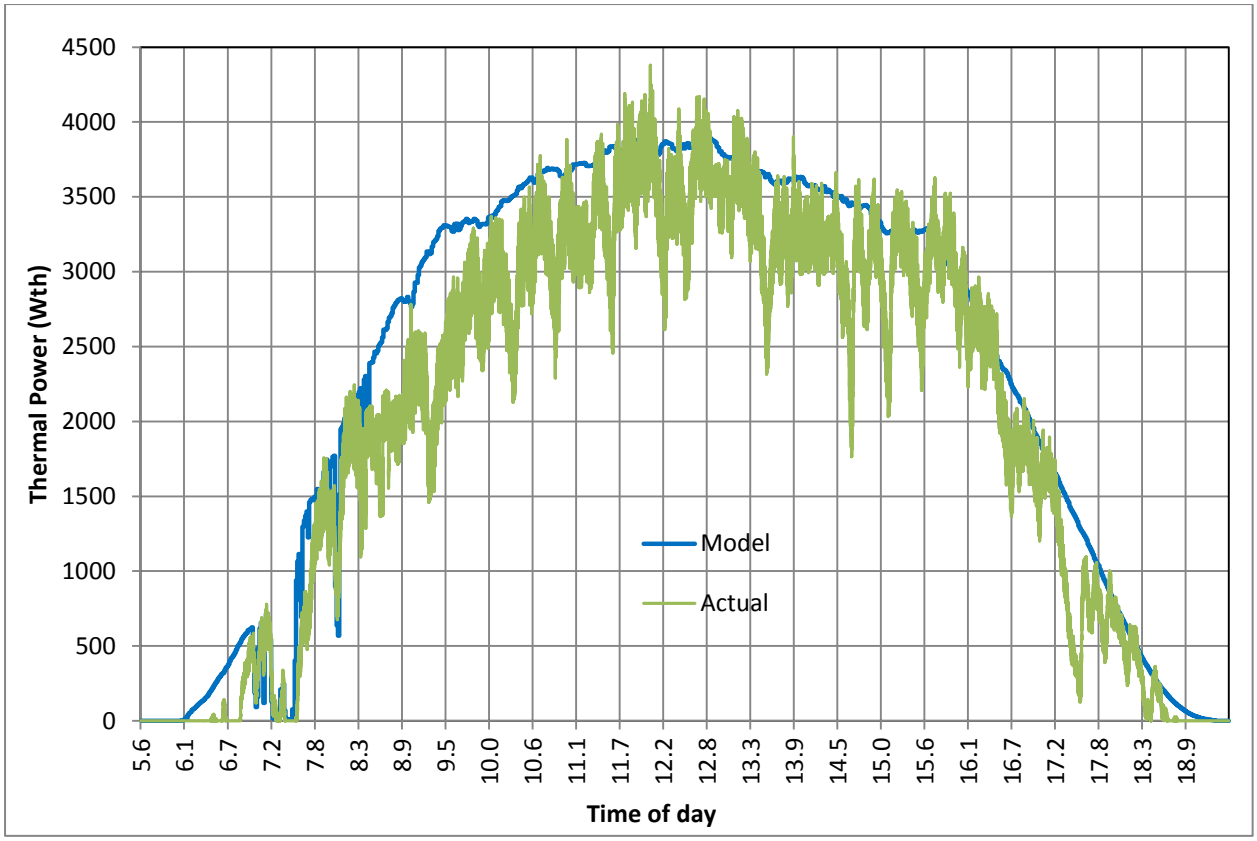


**Figure 49 MATLAB model vs experimental results (19/11/2012)**

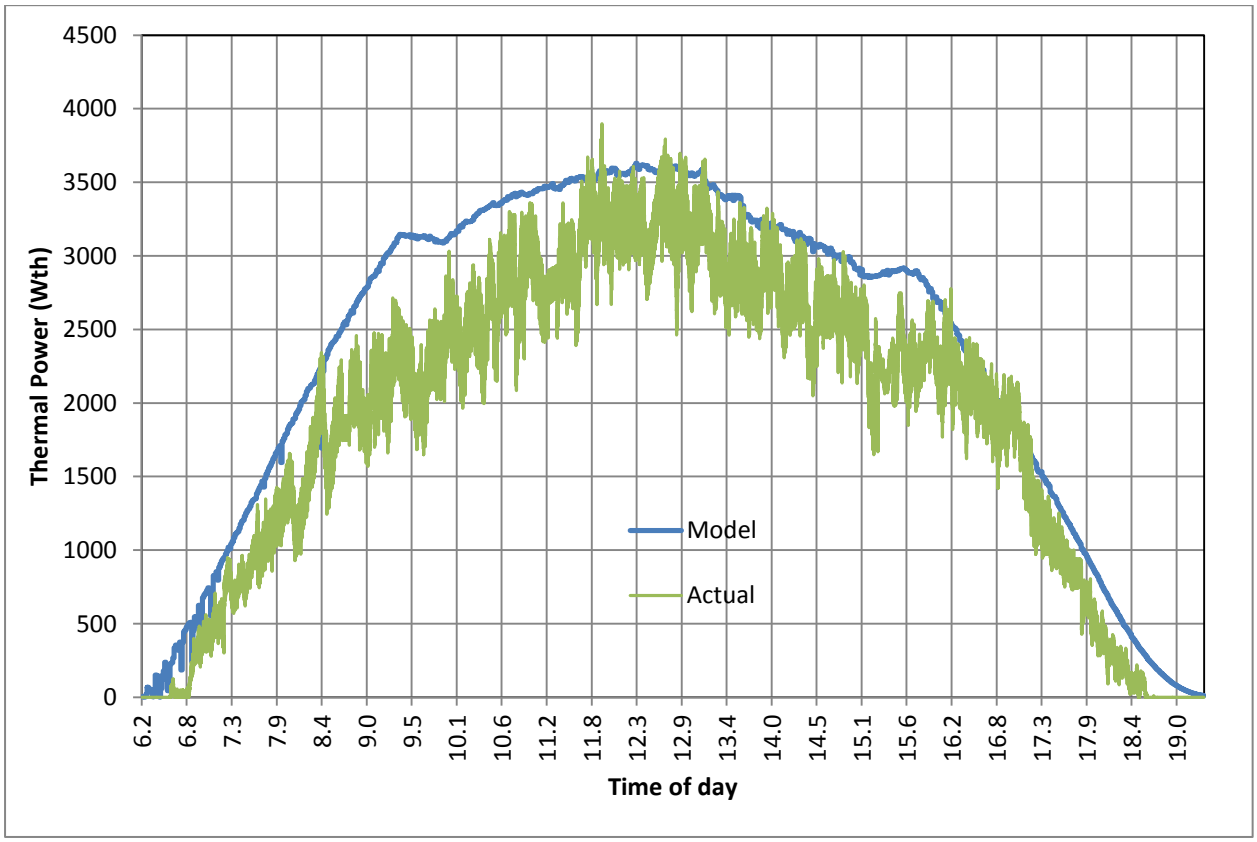


**Figure 50 MATLAB model vs experimental results (30/11/2012)**

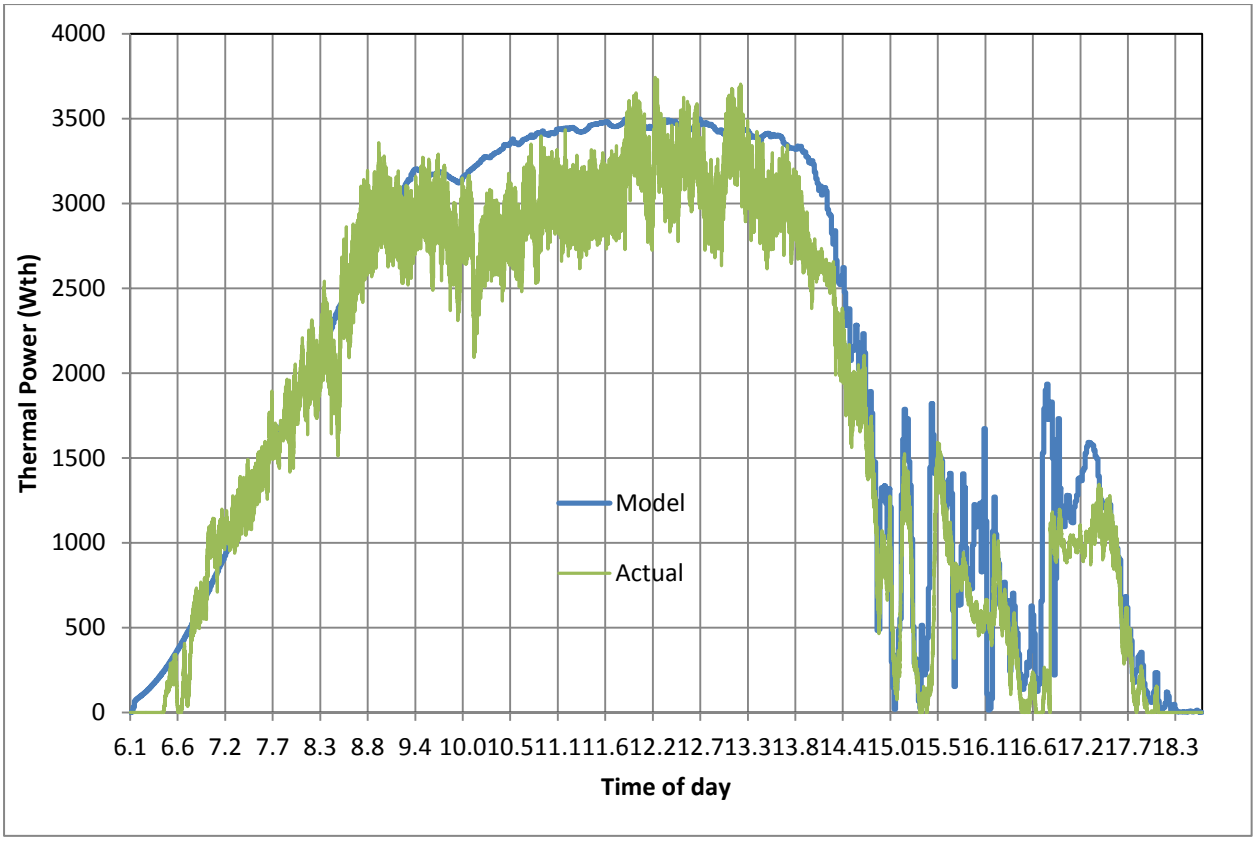


**Figure 51 MATLAB model vs experimental results (01/12/2012)**

Initial work on comparing model predictions and experimental results showed a noticeable discrepancy. This was due to the basic MATLAB model not taking thermal losses into account. When these losses were implemented, the model showed greater conformity with the experimental results. The highest radiation loss predicted was approximately 340 W and the highest convection loss was 150 W. The calculations, however, are based on conservative worst case scenarios close to black body radiation and free convection. For this reason, the model sometimes over predicts the thermal losses and this can be seen in the figures above when the predicted value is less than the experimental value. For more information on the calculation of these losses, refer to Appendix C. More work on the radiation and convection losses from the receiver would further improve the accuracy of the model, however, this is beyond the scope of this thesis. The introduction of a selectively coated absorber tube would also reduce the highest thermal loss, namely the radiation loss.

The modelled and actual data follow a similar trend, with the model slightly over predicting the performance. The average difference in power between the actual and predicted performance was 9.5 %, 19.8 % and 7.3 % respectively for the three test days shown above. This difference is because the model cannot predict certain errors such as alignment errors

and slippage of the tracking motor. The worst performance of 19.8 % was due to this day (30/12/2102) having a consistently stronger wind load on the mirrors than the other two days shown. The average wind speed on the 30/11/2012 was 8.7 m/s with gusts over 18 m/s. This noticeably reduced performance due to mirrors vibrating in the wind and increased convection losses. The mirror mounting and tracking system have the greatest scope for improvement and it is believed this would reduce the discrepancy between the predicted and actual performance.

To investigate the actual efficiency of the experiment, the produced thermal power was compared to the total incoming flux for each particular instant in time. This is plotted against the change in temperature (delta T) above ambient as shown in Figure 52 below. The efficiency data was grouped in each unit degree rise in temperature and the average was plotted as a single point to simplify the graph. The reduction in efficiency for rising delta T was also calculated with the model and shown below. This is only shown for each 5 degree rise in temperature.

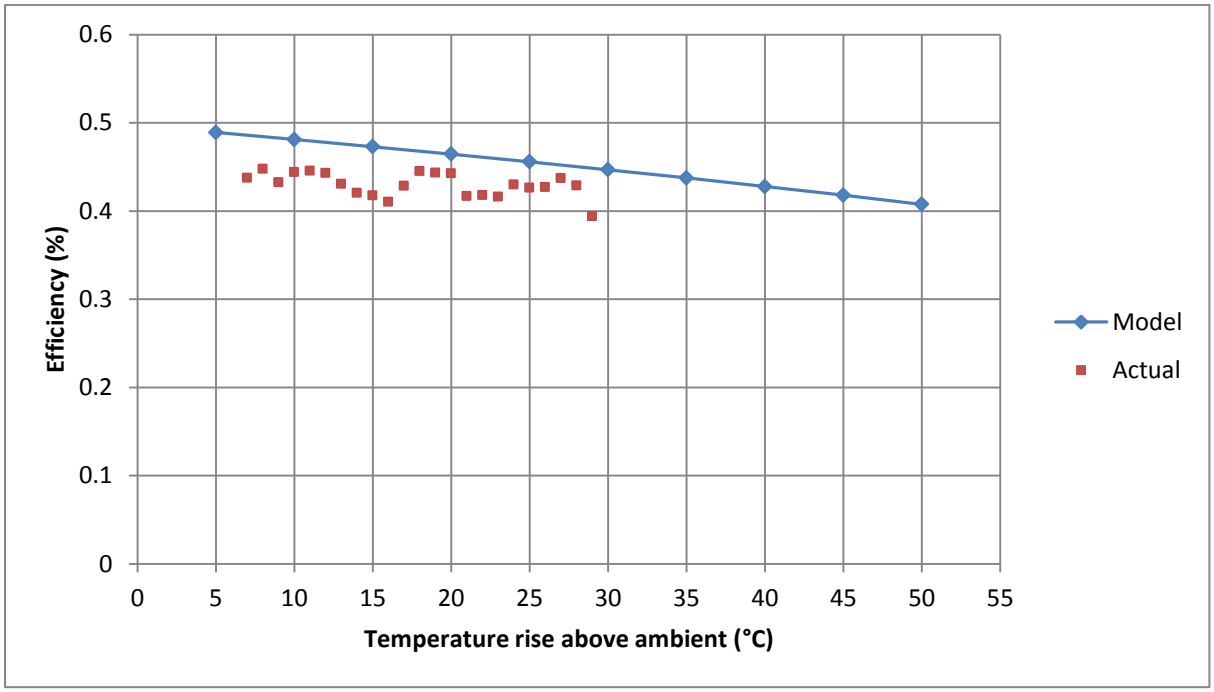


**Figure 52 Efficiency curve for experiment vs model**

The graph indicates that the average conversion efficiency to thermal energy is approximately 43 %. The experiment was only run at below boiling temperatures and therefore only a narrow section of the efficiency graph can be plotted. The model does predict that the efficiency will drop as higher temperatures are reached.

## 6.4. STAGNATION TEST

A test was carried out to determine the time required for the system to reach boiling point should the pump stop. The experiment was not designed to operate continuously at boiling point or beyond and there is no pressure release valve or high temperature piping at the outlet. The aim of the stagnation test was to determine how quickly boiling occurs and whether the system could be altered to produce steam at a later stage.

Initially the pump was run to fill the absorber tube with water at ambient temperature. It was then completely switched off and the tracker was started. The thermocouples at the inlet and outlet are installed in the absorber tube and so will still read the water temperature if no flow was present. Due to the overhang on the southern side, the outlet thermocouples were closest to the concentrated flux and registered the temperature rise first. Slowly the stagnant water in the tube heated up through natural convection and conduction until the whole tube was full of water at boiling point. Once boiling point was reached, the pump was switched on again and the tube was quickly flushed. This was to protect the system from pressure build-up and high temperatures. The whole process was repeated a second time and Figure 53 below shows the trends in temperature.

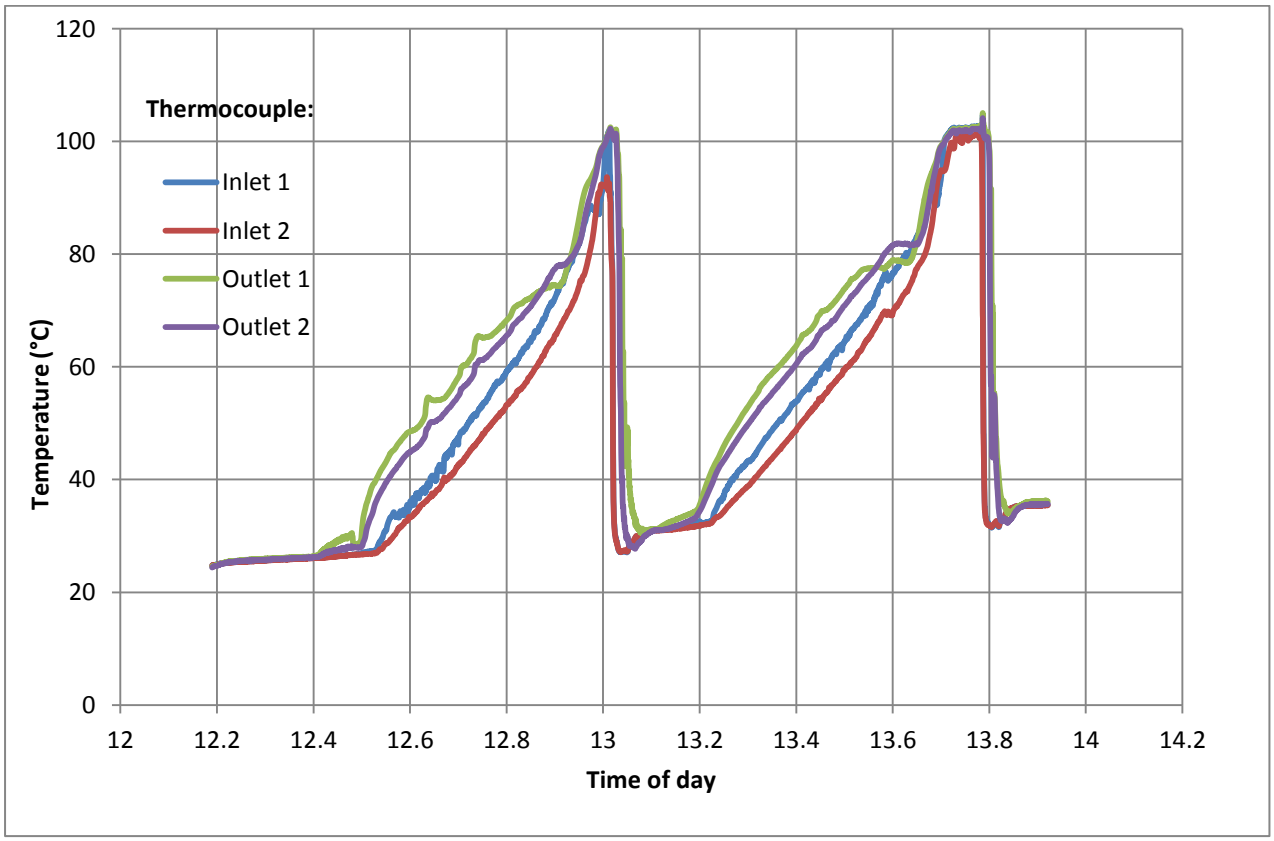


**Figure 53 Stagnation test**

The stagnation test shows that at a DNI of approximately 1020 W/m$^2$ the system takes roughly 30 minutes to heat up 30 litres of water to boiling point. There is a temperature profile across the absorber tube due to the location of the concentrated flux. This profile is present until boiling is reached at which point there is a constant temperature in the tube and it acts as a boiler drum. This boiling could be maintained by accurately controlling the flow rate into the tube after boiling commences.

## 6.5. EXPERIMENT COST ANALYSIS

A core aim of the project was to develop a low cost LFR system. The experiment that was built, however, was designed as a flexible test bench and therefore some aspects of its design have introduced extra cost in order to ensure flexibility. A commercial design would remove this flexibility and strive to drive down costs as far as possible. Nevertheless, the costs for building the experiment were investigated in order to compare it to other forms of generating heated water such as electric geysers. The total cost of the experiment is shown in Table 12 below along with how this cost was divided into the four main physical components of the system plus the labour and design costs. The cost in R/kW$_{th}$ of the 4 kW$_{th}$ peak system is also shown.

**Table 12 Cost of experiment**

| Description | Value | Percentage of total |
|---|---|---|
| Structure | R8 552 | 13.9 % |
| Mirrors and mounting | R16 754 | 27.3 % |
| Tracker | R14 380 | 23.5 % |
| Receiver | R7 361 | 12.0 % |
| Labour | R6 280 | 10.2 % |
| Design time | R8 000 | 13.1 % |
| **Total** | **R61 327** | |
| | | |
| **R/kW$_{th}$** | **R15 332** | |

The mirrors and mounting mechanisms comprise the greatest portion of the cost and this is acceptable due to the mirrors covering a much larger surface area than the receiver or

trackers. It also suggests that any cost savings in this area would have a large impact on the total cost of a LFR array. It is surprising though to see how much of the total cost the tracker represents. If another module of mirrors was installed next to the current module and driven off the same tracker, this would bring down the percentage of total cost for the tracker to expected levels. This is what happens in practice with a single motor running a 50 m row of mirrors.

The flexibility of the experimental test bench to test different mirror spacing's and mirror widths has meant the inclusion of adjustable mounting rails and detachable mirror mounts. To achieve the full low cost potential of LFR, these features would be removed in a commercial design. For instance, removing the adjustable mirror mounts from the design would save R6631 from the mirrors and mounting total in Table 12 above. In order to simulate what the effect of scaling up the system would have on system price, a table of estimated costs for a slightly larger system is shown in Table 13 below. For this system, the footprint is doubled so the peak thermal power is 8 kWth.

**Table 13 Projected costs of larger experiment**

| Description | Value | Percentage of total |
|---|---|---|
| Structure | R17 104 | 19.7 % |
| Mirrors and mounting | R20 246 | 23.3 % |
| Tracker | R14 380 | 16.5 % |
| Receiver | R14 722 | 16.9 % |
| Labour | R12 560 | 14.4 % |
| Design time | R8 000 | 9.2 % |
| **Total** | **R87 012** | |
| | | |
| **R/kW$_{th}$** | **R10 877** | |

The structure, receiver and labour segments were doubled to achieve a doubling of system footprint. The mirror and mounting system was first reduced by R6631 as previously mentioned and then doubled. The tracker segment remains the same as the previous tracker can drive two adjacent arrays. The design time also remained the same as no new design is required in doubling the system.

It becomes evident that economies of scale start to have an effect on system cost. The cost per $kW_{th}$ is reduced by approximately 50% when doubling the size of the array. The $R/kW_{th}$ value for the system is still high, however, when compared to conventional sources of thermal energy such as electric geysers. A brief investigation of quoted prices for equivalently sized electric geysers indicates that the capital cost of a system that can heat the same 500 litre tank of water would cost approximately R20 000 as opposed to R61 327 for the LFR system. In terms of lifecycle cost though, the LFR system may be competitive. Equivalent conventional electric geysers draw over 4kW when operating which results in much higher operational costs than the LFR system. Comparison to commercially available solar rooftop geysers also indicates that the LFR system is more expensive than other renewable energy options. Standard solar rooftop geysers are approximately R30 000 but this does include the Eskom rebate.

There remains potential for dramatic cost reductions of the LFR system when scaling up to a plant size such as 50 $MW_e$. A presentation by Rudiger Wolf of SHP in 2004 indicates that a standalone 50 $MW_e$ LFR plant in Spain would cost approximately 6 500 $R/kW_{th}$ (Wolf 2004). This assumes inflation at 5 % per annum and a Euro/Rand exchange rate of 13.3. This amount includes all power plant balance of plant such as thermal storage and power block.

The investigation of the potential for local manufacture was also one of the aims identified. One method to study this aspect is to split the cost into material categories. For example, South Africa has an established steel industry so it is assumed that all material needs for that category could be met locally. The effect of the volatility of a given market on CSP plant manufacture can also be analysed. Figure 54 shows the percentage of total cost for each material category.

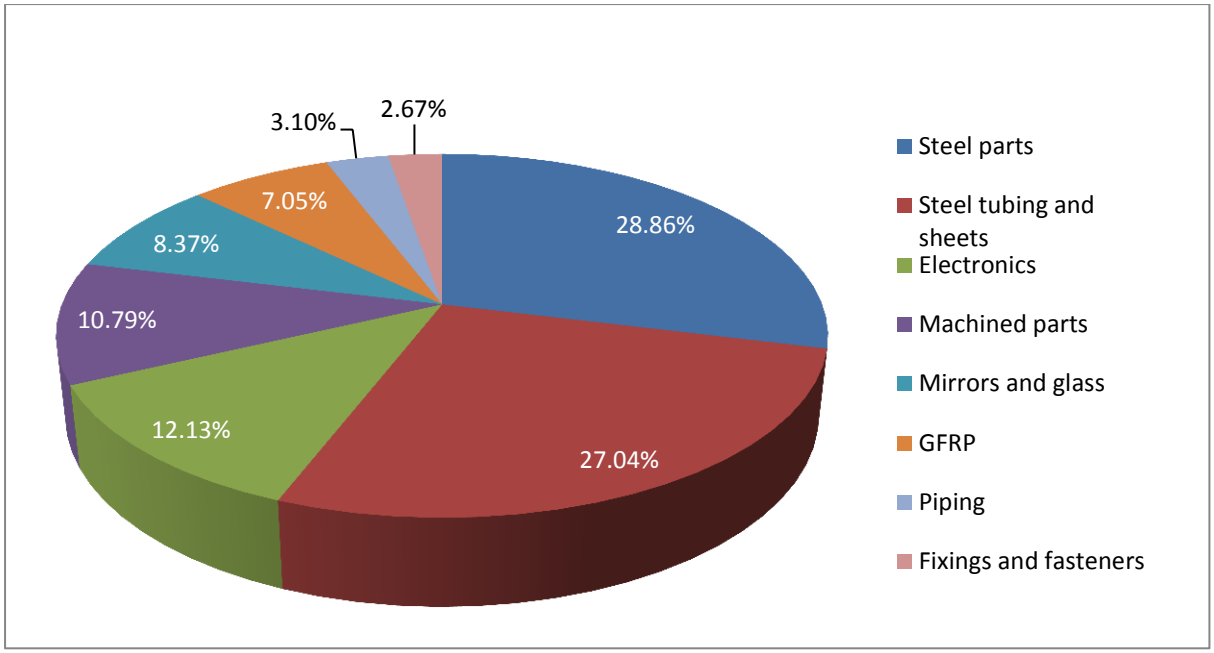


**Figure 54 Division of cost into material segments**

It is evident that processed steel parts and steel extrusions encompass over half of the total material costs. This is a good feature of LFR systems when aiming for local manufacturing. As South Africa is a resource rich nation, further enhancement of produced steel components into finished products is important for a developing country and one of the aims of national government. The steel parts, machined parts and piping categories are all directly related to the steel industry. The GFRP backing would likely also be replaced by steel or aluminium backing in commercial plants. The category divisions above also take into account the labour costs. Therefore skilled metal-working labour is also a requirement and a major beneficiary of developing CSP plants. The recent volatility of this sector is a major concern, however, as it would dramatically increase costs.

Currently, the electronics category is the only equipment segment that is sourced internationally. Further reducing of this level would be moving in the right direction although the current level below the 25 % set in the specifications is acceptable. The cheap glass used for the experiment is sufficient for the project's needs but a commercial design would likely strive to use low iron glass. Currently this is not available in South Africa and would probably push the glass category well above 10 % of system cost.

# CHAPTER 7. CONCLUSIONS

## 7.1. OVERVIEW OF PROJECT

The core design aim of the project to develop a system that demonstrates the LFR principle has been achieved. The system automatically tracks the sun through the use of a GPS timing chip which makes it possible to switch it on at any date in the year or at any time of day. This allows any staff member to use it as a demonstration system when required. The achieved power is also close to the expected performance from the model. Improvements in the tracking system and changes to the mirror mounting would further enhance its performance.

While the experiment did show a degree of fluctuation in the power production, this may be acceptable if the system is used just to heat water. At the end of a full day's operation, all of the water in the 500 litre tank was heated up to 60 °C. This may be ideal if the system is to be used to provide large quantities of low temperature water. While the capital cost of the system is higher than conventional electric geysers or boilers, the fuel savings over a number of years may make it economically attractive. This is even more likely with rising electricity costs. Such as system could provide low temperature water or steam to markets such as food and beverage industries.

The objective of achieving a high level of local manufacturing has been realized with only 16.4 % of the total experiment cost being sourced internationally. The material with greatest share of total cost was steel material and parts, which was locally sourced. This indicates the potential of LFR systems as a locally produced CSP product. The tracking system was sourced internationally from reputed manufacturers to guarantee operation of the experiment. With extensive due diligence and testing, motors could be sourced from local manufacturers in future and further increase local content of the system.

The method of first using models to predict optical performance before conceptual design proved to be beneficial. The sensitivity analyses indicated trends in performance that could be expected should certain design choices be made. This led to a design that was appropriate for the given footprint on the solar roof and was in line with what the system aimed to demonstrate. The models can be used to predict the performance of future designs or scaling up of the current design.

## 7.2. OPERATION OF LFR EXPERIMENT

As per the specifications, the system allows full rotation of the mirrors and the stow position protects the mirrors at night or during rough weather. The structure and receiver design is rigid enough to withstand strong winds and heavy rain. The initial means of mounting of the mirrors was not sufficient but the subsequent modifications have rectified the problem. The flexibility of the design was an advantage because mirrors were easily removed for modifications. This led to a need for a larger gap between mirrors which was also achievable due to the flexible mounting design.

The single drive tracking system performed adequately and demonstrated that such a system is feasible. The step size and accuracy of the tracker was within the required performance criteria for a low cost system. The chain and sprocket design allowed mirror spacing to be easily altered. It did, however, introduce errors due to tooth backlash and loss of tension away from the driven sprocket. It is recommended that future designs investigate the use of a smaller motor per mirror row or a linear actuator driven crank system.

When running the experiment, it is important to match the flow rate through the absorber tube with its tube diameter and related volume of water present in the tube at any given time. A high enough flow rate is needed that turbulent flow will be present and therefore it's higher heat transfer rate so that the array is operating at its full potential. In a scaled up LFR plant there will be a maximum possible heat transfer into the water or steam depending on the size of the installation and its peak thermal power. The minimum mass flow rate through the circuit to achieve the required heat transfer will then be the point at which the flow rate is still in the turbulent flow regime. Any lower and the array will not be operating efficiently. Therefore the maximum possible temperature achievable will be a function of this minimum flow rate and the design thermal power input for the given installation.

If the objective of the LFR plant is a specific steam temperature, then the size of the absorber tube and length of the array will place a constraint on the maximum achievable flow rate. This also means that if power input into the array drops then the flow rate will need to be throttled to achieve the required temperature. If this flow rate drops too low into the laminar flow regime, then the flow rate will need to be throttled even further due to the lower heat transfer coefficient. A dramatic drop in flow rate may occur then if the power input drops too low. Turbines or process machinery will then need to be sized accordingly.

## 7.3. FUTURE WORK

As a first attempt at building a LFR system, the experiment has indicated a number of areas that warrant further work. These regions of study are either beyond the scope of the project or have arisen due to lessons learnt from the construction of the experiment. Should the scope of a future project include pre-commercial design, it is believed that the tracking system is an area that future efforts could be focused on. The chain and sprocket design would need to be re-evaluated in favour of potentially using a motor to actuate each mirror row. This would allow smarter tracking algorithms to be used and improve accuracy of the tracker. For example, using a simple DC motor with a planetary gearbox and an encoder will reduce the chance of the motor slip experienced with stepper motors and greatly improve accuracy.

Another area of study could include the sizing up of mirror widths and increasing the receiver height. This would only be appropriate for a larger installation in which the footprint is not limited. Wider mirrors and a higher receiver would allow mirror curvature to be introduced. Due to the rigidity of glass mirrors, this is not feasible for small mirror widths as they are likely to break. Alternatively, a flexible reflective material could be investigated as a primary mirror surface. Mirror curvature improves the concentration ratio and allows the receiver width to be reduced. A higher accuracy tracking system would also be required.

The design of the absorber tube and secondary concentrator could be investigated. Selective coating of a non-evacuated tube is an active research area as well as higher temperature selective coatings. The installation of high pressure and high temperature piping and absorber tubing would allow the system to be tested for potential steam production. The stagnation test could then be conducted over a longer period with a slow incremental increase in flow rate to see at what flow rate boiling can be maintained.

The highest level of redesign required to move the project to a pre-commercial phase is the mirror mounting system. The current design is meant to be flexible and allow regular alterations. In contrast, a commercial system will have a fixed mirror pivoting system. A simple yet accurate method of mounting the mirrors is required. The mirrors and mirror support structure would normally be assembled in a serial production facility and transported to site. Some form of support structure and bearing system should be designed that allows the preassembled mirror units to be lifted on with no alignment calibration required.

# REFERENCES


Abbas, R, M J Montes, M Piera, and J M Martínez-Val. “Solar radiation concentration features in Linear Fresnel Reflector arrays.” *Energy Conversion and Management* 54 (2012): 133-144.

Abbas, R; Munoz, J; Martinez-Val, J M. “Steady state thermal analysis of an innovative receiver for linear Fresnel reflectors.” *Applied Energy*, no. 92 (2012): 503-515.

African Development Bank. *Eskom Renewable Energy Project - Porject appraisal report.* Abidjan, Côte d’Ivoire: African Development Bank, 2011.

Alliotte, R. “Superheated direct steam generation: alternative configuration for CLFR solar plants.” *Solarpaces.* Andalucia, 2011.

Barale, G, A Heimsath, P Nitz, and A Toro. “Optical design of a linear Fresnel collector for Sicily.” *Solarpaces.* Perpignan, 2010.

Blanco-Muriel, M, D C Alarcon-Padilla, T Lopez-Moratalla, and M Lara-Coira. “Computing the solar vector.” *Solar Energy* 70, no. 5 (2001): 431-441.

Canavarro, D, M Collares-Pereira, and L L Guerreiro. “Increasing the efficiency of conventional LFR technologies: a new CLFR "Etendue Matched" CSP collector.” *Solarpaces.* Andalucia, 2011.

Cengel, Y A, and M A Boles. *Thermodynamics: An engineering approach (4th edition).* New York: McGraw-Hill, 2002.

Chaves, J, and M Collare-Pereira. “Etendue-matched two stage concentrators with multiple receivers.” *Solar Energy* 84 (2010): 196-207.

Conlon, W M, P Johnson, and R Hanson. “Superheated steam from CLFR solar steam generators.” *ASME Power Conference.* Denver, USA, 2011.

De La Torre, F, J J Veynandt, M Bezian, M El Hafi, and R Fourniner. “Design computation in central receiver systems using monte carlo methods and EDStar programming environmnet.” *Solarpaces.* Perpignan, France, 2010.

Department of Energy. *Executive summary of the draft integrated electricity resource plan 2010.* Pretoria: The Government Printing Works, 2010.

Eck, M, R Uhlig, M Mertins, A Häberle, and H Lerchenmüller. “Thermal load of direct steam generating absorber tubes with large diameter in horizontal linear Fresnel collectors.” *Heat Transfer Engineering* 28, no. 1 (2007): 42-48.

Facão, Jorge, and Armando Oliveira. “Numerical simulation of a trapezoidal cavity receiver for a linear Fresnel solar collector concentrator.” *Renewable Energy*, no. 36 (2011): 90-96.

Häberle, Andreas, et al. “The Solarmundo line focussing Fresnel collector. Optical and thermal performance and cost calculations.” *Solarpaces.* Zurich: Solarpaces, 2002. 10-21.

Heimsath, A, W Platzer, T Bothe, and W Li. “Characterization of optical components for linear Fresnel collectors by fringe reflection method.” *Solarpaces.* Las Vegas, 2008.

Horta, P, M Collares-Pereira, D Canavarro, and L Guerreiro. “Modelling thermal losses in a new CLFR "etendue matched" non-evacuated collector cavity.” *Solarpaces.* Andalucia, 2011.

International Energy Agency. *Key World Energy Statistics .* Paris: International Energy Agency, 2012.

International Energy Agency. *World energy outlook 2012.* Paris: International Energy Agency, 2012.

IPCC. *Climate change 2007: Impacts, adaption and vulnerability.* New York: Cambridge University Press, 2007.

IPCC. *Renewable energy sources and climate change mitigation - Summary for policy makers and technical summary.* Intergovernmental Panel on Climate Change, 2011.

Lamm, L O. “A new analytic expression for the equation of time.” *Solar Energy* 26 (1981): 465.

Larsen, S, M Altamirano, and A Hernández. “Heat loss of a trapezoidal cavity absorber for a linear Fresnel reflecting solar concentrator.” *Renewable Energy* 39 (2012): 198-206.

Martinez-Val, J, et al. “Thermal performance analysis of linear receivers.” *Solarpaces.* Andalucia, 2011.

Mathur, SS, TC Kandpal, and BS Negi. “Optical design and concentration characteristics of linear Fresnel reflector solar concentrators - II. Mirror elements of equal width.” *Energy Conversion and Management* 31, no. 3 (1991): 221-232.

Mertins, M, H Lerchenmuller, A Haberle, and V Heinzel. “Geometry optimization of Fresnel collectors with economic assessment.” *Eurosun.* 2004. 918-925.

Michalsky, J J. “The astronomical almanac's algorithm for approximate solar position (1950-2050).” *Solar Energy* 40, no. 3 (1988): 227-235.

Mills, D, and GL Morrison. “Compact linear Fresnel reflector solar thermal powerplants.” *Solar Energy* 68, no. 3 (2000): 263-283.

Morin, G, M Mertins, J Kirchberger, and Martin Selig. “Supernova - Construction, control & performance of steam superheating linear Fresnel collector.” *Solarpaces.* Andalucia, 2011.

Morin, G, W Platzer, M Eck, R Uhlig, A Häberle, and M Berger. “Road map towards the demonstration of a linear Fresnel collector using a single tube receiver.” *Solapaces.* Las Vegas, 2006. 20-23.

NREL. *Parabolic trough technology overview.* NREL, 2002.

Olcese, M, and S Amorosi. “The potential of new tracking methods combining the existing linear Fresnel collectors with the innovatice Solar Island concept.” *Solarpaces.* Andalucia, 2011.

Shigley, J E, C R Mischeke, and R G Budynas. *Mechanical engineering design (7th edition).* New York: McGraw-Hill, 2004.

Singh, PL, RM Sarviya, and JL Bhagoria. “Thermal performance of linear Fresnel reflecting solar concentrator with trapezoidal cavity absorbers.” *Applied Energy* 87 (2010): 541-550.

Stine, W B, and R W Harrigan. *Solar energy systems design.* John Wiley and Sons, 1986.

Veynandt, F, J De La Torre, J J Bezian, and A Ghatuary. “Design optimization of a solar power plant based on linear Fresnel reflector.” *Eurosun.* Glasgow, 2006.

Veynandt, Francois, and Jean-Jacques Bézian. “Optical accuracy of linear Fresnel collectors.” *Solarpaces.* Granada: Solarpaces, 2011. 10-18.

Wolf, Rudiger. “Compact Linear Fresnel Arrays - Solar thermal power generation ready to take off.” *Clean Energy Power.* Berlin, 2004.

# APPENDIX A. COLLECTOR SIMULATION CODE

Please note that the pasted code may have moved long lines of code to the next line.

```
function [output_vec] = modelLFRoptic(input_vec);

clc
figure(2)
newplot
format short

set(gcf, 'Units','normalized','Position',[0 0.17 1 0.8])
set(gca,'LooseInset',2*(get(gca,'TightInset')))

sun_angle = input_vec(1);
num_mirrors = input_vec(2);
width_mirror = input_vec(3);
gap_mirror = input_vec(4);
gap_increment = input_vec(5);
do_offset = input_vec(6);
offset_increment_y = input_vec(7);
offset_increment_x = input_vec(8);
ray_mirror = input_vec(9);
receiver_height = input_vec(10);
receiver_width = input_vec(11);

receiver_depth = 0.1;
aperture_width = 0;
output_vec = [];
footprint =0;
shaded_aperture = 0;
plot_centre = 0;
received_flux = 0;
total_flux = 0;
receiver_angles =[];
mirror_flux = [];
subtend_angle = (16/60)*pi()/180;


% Calculate mirror gaps
%_____________________________________________________________________________

mirror_gaps(num_mirrors/2+1) = gap_mirror;
mirror_gaps(num_mirrors/2) = gap_mirror;
for i = (num_mirrors/2+2):num_mirrors
    mirror_gaps(i) =  mirror_gaps(i-1)+gap_increment;
end
for i = (num_mirrors/2-1):-1:1
    mirror_gaps(i) = mirror_gaps(i+1) +gap_increment;
end
```

```
% Prevent divide by zero
%_____________________________________________________________________________

if sun_angle >= ((pi()/2)-(0.5*pi()/180))
    sun_angle = (89.5*pi()/180);
elseif sun_angle <= ((-1)*(pi()/2)+(0.5*pi()/180))
    sun_angle = (-1)*(89.5*pi()/180);
end


% Calculate offsets
%_____________________________________________________________________________

if do_offset == 1

    offset_x(num_mirrors/2+1) = 0.00001;
    offset_x(num_mirrors/2) = -0.00001;
    offset_y(num_mirrors/2+1) = -0.00001;
    offset_y(num_mirrors/2) = -0.00001;
    for i = (num_mirrors/2+2):num_mirrors
        offset_x(i) =  offset_x(i-1)+offset_increment_x;
        offset_y(i) =  offset_y(i-1)-offset_increment_y;
    end
    for i = (num_mirrors/2-1):-1:1
        offset_x(i) = offset_x(i+1) -offset_increment_x;
        offset_y(i) = offset_y(i+1) -offset_increment_y;
    end

else
    for t = 1:num_mirrors
        offset_x(t) = 0;
        offset_y(t) = 0;
        delta_x(t) = 0;
        delta_y(t) = 0;

    end
end


% Calculate position of centre points
%_____________________________________________________________________________

x_pos(num_mirrors/2+1) = mirror_gaps(num_mirrors/2+1)/2+width_mirror/2;
x_pos(num_mirrors/2) = (-mirror_gaps(num_mirrors/2)/2)-width_mirror/2;

for i = (num_mirrors/2+2):num_mirrors
    x_pos(i) = x_pos(i-1)+width_mirror+mirror_gaps(i);
end
for i = (num_mirrors/2-1):-1:1
    x_pos(i) = x_pos(i+1)-width_mirror-mirror_gaps(i);
end

% Solve for offset thetas
%_____________________________________________________________________________

hold on

for l =1:num_mirrors
```

```
    plot(x_pos(l),0,'+r')

    if do_offset == 1
        h_offset(l) = sqrt((offset_x(l))^2+(offset_y(l))^2);

        alpha(l) = atan(abs(offset_y(l))/abs(offset_x(l)));
        equ =
['(',num2str(x_pos(l)),'+',num2str(h_offset(l)),'*cos(',num2str(alpha(l)),'
-
x))/(',num2str(receiver_height),'+',num2str(h_offset(l)),'*sin(',num2str(al
pha(l)),'-x))-tan(2*x+',num2str(sun_angle),')'];
        x0 = [0,0];
        [x,fval] = fsolve(equ,x0);
        theta(l) = x(1,1);
    end
end

% Setup base graph
%_____________________________________________________________________

xmax = 4;
xmin = -4;
ymin = -0.5;
ymax = 3.5;

axis([xmin xmax ymin ymax])
plot(0,receiver_height,'+r')
plot([-7 7],[0 0],'r')

x_receiver = [(receiver_width/2) (receiver_width/2) -1*(receiver_width/2) -
1*(receiver_width/2)];
y_receiver = [receiver_height (receiver_height+receiver_depth)
(receiver_height+receiver_depth) receiver_height];

plot(x_receiver,y_receiver,'k')

% Receiver shading
%_____________________________________________________________________

if sun_angle >= 0

    l_shadow =
tan(sun_angle+subtend_angle)*(receiver_height+receiver_depth);
    x2_shadow = (-1)*((receiver_width/2)+l_shadow);
    l2_shadow = receiver_height*tan(sun_angle-subtend_angle);
    x1_shadow = (receiver_width/2)-l2_shadow;
    %x1_shadow = x2_shadow + (receiver_width +
sin(sun_angle)*receiver_depth);
    x_shadow = [x1_shadow x2_shadow];
    y_shadow = [0 0];%[(width_mirror/2) (width_mirror/2)];
    shadow_leftx = [x2_shadow (-(receiver_width/2))];
    shadow_lefty = [0 (receiver_height+receiver_depth)];
    shadow_rightx = [x1_shadow (receiver_width/2)];
    shadow_righty = [0 receiver_height];

elseif sun_angle < 0
```

```
    l_shadow = (-1)*tan(sun_angle-
subtend_angle)*(receiver_height+receiver_depth);
    x1_shadow = ((receiver_width/2)+l_shadow);
    l2_shadow = (-1)*receiver_height*tan(sun_angle+subtend_angle);
    x2_shadow = (-1)*(receiver_width/2)+l2_shadow;
    %x2_shadow = x1_shadow - (receiver_width -
sin(sun_angle)*receiver_depth);
    x_shadow = [x1_shadow x2_shadow];
    y_shadow = [0 0];%[(width_mirror/2) (width_mirror/2)];
    shadow_leftx = [x2_shadow (-(receiver_width/2))];
    shadow_lefty = [0 (receiver_height)];
    shadow_rightx = [x1_shadow (receiver_width/2)];
    shadow_righty = [0 (receiver_height+receiver_depth)];

end

%_____________________________________________________________________________
% Flux initialisation

flux_vector = zeros(2,501);
mirror_flux = zeros(num_mirrors,501);
increment = 0;

for i = 1: length(flux_vector)

    flux_vector(1,i) = -250 + increment;
    increment = increment + 1;

end

%_____________________________________________________________________________
%_____________________________________________________________________________

for i = 1: num_mirrors


    if do_offset == 1

        if offset_x(i)<=0 && offset_y(i)<=0 && theta(i)<=0

            if abs(theta(i))>alpha(i)
                delta_x(i) = -h_offset(i)*cos(-alpha(i)-theta(i));
                delta_y(i) = h_offset(i)*sin(-alpha(i)-theta(i));
            else
                delta_x(i) = -h_offset(i)*cos(alpha(i)+theta(i));
                delta_y(i) = -h_offset(i)*sin(alpha(i)+theta(i));
            end

        elseif offset_x(i)<=0 && offset_y(i)<=0 && theta(i)>0

            if (alpha(i)+theta(i))>=(pi()/2)
                delta_x(i) = -h_offset(i)*cos(alpha(i)+theta(i));
                delta_y(i) = -h_offset(i)*sin(alpha(i)+theta(i));
            else
                delta_x(i) = -h_offset(i)*cos(alpha(i)+theta(i));
                delta_y(i) = -h_offset(i)*sin(alpha(i)+theta(i));
            end
```

```
        elseif offset_x(i)>0 && offset_y(i)<=0 && theta(i)<=0

            if (alpha(i)+abs(theta(i)))>=(pi()/2)
                delta_x(i) = h_offset(i)*cos(alpha(i)-theta(i));
                delta_y(i) = -h_offset(i)*sin(alpha(i)-theta(i));
            else
                delta_x(i) = h_offset(i)*cos(alpha(i)-theta(i));
                delta_y(i) = -h_offset(i)*sin(alpha(i)-theta(i));
            end

        elseif offset_x(i)>0 && offset_y(i)<=0 && theta(i)>0

            if theta(i) >= alpha(i)
                delta_x(i) = h_offset(i)*cos(alpha(i)-theta(i));
                delta_y(i) = -h_offset(i)*sin(alpha(i)-theta(i));
            else
                delta_x(i) = h_offset(i)*cos(alpha(i)-theta(i));
                delta_y(i) = -h_offset(i)*sin(alpha(i)-theta(i));
            end
        end
    end


    phi(i) = atan((x_pos(i)+delta_x(i))/(receiver_height-delta_y(i
    if do_offset == 0
        theta(i) = (phi(i)-sun_angle)/2;
    end

    x1(i) = x_pos(i)+delta_x(i)+(width_mirror/2)*cos(theta(i));
    x2(i) = x_pos(i)+delta_x(i)-(width_mirror/2)*cos(theta(i));

    y1(i) = delta_y(i)+(width_mirror/2)*sin(theta(i));
    y2(i) = delta_y(i)-(width_mirror/2)*sin(theta(i));

end
%_____________________________________________________________________________
%_____________________________________________________________________________
% MAIN LOOP


for k = 1:num_mirrors

    x1current = x1(k);
    x2current = x2(k);

    y1current = y1(k);
    y2current = y2(k);

    xplot = [x1current x2current];
    yplot = [y1current y2current];

    %_____________________________________________________________________________
    %_____________________________________________________________________________
    % BLOCKING
    blocked = 0;

    if theta(k) < 0 && phi(k) < 0 && k < num_mirrors
```

```
        if (x1current + tan(phi(k)-subtend_angle)*(y1current-delta_y(k))) >
(x2(k+1) + tan(phi(k)-subtend_angle)*(y2(k+1)-2*delta_y(k+1)+delta_y(k)))

            blocked = 1;

            %
            l1 = (x1current + tan(phi(k)-subtend_angle)*(y1current-
delta_y(k)))- (x2(k+1) + tan(phi(k)-subtend_angle)*(y2(k+1)-delta_y(k)));
            %
            w1 = l1*cos(phi(k)-subtend_angle);
            h1 = w1/(sin((pi()/2) + (phi(k)-subtend_angle) -theta(k)));
            blockedx = h1* cos(theta(k));
            blockedy = (-1)*h1* sin(theta(k));
            %
            x1current = x1current - blockedx;
            y1current = y1current + blockedy;


        end
    end

    if theta(k) > 0 && phi(k) > 0 && k > 1
        %
        %
        %
        if (x2current + tan(phi(k)+subtend_angle)*(y2current-delta_y(k))) <
(x1(k-1) + tan(phi(k)+subtend_angle)*(y1(k-1)-delta_y(k)))
            %
            %

            blocked = 1;
            %
            l1 = (x1(k-1) + tan(phi(k)+subtend_angle)*(y1(k-1)-
delta_y(k)))-(x2current + tan(phi(k)+subtend_angle)*(y2current-
delta_y(k)));
            %
            %
            w1 = l1*cos(phi(k)+subtend_angle);
            h1 = w1/(sin((pi()/2) - phi(k)+subtend_angle +theta(k)));
            blockedx = h1 * cos(theta(k));
            blockedy = h1 * sin(theta(k));
            %
            x2current = x2current + blockedx;
            y2current = y2current + blockedy;
            %
        end
        %
        %
    end

%_____________________________________________________________________
    % ray tracing

    x_in_centre_top = (x_pos(k)+delta_x(k)+(receiver_height-
delta_y(k))*tan(sun_angle));
    x_in_centre_mirror = (x_pos(k)+delta_x(k));
    y_in_centre_top = receiver_height;
    y_in_centre_mirror = delta_y(k);
```

```
    x_in_centre = [x_in_centre_top x_in_centre_mirror];
    y_in_centre = [y_in_centre_top y_in_centre_mirror];

    x_out_centre_mirror = (x_pos(k)+delta_x(k));
    x_out_centre_top = (x_pos(k)+delta_x(k))-((receiver_height-
delta_y(k))/tan((pi()/2)-phi(k)));
    y_out_centre_mirror = (delta_y(k));
    y_out_centre_top = receiver_height;

    x_out_centre = [x_out_centre_mirror x_out_centre_top];
    y_out_centre = [y_out_centre_mirror y_out_centre_top];

    x_in_left_top = x2current +(receiver_height+delta_y(k)-
y2current)*tan(sun_angle-subtend_angle);
    y_in_left_top = receiver_height;
    x_in_right_top = x1current +(receiver_height+delta_y(k)-
y1current)*tan(sun_angle+subtend_angle);
    y_in_right_top = receiver_height;

    x_out_left_top = x2current - (receiver_height-y2current)/tan((pi()/2)-
phi(k)-subtend_angle);
    y_out_left_top = receiver_height;

    x_out_right_top = x1current - (receiver_height-y1current)/tan((pi()/2)-
phi(k)+subtend_angle);
    y_out_right_top = receiver_height;

%_____________________________________________________________________________
    % SHADING

%_____________________________________________________________________________


    if sun_angle < 0 && theta(k) > 0 && k > 1

        xn_1 = x1(k-1);
        yn_1 = y1(k-1);

        unshaded = (x_pos(k)+delta_x(k)-(xn_1 + (tan((-1)*(sun_angle-
subtend_angle))*(yn_1-delta_y(k)))))*sin((pi()/2)+(sun_angle-
subtend_angle));
        test = sin((pi()/2)+(sun_angle-
subtend_angle+theta(k)))*(width_mirror/2);

        if unshaded < test

            shaded = 1;

            xnew = x_pos(k)+delta_x(k)- (unshaded/sin((pi()/2)+(sun_angle-
subtend_angle)+theta(k)))*cos(theta(k));
            ynew = delta_y(k)+(-1)*(unshaded/sin((pi()/2)+(sun_angle-
subtend_angle)+theta(k)))*sin(theta(k));
            %
            %
            if blocked ==1 && xnew < x2current
                %
            else
```

```
                %
                x2current = xnew;
                y2current = ynew;

                x_in_left_top = x2current + (receiver_height-
y2current+delta_y(k))*tan(sun_angle-subtend_angle);
                y_in_left_top = receiver_height;


                x_out_left_top = x2current - (receiver_height-
y2current)/tan((pi()/2)-phi(k));%+subtend_angle);
                y_out_left_top = receiver_height;

            end

            if xnew > x_in_centre_mirror

                x_in_centre = [x_in_left_top x2current];
                y_in_centre = [y_in_left_top y2current];
                x_out_centre = [x_out_left_top x2current];
                y_out_centre = [y_out_left_top y2current];

            end
        end
    end

    if sun_angle > 0 && theta(k) < 0 && k < num_mirrors

        xn_1 = x2(k+1);
        yn_1 = y2(k+1);

        unshaded = (xn_1 -x_pos(k)-delta_x(k)-
(tan(sun_angle+subtend_angle)*(yn_1-delta_y(k))))*sin((pi()/2)-
(sun_angle+subtend_angle) );
        test = sin((pi()/2)-
(sun_angle+subtend_angle+theta(k)))*(width_mirror/2);

        if unshaded < test

            shaded = 1;

            xnew = x_pos(k)+delta_x(k)+ (unshaded/sin((pi()/2)-
(sun_angle+subtend_angle)-theta(k)))*cos(theta(k));
            ynew = delta_y(k)+(unshaded/sin((pi()/2)-
(sun_angle+subtend_angle)-theta(k)))*sin(theta(k));

            if blocked ==1 && xnew > x1current
                %
            else
                %

                x1current = xnew;
                y1current = ynew;

                x_in_right_top = x1current + (receiver_height-
y1current+delta_y(k))*tan(sun_angle+subtend_angle);
                y_in_right_top = receiver_height;
```

```
                x_out_right_top = x1current - (receiver_height-
y1current)/tan((pi()/2)-phi(k));%-subtend_angle);
                y_out_right_top = receiver_height;
                %
            end
            %

            if xnew < x_in_centre_mirror

                x_in_centre = [x_in_right_top x1current];
                y_in_centre = [y_in_right_top y1current];
                x_out_centre = [x_out_right_top x1current];
                y_out_centre = [y_out_right_top y1current];
            end
        end
    end

    %_____________________________________________________________
    % Receiver shading
    %_____________________________________________________________

    if sun_angle>=0
        x2_sun = x2current+(width_mirror-y2current)/tan((pi()/2)-sun_angle-
subtend_angle);
        y2_sun = width_mirror;
        x1_sun = x1current+(width_mirror-y1current)/tan((pi()/2)-
sun_angle+subtend_angle);
        y1_sun = width_mirror;
        x2_shade = x2_shadow+width_mirror/tan((pi()/2)-sun_angle-
subtend_angle);
        x1_shade = x1_shadow+width_mirror/tan((pi()/2)-
sun_angle+subtend_angle);


    elseif sun_angle<0
        x2_sun = x2current-(width_mirror-y2current)/tan((pi()/2)+sun_angle-
subtend_angle);
        y2_sun = width_mirror;
        x1_sun = x1current-(width_mirror-
y1current)/tan((pi()/2)+sun_angle+subtend_angle);
        y1_sun = width_mirror;
        x2_shade = x2_shadow-
width_mirror/tan((pi()/2)+sun_angle+subtend_angle);
        x1_shade = x1_shadow-width_mirror/tan((pi()/2)+sun_angle-
subtend_angle);
    end

    % Check if shaded
    if x1_shade>= x1_sun &&    x2_shade<= x2_sun
        complete =1
        %Complete shading of mirror
        shaded_aperture = 1;

    elseif x1_shade> x1_sun && x2_shade> x2_sun && x2_shade< x1_sun
        rightshade =1;
        % Righthand shade of mirror

        if sun_angle <=0
```

```
            reduce = (-1)*(width_mirror-y2current)*tan(sun_angle-
2*subtend_angle)+(width_mirror-y2current)*tan(sun_angle);
            w2 = (x2_shade-x2_sun-reduce)*cos(sun_angle+subtend_angle);
            h2 = w2/(cos((-1)*sun_angle-theta(k)));
            xdif = h2*cos(theta(k));
            ydif = h2*sin(theta(k));
            x1current = x2current +xdif;
            y1current = y2current +ydif;
        elseif sun_angle >0
            w2 = (x2_shade-x2_sun)*cos(sun_angle-subtend_angle);
            h2 = w2/(cos(sun_angle+theta(k)));
            xdif = h2*cos(theta(k));
            ydif = h2*sin(theta(k));
            x1current = x2current +xdif;
            y1current = y2current +ydif;
        end

    elseif x1_shade< x1_sun && x2_shade< x2_sun && x1_shade> x2_sun
        leftshade =1;
        %Lefthand shade of mirror

        if sun_angle <=0

            w2 = (x1_sun - x1_shade)*cos(sun_angle+subtend_angle);
            h2 = w2/(cos((-1)*sun_angle-theta(k)));
            xdif = h2*cos(theta(k));
            ydif = h2*sin(theta(k));
            x2current = x1current -xdif;
            y2current = y1current -ydif;

        elseif sun_angle> 0

            w2 = (x1_sun - x1_shade)*cos(sun_angle-subtend_angle);
            h2 = w2/(cos(sun_angle+theta(k)));
            xdif = h2*cos(theta(k));
            ydif = h2*sin(theta(k));
            x2current = x1current -xdif;
            y2current = y1current -ydif;

        end

    elseif x1_shade< x1_sun && x2_shade> x2_sun
        middleshade =1

    end

    x_in_right_top = x1current + (receiver_height-
y1current+delta_y(k))*tan(sun_angle+subtend_angle);
    y_in_right_top = receiver_height;

    x_out_right_top = x1current - (receiver_height-y1current)/tan((pi()/2)-
phi(k)+subtend_angle);
    y_out_right_top = receiver_height;

    x_in_left_top = x2current + (receiver_height-
y2current+delta_y(k))*tan(sun_angle-subtend_angle);
    y_in_left_top = receiver_height;
```

```
    x_out_left_top = x2current - (receiver_height-y2current)/tan((pi()/2)-
phi(k)-subtend_angle);
    y_out_left_top = receiver_height;

    if x1current < x_in_centre_mirror

        x_in_centre = [x_in_right_top x1current];
        y_in_centre = [y_in_right_top y1current];
        x_out_centre = [x_out_right_top x1current];
        y_out_centre = [y_out_right_top y1current];
    end

    if x2current > x_in_centre_mirror

        x_in_centre = [x_in_left_top x2current];
        y_in_centre = [y_in_left_top y2current];
        x_out_centre = [x_out_left_top x2current];
        y_out_centre = [y_out_left_top y2current];

    end

    %_____________________________________________________________________
    % receiver angles

    receiver_height_above_glazing = 0.02;

    receiver_angles(k,1) = x1current - (receiver_height-
receiver_height_above_glazing-y1current)/tan((pi()/2)-
phi(k)+subtend_angle);
    receiver_angles(k,2) = ((pi()/2)+phi(k)+subtend_angle);
    receiver_angles(k,3) = x2current - (receiver_height-
receiver_height_above_glazing-y2current)/tan((pi()/2)-phi(k)-
subtend_angle);
    receiver_angles(k,4) = ((pi()/2)+phi(k)-subtend_angle);

%_____________________________________________________________________

    plot(xplot, yplot,'k')

    if ray_mirror == 0 || ray_mirror == k

        if shaded_aperture ==0

            if plot_centre == 1

                plot(x_in_centre,y_in_centre,'y')
                plot(x_out_centre,y_out_centre,'c')
            end
            plot([x_in_left_top x2current],[y_in_left_top y2current],'y')
            plot([x_in_right_top x1current],[y_in_right_top y1current],'y')
            plot([x_out_left_top x2current],[y_out_left_top y2current],'c')
            plot([x_out_right_top x1current],[y_out_right_top
y1current],'c')
        end

        plot(x_shadow,y_shadow,'k','LineWidth',2)
        plot(shadow_leftx,shadow_lefty,'--k','LineWidth',1)
        plot(shadow_rightx,shadow_righty,'--k','LineWidth',1)
```

```
    end

    %_____________________________________________________________________
    % Aperture area

    new_aperture = 0;
    illuminated_length = (x1current-x2current)/(cos(theta(k)));

    if sun_angle > 0 && theta(k) > 0 && shaded_aperture == 0

        new_aperture = sin((pi()/2)-sun_angle-theta(k))*illuminated_length;
        aperture_width = aperture_width + new_aperture;

    elseif sun_angle > 0 && theta(k) < 0 && shaded_aperture == 0

        new_aperture = sin((pi()/2)-sun_angle-theta(k))*illuminated_length;
        aperture_width = aperture_width + new_aperture;

    elseif sun_angle < 0 && theta(k) > 0 && shaded_aperture == 0

        new_aperture = sin((pi()/2)+sun_angle+theta(k))*illuminated_length;
        aperture_width = aperture_width + new_aperture;

    elseif sun_angle < 0 && theta(k) < 0 && shaded_aperture == 0

        new_aperture = sin((pi()/2)+sun_angle+theta(k))*illuminated_length;
        aperture_width = aperture_width + new_aperture;

    elseif sun_angle == 0 && theta(k) < 0 && shaded_aperture == 0

        new_aperture = sin((pi()/2)+theta(k))*illuminated_length;
        aperture_width = aperture_width + new_aperture;

    elseif sun_angle == 0 && theta(k) > 0 && shaded_aperture == 0

        new_aperture = sin((pi()/2)-theta(k))*illuminated_length;
        aperture_width = aperture_width + new_aperture;

    end

    shaded = 0;
    shaded_aperture = 0;

    %_____________________________________________________________________
    % Flux calculation

    x_out_left_top_inner = x2current - (receiver_height-
y2current)/tan((pi()/2)-phi(k)+subtend_angle);

    x_out_right_top_inner = x1current - (receiver_height-
y1current)/tan((pi()/2)-phi(k)-subtend_angle);

    rightedge = floor(1000*x_out_right_top)/1000;
    leftedge = ceil(1000*x_out_left_top)/1000;
    rightedgeinner = floor(1000*x_out_right_top_inner)/1000;
    leftedgeinner = ceil(1000*x_out_left_top_inner)/1000;
```

```
    ray_length = (rightedge - leftedge);
    projection_factor = new_aperture/ray_length;

    for point = (1000*leftedge):1:(1000*rightedge)

        for vec = 1: length(flux_vector)

            if flux_vector(1,vec) == point

                if point< (1000*leftedgeinner)
                    flux_vector(2,vec) = flux_vector(2,vec) +
projection_factor/2;
                    total_flux = total_flux + projection_factor/2;
                    mirror_flux(k,vec) = projection_factor/2;
                elseif point >= (1000*leftedgeinner) && point <=
(1000*rightedgeinner)
                    flux_vector(2,vec) = flux_vector(2,vec) +
projection_factor;
                    total_flux = total_flux + projection_factor;
                    mirror_flux(k,vec) = projection_factor;
                elseif point > (1000*rightedgeinner)
                    flux_vector(2,vec) = flux_vector(2,vec) +
projection_factor/2;
                    total_flux = total_flux + projection_factor/2;
                    mirror_flux(k,vec) = projection_factor/2;
                end
            end
        end
    end
    %_____________________________________________________________________
end

hold off

x_flux = flux_vector(1,:);
y_flux = flux_vector(2,:);

for vec = 1: length(flux_vector)

    if flux_vector(1,vec) >= (-1000*(receiver_width/2)) &&
flux_vector(1,vec) <= (1000*(receiver_width/2))
     received_flux = received_flux + flux_vector(2,vec);
    end

end

footprint = 2*(x_pos(num_mirrors)+delta_x(num_mirrors)+(width_mirror/2));

output_vec(1,1) = aperture_width;
output_vec(1,2) = footprint;
output_vec(1,3) = received_flux;

csvwrite('angles.txt',theta)
csvwrite('mirrorflux.txt',mirror_flux)
format long e
csvwrite('receiverangles.txt',receiver_angles)
format short
```

# APPENDIX B. RECEIVER SIMULATION CODE

Please note that the pasted code may have moved long lines of code to the next line.

The receivertraceLFR code requires a surface input file, denoted by “surface_file” below. This is a surface specific file depending on the secondary concentrator surface. Two examples of surface files are included below the main code, namely “ReceiverTrapezoidal” and “ReceiverParabolic”. A an example of a call to the simulation code is:

```
[flux num_rays num_hit flux_in] =
receivertraceLFR(1,0.0445,0.8,'ReceiverTrapezoidal',1,1,8)
```

Main code - receivertraceLFR

```
function [absorbed_flux num_rays num_hit total_flux_in] =
receivertraceLFR(num_pipes,radius_of_pipe,height_above_glazing,surface_file
,ray_spacing,do_plot,num_mirror)

global sec_domain
global sec_range
global func
global height
global do_plot
global rec_dim_pos
global flat_surface
global circ_domain
global height_above_glazing

%_____________________________________________________________________________
% Plot initial graph

if do_plot == 1
    figure(3)
    set(gcf,'NextPlot','replacechildren');
    newplot
    hold on
    axis([-0.2 0.2 0 0.2])
    set(gcf, 'Units','normalized','Position',[0 0.1 1 0.8])
    set(gca,'LooseInset',2*(get(gca,'TightInset')))
end
%_____________________________________________________________________________
% Initiate variables

mirror_flux = csvread('mirrorflux.txt');
ray_flux = 0;
reflection_loss = 0.8;
num_rays = 0;
num_hit = 0;
```

```
total_flux_in = 0;
absorbed_flux = 0;

tempvector = csvread('receiverangles.txt');

x1vec = tempvector(:,1);
alpha1vec = tempvector(:,2);
x2vec = tempvector(:,3);
alpha2vec = tempvector(:,4);
%_____________________________________________________________________________

% Secondary reflector surface file

eval(surface_file);

%_____________________________________________________________________________
% Initiate variables

x_offset_circle = 0;
y_offset_circle = height_above_glazing;

%_____________________________________________________________________________
% Determines pipe geometry

if num_pipes ==1
    x_offset_circle(1) = 0;
    y_offset_circle(1) = height_above_glazing;
    circ_domain = [-radius_of_pipe radius_of_pipe];

elseif num_pipes ==2
    x_offset_circle(1) = radius_of_pipe;
    y_offset_circle(1) = height_above_glazing;
    x_offset_circle(2) = (-1)*radius_of_pipe;
    y_offset_circle(2) = height_above_glazing;
    circ_domain = [0 2*radius_of_pipe; -2*radius_of_pipe 0];

elseif num_pipes ==3
    x_offset_circle(1) = 0;
    y_offset_circle(1) = height_above_glazing;
    x_offset_circle(2) = 2*radius_of_pipe;
    y_offset_circle(2) = height_above_glazing;
    x_offset_circle(3) = (-1)*2*radius_of_pipe;
    y_offset_circle(3) = height_above_glazing;
    circ_domain = [-radius_of_pipe radius_of_pipe;radius_of_pipe
3*radius_of_pipe;-3*radius_of_pipe -radius_of_pipe];

elseif num_pipes ==4
    x_offset_circle(1) = radius_of_pipe;
    y_offset_circle(1) = height_above_glazing;
    x_offset_circle(2) = (-1)*radius_of_pipe;
    y_offset_circle(2) = height_above_glazing;
    x_offset_circle(3) = 3*radius_of_pipe;
    y_offset_circle(3) = height_above_glazing;
    x_offset_circle(4) = (-1)*3*radius_of_pipe;
    y_offset_circle(4) = height_above_glazing;
    circ_domain = [0 2*radius_of_pipe;-2*radius_of_pipe 0;2*radius_of_pipe
4*radius_of_pipe;-4*radius_of_pipe -2*radius_of_pipe];

elseif num_pipes ==5
```

```
    x_offset_circle(1) = 0;
    y_offset_circle(1) = height_above_glazing;
    x_offset_circle(2) = 2*radius_of_pipe;
    y_offset_circle(2) = height_above_glazing;
    x_offset_circle(3) = (-1)*2*radius_of_pipe;
    y_offset_circle(3) = height_above_glazing;
    x_offset_circle(4) = 4*radius_of_pipe;
    y_offset_circle(4) = height_above_glazing;
    x_offset_circle(5) = (-1)*4*radius_of_pipe;
    y_offset_circle(5) = height_above_glazing;
    circ_domain = [-radius_of_pipe radius_of_pipe;radius_of_pipe
3*radius_of_pipe;-3*radius_of_pipe -radius_of_pipe;3*radius_of_pipe
5*radius_of_pipe;-5*radius_of_pipe -3*radius_of_pipe];

end

num_sections = length(func);

%_____________________________________________________________________________
% Plots pipes
%_____________________________________________________________________________

if do_plot == 1

    y_pipe = [];
    x_pipe = [];
    y_temp =[];

    resolution = 100;
    step = radius_of_pipe*2/resolution;
    for t = 1:num_pipes

        for k = 1:resolution+1
            y_temp(k,1) = height_above_glazing - radius_of_pipe+(k-1)*step;
            x_pipe(k,t) = x_offset_circle(t)+ sqrt((radius_of_pipe)^2-
(y_temp(k,1)-y_offset_circle(t))^2);
            y_pipe(k,1) = y_temp(k,1);
        end

        for m = 1:resolution+1
            x_pipe(m+resolution+1,t) = x_offset_circle(t)+(-
1)*sqrt((radius_of_pipe)^2-(y_temp(resolution +2 -m,1)-
y_offset_circle(t))^2);
            y_pipe(m+resolution+1,1) = y_temp(resolution+2 -m,1);

        end
    end

    for r = 1:num_pipes
        figure(3)
        plot(x_pipe(:,r),y_pipe(:,1))
    end
end
%_____________________________________________________________________________

%_____________________________________________________________________________
%_____________________________________________________________________________
% MAIN LOOP
```

```
for i = num_mirror:num_mirror

    absorbed_flux = 0;
    x1 = (floor(1000*x1vec(i,1)))/1000;
    alpha1 = alpha1vec(i,1);
    x2 = (ceil(1000*x2vec(i,1)))/1000;
    alpha2 = alpha2vec(i,1);

    right = floor(1000*x1);
    left = ceil(1000*x2);
    iterations = round((right -left)/ray_spacing);
    anglechange = alpha1-alpha2;
    angledelta = anglechange/iterations;
    angleiter = alpha2;
    xstart = x2;
    ystart = 0;

    xvec = []; yvec =[];

    %_____________________________________________________________________
    % START RAYS FOR MIRROR

    for j = 1:iterations

        j
        num_rays = num_rays +1;
        ray_flux = mirror_flux(i,floor(1000*(xstart+0.251)));
        total_flux_in = total_flux_in + ray_flux;

        gamma = NaN;
        xtemp = xstart;
        ytemp = ystart;
        mtemp = tan(angleiter
        ctemp = (-1)*mtemp*xtemp;
        omega1 = angleiter;
        omega2 = 0;
        vert = 0;
        straight_down = 0;

        error_val = 0.000001;
        ytemptop = height;
        xtemptop = (ytemptop -ctemp)/mtemp;

        y_inter_vec =[];
        x_inter_vec =[];

        cont_loop =1;
        direction = 1;
        last_inter = 0;

        if xtemp <= sec_domain(1,1) || xtemp >= sec_domain(num_sections,2)
            cont_loop = 0;
        end

        %_____________________________________________________________
        % START WHILE LOOP FOR EACH RAY
```

```
        while cont_loop ==1
            %_____________________________________________________________________
            % Check if intercept

            dist = [];

            for h = 1: num_pipes
                if last_inter == h
                    dist(h) = 10;
                else

                    if vert == 1 && direction == 0
                        if xtemp >= circ_domain(h,1) && xtemp<=
circ_domain(h,2)

                            x_inter(h) = xtemp;
                            y_inter(h) = y_offset_circle(h) +
sqrt((radius_of_pipe)^2-(x_inter(h)-x_offset_circle(h))^2);
                            actualintercept =1
                            dist(h) = 0;

                        else
                            actualintercept =0
                            dist(h) = 10;
                            straight_down = 1;
                        end
                    else

                        linefunc = strcat(num2str(mtemp),'*x
+',num2str(ctemp));
                        equ2 = ['(x-
',num2str(x_offset_circle(h)),')^2+(',linefunc,'-
',num2str(y_offset_circle(h)),')^2-(',num2str(radius_of_pipe),')^2'];

                        if direction == 1 && mtemp <0
                            x0 = [5];
                        elseif direction == 1 && mtemp >= 0
                            x0 = [-5];
                        elseif direction == 0 && mtemp <0
                            x0 = [-5];
                        elseif direction == 0 && mtemp >= 0
                            x0 = [5];
                        end

                        options = optimset('TolFun',1e-14);

                        [x_inter(h),fval] = fsolve(equ2,x0,options);
                        eval(['x=',num2str(x_inter(h)),';']);
                        y_inter(h) = eval(linefunc);

                        check_temp2 = (x_inter(h)-
x_offset_circle(h))^2+(y_inter(h)-y_offset_circle(h))^2-(radius_of_pipe)^2;
                        actualintercept =0;
                        if check_temp2 < error_val

                            actualintercept =1
                            dist(h) = sqrt((x_inter(h)-
xtemp)^2+(y_inter(h)-ytemp)^2);
                        else
```

```
                        actualintercept =0
                        dist(h) = 10;
                    end

                end
            end

        end

        vert = 0;


        for m = (num_pipes+1):(num_pipes+num_sections)

            equ3 = [strcat(linefunc,'-(',func(m-num_pipes,1),')')];

            if direction == 1 && mtemp <0
                x0 = [-5];
            elseif direction == 1 && mtemp >= 0
                x0 = [5];
            elseif direction == 0 && mtemp <0
                x0 = [5];
            elseif direction == 0 && mtemp >= 0
                x0 = [-5];
            end

            options = optimset('TolFun',1e-14);

            [x_inter(m),fval] = fsolve(equ3,x0,options);
            eval(['x=',num2str(x_inter(m)),';']);

            y_inter(m) = eval(linefunc);

            dist(m) = sqrt((x_inter(m)-xtemp)^2+(y_inter(m)-ytemp)^2)

            if x_inter(m) >= (sec_domain(m-num_pipes,1)+0.00001) &&
x_inter(m) <= (sec_domain(m-num_pipes,2)-0.00001)

                check = 60
            else
                dist(m) = 10
                check = 50
            end

            if last_inter == m
                if flat_surface == 1

                    check = 40
                    dist(m) = 10;

                else
                    if x_inter(m) > (xtemp-0.0001) && x_inter(m) <
(xtemp+0.0001)
                        if direction == 0 && mtemp >=0

                            solve_domain = [sec_domain(last_inter-
num_pipes,1)]
```

```
                            elseif direction == 1 && mtemp <= 0

                                solve_domain = [sec_domain(last_inter-
num_pipes,1)]
                            elseif direction == 1 && mtemp > 0
                                solve_domain = [sec_domain(num_sections,2)]
                            elseif direction == 0 && mtemp <0
                                solve_domain = [sec_domain(num_sections,2)]
                        end

                            options = optimset('TolX',1e-10);
                            equ3 = (cell2mat(equ3));

                            [x_inter(m),fval] =
fzero(equ3,solve_domain,options);

                            eval(['x=',num2str(x_inter(m)),';']);

                            y_inter(m) = eval(linefunc);

                            dist(m) = sqrt((x_inter(m)-
xtemp)^2+(y_inter(m)-ytemp)^2);

                            if x_inter(m) > (xtemp-0.00001) && x_inter(m) <
(xtemp+0.00001)
                                dist(m) = 10;
                            end
                        end
                    end
                end

            end

            dist

            [min_dist surface] = min(dist);

            if direction == 0 && mtemp <=0
                if x_inter(surface) < xtemp && last_inter == (num_pipes +1)
                    dist(surface) = 10;
                    [min_dist surface] = min(dist);
                end

            elseif direction == 0 && mtemp >0 && last_inter == (num_pipes +
num_sections)
                if x_inter(surface) > xtemp
                    dist(surface) = 10;
                    [min_dist surface] = min(dist);
                end
            end

            if surface > num_pipes && surface < (num_pipes+num_sections +1)
                if gamma > (pi()/2)

                    if sec_domain(surface-num_pipes,1) > xtemp &&
y_inter(surface) > sec_range(surface-num_pipes-1,2)
                        dist(surface) = 10;
                        [min_dist surface] = min(dist);
```

```
                    end

                    if flat_surface == 1 && num_sections == 4

                        if last_inter > 1 && surface > 1
                        if sec_domain(surface-num_pipes,1) > xtemp &&
y_inter(surface) > sec_range(last_inter-num_pipes,2)


                            dist(surface) = 10;
                            [min_dist surface] = min(dist);
                        end
                        end
                    end

                elseif gamma < (pi()/2) && gamma > 0

                    check = 30
                    if sec_domain(surface-num_pipes,2) < xtemp &&
y_inter(surface) > sec_range(surface-num_pipes+1,1)


                        dist(surface) = 10;
                        [min_dist surface] = min(dist);
                    end

                    if flat_surface == 1 && num_sections == 4
                        if last_inter>1 && surface >1
                        surface
                        if sec_domain(surface-num_pipes,2) < xtemp &&
y_inter(surface) > sec_range(last_inter-num_pipes,1)
                            dist(surface) = 10;
                            [min_dist surface] = min(dist);
                        end
                        end
                    end

                elseif gamma == 0

                    if last_inter< surface
                        if sec_domain(surface-num_pipes,1) > xtemp &&
y_inter(surface) > sec_range(surface-num_pipes-1,2)

                            dist(surface) = 10;
                            [min_dist surface] = min(dist);
                        end
                    elseif last_inter> surface

                        if sec_domain(surface-num_pipes,2) < xtemp &&
y_inter(surface) > sec_range(surface-num_pipes+1,1)

                            dist(surface) = 10;
                            [min_dist surface] = min(dist);
                        end
                    end
                end
            end
```

```
if dist(surface) < 0.0001 && y_inter(surface) < 0.01
    dist(surface) =10;
end

no_inter = 0;
test_vec = [];
for check_inter = 1: (num_pipes + num_sections)
    if dist(check_inter) == 10
        test_vec(check_inter) = 1;
    else
        test_vec(check_inter) = 0;
    end
end
flag_inter = min(test_vec);
if flag_inter == 1
    no_inter = 1;
end

 if y_inter(surface) < 0 || y_inter(surface) > (height+0.001)
    dist(num_pipes+num_sections+1) = 0;
    [min_dist surface] = min(dist);
elseif no_inter ==1
    dist(num_pipes+num_sections+1) = 0;
    [min_dist surface] = min(dist);
elseif straight_down == 1
    dist(num_pipes+num_sections+1) = 0;
    [min_dist surface] = min(dist);
else
    dist(num_pipes+num_sections+1) = 10;
end

last_inter = surface;

%_____________________________________________________________________
%_____________________________________________________________________
% Check for reflections

if surface > num_pipes && surface < (num_pipes+num_sections+1)

    tempfunc = cell2mat(func(surface-num_pipes));

    deriv = diff(cell2mat(func(surface-num_pipes)),1,'x');

     x = x_inter(surface);
    deriv = eval(deriv);

    if deriv >= 0
        gamma = atan(deriv);
    elseif deriv< 0
        gamma = atan(deriv)+ pi();
    end

    normal_grad = (-1)/deriv;
    if normal_grad == inf || normal_grad == (-inf)
        normal_grad = 1;
        infinite_check = 0;
    else
        infinite_check = 1;
    end
```

```
                if normal_grad > 0
                    sign = -1;
                else normal_grad <= 0
                    sign = 1;
                end

                normal_c = y_inter(surface) -
(normal_grad*x_inter(surface));

                normal_x = x_inter(surface)+ sign* 0.002*infinite_check;
                normal_y = y_inter(surface)+ sign* 0.002*normal_grad;

                xtempnew = x_inter(surface);
                ytempnew = y_inter(surface);

                %_____________________________________________________________
                %_____________________________________________________________
                % Check reflections

                 if gamma >0 && gamma < (pi()/2)
                    if gamma<=omega1 && omega1<(pi()/2)
                          omega2 = 2*gamma-omega1;
                        if omega2 < 0
                            direction = 0;
                        else
                            direction = 1;
                        end

                        mtemp = tan(omega2);

                        if do_plot ==1
                            figure(3)
                            plot([xtemp xtempnew],[ytemp ytempnew],'r')
                        end

                    elseif omega1 >= (pi()/2) && omega1<((pi()/2)+gamma)
                        omega2 = 2*gamma-omega1;

                         if omega2> 0
                            direction = 1;
                        else
                            direction = 0;
                        end

                        mtemp = tan(omega2);

                        if do_plot == 1
                            figure(3)
                            plot([xtemp xtempnew],[ytemp ytempnew],'r')
                        end

                    elseif omega1>= ((pi()/2)+gamma) && omega1< (pi())
                        omega2 = 2*gamma - omega1;

                        direction = 0;

                        mtemp = tan(omega2);
```

```
            if do_plot == 1
                figure(3)
                plot([xtemp xtempnew],[ytemp ytempnew],'r')
            end

        elseif omega1>=(pi()) && omega1<=(pi()+gamma)



            omega2 = 2*gamma-omega1 +2*pi();
            mtemp = tan(omega2);
            direction = 0;

            if do_plot ==1
                figure(3)
                plot([xtemp xtempnew],[ytemp ytempnew],'r')
            end
        end

    elseif gamma >= (pi()/2) && gamma < (pi())

        if omega1> (pi()/2) && omega1 <= gamma

            check = 8
            omega2 = 2*gamma - omega1

            if omega2 > pi()
                direction = 0;
            else
                direction = 1;
            end

            mtemp = tan(omega2);

             if do_plot == 1
                figure(3)
                plot([xtemp xtempnew],[ytemp ytempnew],'r')
            end

        elseif omega1>(gamma - pi()/2) && omega1<= (pi()/2)

             check = 9

            omega2 = 2*gamma - omega1

            if omega2 <= pi()
                mtemp = tan(omega2);
                direction = 1;
            else
                mtemp = tan(omega2);
                direction = 0;
            end

            if do_plot == 1
                figure(3)
                plot([xtemp xtempnew],[ytemp ytempnew],'r')
            end
```

```
                elseif omega1>=0 && omega1<= (gamma -(pi()/2))

                    check = 10

                    omega2 = 2*gamma - omega1;

                    mtemp = tan(omega2)
                    direction = 0;

                    if do_plot == 1
                        figure(3)
                        plot([xtemp xtempnew],[ytemp ytempnew],'r')
                    end

                elseif omega1>= (pi()+gamma) && omega1 <= (2*pi())

                    check = 11

                    omega2 = 2*gamma - omega1;

                    mtemp = tan(omega2);
                    direction = 0;

                    if do_plot == 1
                        figure(3)
                        plot([xtemp xtempnew],[ytemp ytempnew],'r')
                    end
                end

            elseif gamma == 0 || gamma == (pi())

                if omega1>0 && omega1< (pi()/2)
                    omega2 = -omega1;
                    mtemp = tan(omega2);
                    direction = 0;
                else
                    omega2 = 2*pi()-omega1;
                    mtemp = tan(omega2);
                    direction = 0;
                end

                if do_plot == 1
                    figure(3)
                    plot([xtemp xtempnew],[ytemp ytempnew],'r')
                end
            end

            ray_flux = ray_flux *reflection_loss;

        elseif surface <= num_pipes
            if do_plot == 1
                figure(3)
                plot([xtemp x_inter(surface)],[ytemp
y_inter(surface)],'y')
            end

            absorbed_flux = absorbed_flux + ray_flux;
```

```
            num_hit = num_hit +1;

            hit = 1
            cont_loop =0;
            xtempnew = x_inter(surface);
            ytempnew = y_inter(surface);

        elseif surface > (num_pipes + num_sections)

            ray_flux = 0;
            missed = 1
            cont_loop =0;

            if direction == 1
                xtempnew = (height-ctemp)/mtemp;
                ytempnew = height;
                if do_plot ==1
                    figure(3)
                    plot([xtemp xtempnew],[ytemp ytempnew],'c')
                end
            elseif direction == 0
                xtempnew = (-1)*ctemp/mtemp;
                ytempnew = 0;
                if do_plot ==1
                    figure(3)
                    plot([xtemp xtempnew],[ytemp ytempnew],'c')
                end
            end
        end

%_____________________________________________________________________________
        % Update variables for next reflection


        if omega2 < (3.03*pi()/2) && omega2 >(2.97*pi()/2)
            vert = 1
        elseif omega2 < (pi()/(-2.03)) && omega2 > (pi()/(-1.97))
            vert = 1
        end

        omega1 = omega2;
        xtemp = xtempnew;
        ytemp = ytempnew;

        if omega1 <0
            omega1 = omega1 + 2*pi();
        end
        %mtemp = tan(omega1);
        ctemp = ytemp - mtemp*xtemp;

    end


    % END WHILE LOOP FOR EACH RAY
    %_____________________________________________________________________
    %_____________________________________________________________________
```

```
        xstart = xstart + ray_spacing/1000;

        angleiter = angleiter + angledelta;
    end

    %_____________________________________________________________________
    % END RAYS FOR MIRROR

    filename_string =
strcat('C:\Users\Work\Documents\Design\Secondaryconcentrator\',num2str(rec_
dim_pos(1,1)),'mirror',num2str(i),'.png');

    hgexport(gcf, filename_string, ...
        hgexport('factorystyle'), 'Format', 'png');
end
```

## Surface file – ReceiverTrapezoidal

```
global sec_domain
global sec_range
global func
global height
global do_plot
global flat_surface

flat_surface = 1;

height = 0.14;
length_rec = 0.27;
side_inclination = 70;

xleftbottom = (-1)*length_rec/2;
yleftbottom = 0;
xrightbottom = length_rec/2;
yrightbottom =0;

xlefttop = xleftbottom + height/(tan(side_inclination*pi()/180));
ylefttop = height;
xrighttop = xrightbottom - height/(tan(side_inclination*pi()/180));
yrighttop = height;

m1rec = tan(side_inclination*pi()/180);
m2rec = 0;
m3rec = tan(pi() - side_inclination*pi()/180);

c1rec = (-1)*m1rec*xleftbottom;
c2rec = height;
c3rec = (-1)*m3rec*xrightbottom;
```

```
m1recinv = (-1)/m1rec;
m3recinv = (-1)/m3rec;

if m2rec == 0
    m2recinv = -1;
else
    m2recinv = (-1)/m2rec;
end

if do_plot == 1
    figure(3)
plot([xrightbottom xrighttop],[yrightbottom yrighttop],'k','LineWidth',1)
plot([xleftbottom xlefttop],[yleftbottom ylefttop],'k','LineWidth',1)
plot([xlefttop xrighttop],[ylefttop yrighttop],'k','LineWidth',1)
end

sec_domain = [xleftbottom xlefttop;xlefttop xrighttop;xrighttop
xrightbottom];
sec_range = [yleftbottom ylefttop;ylefttop yrighttop;yrighttop
yrightbottom];

func1 = [num2str(m1rec),'*x +',num2str(c1rec)];
func2 = [num2str(m2rec),'*x +',num2str(c2rec)];
func3 = [num2str(m3rec),'*x +',num2str(c3rec)];

func = {func1;func2;func3};
```

## Surface file – ReceiverParabolic

```
x_vector = -0.14:0.001:0.14;
focus = 0.06;
vertex_x = 0;
vertex_y = 0.09375;

global sec_domain
global sec_range
global func
global height
global do_plot
global flat_surface

flat_surface = 0;


% Para 1


func = {'(-1)*((x+0.05)^2-4*0.014464286*0.14)/(4*0.014464286)';'(-
1)*((x+0.05)^2-4*0.02*0.14)/(4*0.02)';'(-1)*((x-0.05)^2-
4*0.02*0.14)/(4*0.02)';'(-1)*((x-0.05)^2-
4*0.014464286*0.14)/(4*0.014464286)'};

sec_domain = [-0.14 -0.05;-0.05 0;0 0.05;0.05 0.14];
```

```
x = sec_domain(1,2);

height = eval(cell2mat(func(1)));

for i = 1:4
    for j = 1:2

        x = sec_domain(i,j);
        sec_range(i,j) = eval(cell2mat(func(i)));
    end
end

sec_domain
sec_range

for f = 1: length(x_vector)

x = x_vector(f);

    if x_vector(f) > sec_domain(1,1) && x_vector(f) <= sec_domain(1,2)

        y_vector(f) = eval(char(func(1)));

    elseif x_vector(f) > sec_domain(2,1) && x_vector(f) <= sec_domain(2,2)

        y_vector(f) = eval(char(func(2)));

    elseif x_vector(f) > sec_domain(3,1) && x_vector(f) <= sec_domain(3,2)

        y_vector(f) = eval(char(func(3)));

    elseif x_vector(f) > sec_domain(4,1) && x_vector(f) <= sec_domain(4,2)

        y_vector(f) = eval(char(func(4)));

    end

end

if do_plot ==1
    figure(3)
plot(x_vector,y_vector,'k')
end
```

# APPENDIX C. CALCULATIONS

## C1. TRACKER TORQUE CALCULATION

Due to a number of factors that were difficult to approximate theoretically, the torque requirement to turn the 16 mirrors was calculated experimentally (Shigley, Mischeke and Budynas 2004). A crank handle was connected onto the shaft of the drive sprocket and a force was applied by hanging weights to the crank at a radial distance of 10cms. Approximately 40 kgs was required to easily run the shaft and all 16 mirrors. The required torque was then calculated:

$$T = F \times d = m \times g \times d = 40 \times 9.81 \times 0.1 = 39.2\ Nm$$

The stepper motor that was selected has a rated torque of 3.5 Nm. This torque would then be increased through the use of a 50:1 worm gear set. Inventor 2012 has a built in worm gear calculator that can perform stress analysis on standard worm gear designs. The 3.5 Nm maximum output torque from the stepper motor was entered and resulted in a 75 Nm output torque from the worm gear set. This was also within the allowable stress for the chosen worm gear tooth module. The stepper motor and worm gear set would then be able to supply the required drive torque with some safety factor built in.

## C2. THERMAL LOSS CALCULATIONS

In order to accurately predict power production in the experiment, the expected thermal losses from the absorber tube and receiver need to be calculated. This is done using the standard heat loss equations for radiation and convection (Cengel and Boles 2002). The radiation loss is calculated by:

$$\dot{Q}_R = F_{p \to rec} \times A_p \times \epsilon \times \sigma \times \left({T_p}^4 - {T_{rec}}^4\right) \qquad (20)$$

Where :

| | | |
|---|---|---|
| $F_{p \to rec}$ | = | View factor from pipe to receiver |
| $A_p$ | = | Area of pipe |
| ε | = | Emissivity of pipe |
| σ | = | Stefan–Boltzmann constant (5.670373×10−8 $W.m^{-2}K^{-4}$) |
| $T_p$ | = | Temperature of absorber pipe |

$T_{rec}$ = Temperature of receiver/ambient

The convection loss is calculated from:

$$\dot{Q}_C = h \times A_p \times (T_p - T_{rec}) \quad (21)$$

Where: h = Heat transfer coefficient

# APPENDIX D. TRACKER ALGORITHM CODE

The code below is programmed in the Arduino development environment available from: www.http://arduino.cc/en/Main/Software

```
#include <icrmacros.h>
#include <SoftwareSerial.h>

float stepsize = 1.8/50.0;
float motorpos = 0.0;
float phimirror = atan(120.0/2080.0);
int limitswitch3 = 0;
SoftwareSerial mySerial(2,3);

void setup()
{
  pinMode(13, OUTPUT);
  Serial.begin(9600);
  digitalWrite(13, LOW);
  pinMode(8, OUTPUT);
  pinMode(6, INPUT);
  pinMode(7, OUTPUT);
  pinMode(10, INPUT);
  digitalWrite(8, HIGH);
  digitalWrite(7,HIGH);
  pinMode(2, INPUT);
  mySerial.begin(9600);

  int limitswitch = 0;
  while (limitswitch != 1)
  {
    digitalWrite(8,LOW);
    delay(5);
    digitalWrite(8,HIGH);
    delay(5);
    //Serial.print("1");
    if (digitalRead(6) == LOW)
    {
      delay(1000);
      if (digitalRead(6) == LOW)
      {
        limitswitch = 1;
```

```
        limitswitch3 =1;
      }
    }
  }
  motorpos = 0.0;
  Serial.println("End setup");
  digitalWrite(13,HIGH);
}


// MAIN LOOP
void loop()
{
  int serialStringPosition;
  char inByte;
  char serialString[250];
  const char beginChar = '*';

  int commaPosition =0;
  int commaString[20];
  int numCommas = 0;

  for (int j=0;j<20;j++)
  {
    commaString[j] = 0;
  }
  for (int i=0;i<250;i++)
  {
    serialString[i] = ' ';
  }
  if (digitalRead(10) == LOW)
  {
    delay(2000);
    if (digitalRead(10) == LOW)
    {
     delay(3000);
     if (digitalRead(10) == LOW)
     {
          while (limitswitch3 != 1)
          {
            digitalWrite(8,LOW);
            delay(5);
            digitalWrite(8,HIGH);
            delay(5);
            Serial.print("1");
```

```
          if (digitalRead(6) == LOW)
          {
            delay(1000);
            if (digitalRead(6) == LOW)
            {
              limitswitch3 = 1;
            }
          }
        }
        Serial.println("No track");
        motorpos = 0.0;
        Serial.print("New motorpos: ");Serial.println(motorpos);
  }
  }
}
else{

 if (mySerial.available())
 {
  delay(1);
  serialStringPosition =0;
  //while (mySerial.available())
  //{
   for (int j=0;j<250;j++)
   {
     inByte = mySerial.read();
     serialString[j] = inByte;
     delay(1);
   }
  //}

  Serial.println(serialString);
  int endpos = 0;
  int startpos = 0;

  for (int k=0;k<250;k++)
  {
   if (serialString[k] == '$' && serialString[k+1] == 'G' && serialString[k+2] == 'P')
   {
     if (serialString[k+3] == 'Z' && serialString[k+4] == 'D' && serialString[k+5] == 'A')
     {
       Serial.println("Right string");
       Serial.println(k);
       startpos = k;
       char checkByte = serialString[k];
```

```
      endpos = k;
      while (checkByte != '*')
      {
        endpos++;
        checkByte = serialString[endpos];
      }
      Serial.println(endpos);
    }// End if ZDA
  }// End if $GP
}// End for
if (endpos != 0 && startpos != 0)
{
  for (int l=startpos;l<endpos;l++)
  {
    char currentChar = serialString[l];
    if (currentChar == ',')
    {
      commaString[numCommas] = l;
      numCommas++;
    }
  }
  int checkGPS1 = commaString[0] +1;
  int checkGPS2 = commaString[1];
  int checkGPS3 = commaString[2] +1;
  int checkGPS4 = commaString[3];
  if (checkGPS1 == checkGPS2 || checkGPS3 == checkGPS4)
  {
    Serial.println("GPS not locked on");
  } else
  {
    Serial.println("GPS locked on");
    int h1 = serialString[commaString[0]+1];
    int h2 = serialString[commaString[0]+2];
    int m1 = serialString[commaString[0]+3];
    int m2 = serialString[commaString[0]+4];
    int s1 = serialString[commaString[0]+5];
    int s2 = serialString[commaString[0]+6];
    int D1 = serialString[commaString[1]+1];
    int D2 = serialString[commaString[1]+2];
    int M1 = serialString[commaString[2]+1];
    int M2 = serialString[commaString[2]+2];
    int Y1 = serialString[commaString[3]+1];
    int Y2 = serialString[commaString[3]+2];
    int Y3 = serialString[commaString[3]+3];
    int Y4 = serialString[commaString[3]+4];
```

```
int Hourval = 10*(h1-48) + (h2-48)+ 2;
int Minuteval = 10*(m1-48) + (m2-48);
int Secondval = 10*(s1-48) + (s2-48);
int Yearval = 1000*(Y1-48)+100*(Y2-48)+10*(Y3-48) + (Y4-48);
int Monthval = 10*(M1-48) + (M2-48);
int Dayval = 10*(D1-48) + (D2-48);
Serial.print("Hour: ");Serial.println(Hourval);
Serial.print("Minute: ");Serial.println(Minuteval);
Serial.print("Second: ");Serial.println(Secondval);
//
if (Hourval >0 && Minuteval >0 && Secondval>0 && Yearval >0 && Monthval >0 && Dayval >0)
{
float leapyearcheck1 = Yearval/4.0;
float leapyearcheck2 = Yearval/4;
int leapyear = 0;
if (leapyearcheck1 == leapyearcheck2)
{
  leapyear = 1;
} else
{
  leapyear = 0;
}
int daynumber = 1;
switch (Monthval) {
  case 1:
  daynumber = Dayval;
  break;
  case 2:
  daynumber = Dayval + 31;
  break;
  case 3:
  daynumber = Dayval + 59 +leapyear;
  break;
  case 4:
  daynumber = Dayval + 90 +leapyear;
  break;
  case 5:
  daynumber = Dayval + 120 +leapyear;
  break;
  case 6:
  daynumber = Dayval + 151 +leapyear;
  break;
  case 7:
  daynumber = Dayval + 181 +leapyear;
  break;
```

```
  case 8:
  daynumber = Dayval + 212 +leapyear;
  break;
  case 9:
  daynumber = Dayval + 243 +leapyear;
  break;
  case 10:
  daynumber = Dayval + 273 +leapyear;
  break;
  case 11:
  daynumber = Dayval + 304 +leapyear;
  break;
  case 12:
  daynumber = Dayval + 334 +leapyear;
  break;
}

int daynum = 1;
switch(Yearval) {
  case 2012:
  daynum = daynumber;
  break;
  case 2013:
  daynum = daynumber + 366;
  break;
  case 2014:
  daynum = daynumber + 731;
  break;
  case 2015:
  daynum = daynumber +1096;
  break;
  case 2016:
  daynum = daynumber;
  break;
  case 2017:
  daynum = daynumber + 366;
  break;
  case 2018:
  daynum = daynumber + 731;
  break;
  case 2019:
  daynum = daynumber + 1096;
  break;
  default:
  daynum = daynumber;
```

```
}
float EOT1 = 0.0002087*cos((360.0*0.0*daynum)/365.25);
float EOT2 = 0.0092869*cos((360.0*1.0*daynum)/365.25) - 0.12229*sin((360.0*1.0*daynum)/365.25);
float EOT3 = (-1.0)*0.052258*cos((360.0*2.0*daynum)/365.25) - 0.15698*sin((360.0*2.0*daynum)/365.25);
float EOT4 = (-1.0)*0.0013077*cos((360.0*3.0*daynum)/365.25) -
0.0051602*sin((360.0*3.0*daynum)/365.25);
float EOT5 = (-1.0)*0.0021867*cos((360.0*4.0*daynum)/365.25) -
0.0029823*sin((360.0*4.0*daynum)/365.25);
float EOT6 = (-1.0)*0.000151*cos((360.0*5.0*daynum)/365.25) -
0.00023463*sin((360.0*5.0*daynum)/365.25);
float EOT = 60.0*(EOT1+EOT2+EOT3+EOT4+EOT5+EOT6);
//float xfractiondeg = 360.0*(daynumber -1)/(365.242);
//float xfraction = xfractiondeg*PI/180.0;
//float EOT = 0.258*cos(xfraction)-7.416*sin(xfraction)-3.648*cos(2*xfraction)-9.228*sin(2*xfraction);
float LC = (18.865-30.0)/15.0;
float LCT = Hourval + Minuteval/60.0 + Secondval/3600.0;
float solartime = LCT + (EOT/60.0) + LC;
Serial.print("Solar time: ");Serial.println(solartime);
float phi = -33.9284*PI/180.0;
float omega = 15.0*(solartime-12.0)*PI/180.0;
float delta = asin(0.39795*cos(0.98563*(daynumber-173.0)*PI/180.0));
float alpha = asin(sin(delta)*sin(phi)+cos(delta)*cos(omega)*cos(phi));
float zenith = (PI/2.0)-alpha;
float azimuthtemp = acos((sin(delta)*cos(phi)-cos(delta)*cos(omega)*sin(phi))/cos(alpha));
float azimuth = 0.0;
if (sin(omega)>0.0)
{
  azimuth = 2.0*PI - azimuthtemp;
}
  else if (sin(omega) <= 0.0)
{
  azimuth = azimuthtemp;
}
Serial.print("Azimuth: ");Serial.println(azimuth,4);
Serial.print("Zenith: ");Serial.println(zenith,4);
if (zenith<(PI/2.0) && azimuth != 0.0)
{
  float rho = PI/2.0 - atan((sin((PI/2.0)-zenith))/(cos((PI/2.0)-zenith)*sin(azimuth)));
  float azimuthadj =0.0;
  if (azimuth <= PI)
  {
    azimuthadj = azimuth;
  }
  else if (azimuth > PI)
  {
```

```
   azimuthadj = 2.0*PI-azimuth;
  }
  float sunangle = 0.0;
  float tempsun = 0.0;
  float tiltangle =0.0;
  if (azimuth <= PI)
  {
    tempsun = rho;
    tiltangle = PI/2.0 - atan((sin((PI/2.0)-zenith))/(cos((PI/2.0)-zenith)*cos(azimuthadj)));
  }
    else if (azimuth > PI)
  {
    tempsun = (-1.0)*(PI-rho);
    tiltangle = (-1.0)*PI/2.0 - atan((sin((PI/2.0)-zenith))/(cos((PI/2.0)-zenith)*sin(azimuthadj)));
  }
  sunangle = (PI - tempsun)*180.0/PI;
  float theta = (phimirror - tempsun)/2.0;
  float normalpos = (PI + theta)*180.0/PI;
  Serial.print("Tempsun: ");Serial.println(tempsun,4);
  Serial.print("Sunangle: ");Serial.println(sunangle,4);
  Serial.print("Tiltangle: ");Serial.println(tiltangle,4);
   Serial.print("Rho: ");Serial.println(rho,4);
   Serial.print("Theta: ");Serial.println(theta,4);
   Serial.print("Normalpos: ");Serial.println(normalpos,4);
  Serial.print("Motorpos: ");Serial.println(motorpos,4);
 if (motorpos < 1.0 || normalpos < motorpos + 5.0)
  {
  while (motorpos < normalpos)
  {
    digitalWrite(8,LOW);
    delay(5);
    digitalWrite(8,HIGH);
    delay(5);
    Serial.print("1");
    motorpos = motorpos + stepsize;
    limitswitch3 = 0;
  }
  }
  Serial.println("end");
  Serial.print("New motorpos: ");Serial.println(motorpos);

}
else
{
 // Do nothing
```

```
        }

      }// End if time vals and date vals positive
      } // End if string populated
    }// End if endpos and startpos
  }  // End if serial available
  } // End Elseif pin 10 == LOW first check
} // End loop
```